Wisconsin Highway Research Program

Friction Coefficients For Stainless Steel (PTFE) Teflon Bearings

SPR # 0092-08-13

John Stanton
Department of Civil Engineering
University of Washington

October 2010
WHRP 10-01

Final Research Report
WisDOT Project ID 0092-08-13
Report No. WHRP 10-01

FRICTION COEFFICIENTS FOR STAINLESS STEEL/PTFE (TEFLON) BEARINGS

by

Josef C. Taylor and John F. Stanton

Department of Civil Engineering
University of Washington

Prepared for:
Wisconsin Department of Transportation.
Administrative Contact: Andrew Hanz.
Technical Contact: Travis MacDaniel.

January 2010

Disclaimer

This research was funded through the Wisconsin Highway Research Program by the Wisconsin Department of Transportation and the Federal Highway Administration under Project 0092-08-13. The contents of this report reflect the views of the authors who are responsible for the facts and accuracy of the data presented herein. The contents do not necessarily reflect the official views of the Wisconsin Department of Transportation or the Federal Highway Administration at the time of publication.

This document is disseminated under the sponsorship of the Department of Transportation in the interest of information exchange. The United States Government assumes no liability for its contents or use thereof. This report does not constitute a standard, specification or regulation.

The United States Government does not endorse products or manufacturers. Trade and manufacturers' names appear in this report only because they are considered essential to the object of the document.

Technical Report Documentation Page

1. Report No. WHRP 10-01	2. Government Accession No	3. Recipient's Catalog No
4. Title and Subtitle Friction Coefficients for Stainless Steel (PTFE) Teflon Bearings		5. Report Date: January 2010 6. Performing Organization Code Wisconsin Highway Research Program
7. Authors Josef C. Taylor, John F. Stanton		8. Performing Organization Report No.
9. Performing Organization Name and Address Department of Civil Engineering, Box 3527000, University of Washington, Seattle WA 98195		10. Work Unit No. (TRAIS) 11. Contract or Grant No. WisDOT SPR# 0092-08-13
12. Sponsoring Agency Name and Address Wisconsin Department of Transportation Division of Business Services Research Coordination Section 4802 Sheboygan Ave. Rm 104 Madison, WI 53707		13. Type of Report and Period Covered Final Report, 2008-2010 14. Sponsoring Agency Code
15. Supplementary Notes		

16. Abstract

The research objectives are to determine the coefficients of friction of stainless steel-PTFE surfaces with two different surface finishes: #7 high-luster and #8 mirror, to provide an initial evaluation of the effects of higher friction on the forces in the structure, and to report the results to WisDOT in a way that can be easily and clearly understood, and implemented in bridge design practice through the Bureau of Structures.

17. Key Words Friction, PTFE, Teflon, Stainless steel, Sliding, Bearing.	18. Distribution Statement No restriction. This document is available to the public through the National Technical Information Service 5285 Port Royal Road Springfield VA 22161		
19. Security Classif.(of this report) Unclassified	19. Security Classif. (of this page): Unclassified	20. No. of Pages	21. Price

Form DOT F 1700.7 (8-72) Reproduction of completed page authorized

Executive Summary.

This report describes a study on sliding bridge bearing made from PTFE and stainless steel. Such bearings are commonly made from sheet PTFE and stainless steel polished to a #8 mirror finish. That surface finish is the only one for which the AASHTO LRFD Design Specifications provide design values of the friction coefficient. However, it can be expensive and difficult to obtain.

The objective of the work was to determine the suitability of stainless steel with a 2B surface finish in sliding bearings. 2B stainless steel is produced by cold rolling and is not polished. It is thus more readily available and less expensive, but it has a rougher finish.

A program of tests was undertaken to investigate the coefficient of friction and the wear characteristics of sliding bearings. Three stainless steel surface finishes were used: #8 mirror (as a reference), 2B, and a rough hot-rolled finish that was initially supplied by WisDOT. The results of the tests were analyzed and recommendations were prepared.

Friction between PTFE and a hard material such as stainless steel varies with many parameters, the most important of which are: surface finish, contact pressure, sliding speed, slide path and temperature. The first four of these were addressed in the tests; low temperature testing requires special equipment that lay outside the scope of the project.

The test results shared many characteristics with those found in previous studies. Static, or breakaway, friction is higher than sliding friction. The coefficient of friction is sensitive to contact pressure (unlike, for example, steel on steel, for which it is essentially independent of contact pressure), and increases at low pressure. It increases as sliding speed increases, although, within the range of sliding speeds expected in a non-seismic application, the sensitivity is not great.

By contrast, the effects of slide path were unexpected. For the mirror finish material, the coefficient of friction rose with increasing slide path, for the rough hot-rolled material, it fell, and for the 2B material it remained almost constant, even over one very long slide path test of three-quarters of a mile. At the end of each long slide-path test, the mirror finish material almost always displayed the highest friction coefficient. This result was counter-intuitive, but was consistent across essentially all tests with the three materials.

Wear of the PTFE was also measured, and was found to be very low for the 2B finish.

A general equation was developed from the test data with which to predict the friction coefficient as a function of surface finish, contact pressure, sliding speed and slide path.

Computations were done to estimate the slide path demand in a real bridge. It was found to vary greatly among bridges, and to depend on column stiffness, span length, superstructure type and details, and temperature profile.

2B surface finish stainless steel displayed stable and relatively low friction properties, based on which it was deemed to be a suitable alternative to #8 mirror finish, subject to the caveat that its performance characteristics at low temperature are unknown.

Table of Contents

List of Figures

List of Tables

Acknowledgements

The financial support of the Wisconsin Department of Transportation, and the technical assistance of Travis MacDaniel and Finn Hubbard in particular, is gratefully acknowledged.

The laboratory work could not have been completed without the help of Vince Chaijaroen, the Structures Laboratory manager, whose assistance is much appreciated.

1 Introduction

Bridges, especially those exposed to wide temperature variations or subjected to heavy truck traffic, require bearings that can accommodate the movement of the bridge superstructure while transmitting the least possible force to the substructure. Bearings must perform their duties with minimal maintenance over as long a design life as possible, due to the difficulty of replacing them.

Bearings accommodate movement by one of several different means. Elastomeric bearings deform, steel rocker and roller bearings roll in rigid body rotation, and in sliding bearings one material slides on another. This report concerns a particular type of sliding bearing, made from PTFE (PolyTetraFluoroEthylene, known more commonly by the DuPont™ trade name Teflon™) and polished stainless steel. Teflon is chemically very inert, and was originally developed as an electrical insulator. However its low friction characteristics and its chemical inertness have made it popular in many commercial and residential applications, such as non-stick cookware, in addition to its use in bridge bearings.

Several types of PTFE are used in bridge bearings. In the US, flat sliding bearings are usually made with solid sheet PTFE. That material is most commonly pure PTFE, but in the past it has been reinforced with glass or other fibers to inhibit creep. That practice has largely been discontinued, because the fibers scratch the stainless steel and increase the friction. In Europe and Canada, the sheet PTFE is frequently dimpled and lubricated with grease. Lubrication decreases the friction to very low levels (to less than 0.3% in some cases) and the dimples act as reservoirs, without which the grease would soon be squeezed out from between the PTFE and the stainless steel. In spherical sliding bearings, the PTFE needs to be formed into a spherical shape, and doing so is difficult. Therefore a woven material is often used that is made from PTFE thread backed by reinforcing threads made from other more robust materials, such as glass fibers.

Bearing design in the USA is usually controlled by the requirements of the AASHTO (American Association of State Highway and Transportation Officials) LRFD Bridge Design Specifications (Section 14.7.2). For sliding bearings, they give values of the friction

coefficient to be used for design. Separate values are given for different types of PTFE, but for the stainless steel only one surface finish, namely a #8 mirror polish, is specified. (That finish is highly polished and was originally developed to create mirrors for circumstances in which glass might be subject to breakage. Hence its name). It has given good service and leads to a low coefficient of friction, but is sensitive to scratches and other surface imperfections, which can be cause for rejection. The polishing process is also time consuming and may lead to difficulties in obtaining the material within reasonable lead times, especially after a last minute rejection.

Interest therefore exists in determining whether other, less highly polished but more readily available, stainless steel finishes might provide adequate performance. A finish known as 2B is widely available, and is a potential alternative. It is produced by cold rolling, using highly polished rollers. No further processing is used, and so the material is relatively economical and readily available. It is widely used in the food-processing industry

The report documents tests performed to determine the friction characteristics of sheet PTFE sliding against three different stainless steel finishes. The three finishes were: #8 mirror polished, 2B rolled, and a rolled stainless steel with a relatively rough surface. The tests were performed in the Structural Engineering Laboratory of the Civil Engineering Department of the University of Washington.

2 Previous Work

Significant research has been done on PTFE-Stainless steel friction interfaces. Papers have discussed many different factors that determine the friction characteristics of these interfaces, including the PTFE itself. In addition to plain (unfilled) PTFE, several other materials which use PTFE have been studied. Jordain T. Rheault, (1992) focused on the behavior of different types of PTFE (dimpled-lubricated, woven, unfilled, 15% and 25% glass filled). Lubricated PTFE has much lower friction, but is vulnerable to contamination (Campbell and Manning 1993). Woven PTFE can be draped over compound curves, such as spherical bearings. For this material, static friction is closer to sliding friction. Fiber glass impregnated PTFE is used when wear and creep are a concern, or to allow higher contact pressure, but also has higher friction (Rheault, 1992).

2.1 Parameters that affect friction in PTFE-SS interfaces

Campbell and Kong (1989) identified the following 14 parameters as influencing the friction coefficient:

- Type of PTFE
- Dimpling and lubrication
- Specimen size
- Attachment of the PTFE to the backing plate
- Roughness of the mating surface
- Contact pressure
- Eccentric loading
- Speed of travel
- Length of the travel path
- Load and travel history
- Surface contamination
- Wear
- Creep
- Temperature

2.1.1 Stainless steel finish:

The coefficient of friction is generally believed to increase with increasing surface roughness. Surface rougness is measured with a profilometer. Several scales are used. The

most common is R_a, the arithmetic average of absolute distance from the mean. Campbell and Kong tested PTFE-SS interfaces with SS surface roughness of 1.18 and 13.4 μin R_a. These finishes are slightly smoother than #8 mirror polish, and slightly rougher than 2B rolled finish, respectively. These tests were conducted using lubricated PTFE

2.1.2 Contact Pressure:

The *coefficient* of friction decreases with higher contact pressure. That is, doubling the load on an interface will yield a less than double increase in friction *force*. This is why drag racers, whose success depends on getting as much friction force out of their tires as possible, use very large, slick tires, and inflate them only enough to hold up the car. NCHRP Report 432, High-Load Multi-Rotational Bridge Bearings (Stanton et al. 1999) describes the results from extensive testing of #8 mirror polished SS-PTFE interfaces at contact pressures from 500 to 6000 psi. The report proposed that CoF is approximated as decreasing linearly with increasing contact pressure below 3000 psi, and being constant at higher pressure The tabulated friction values published in AASHTO Bridge Design Specification, (18.1.5.2.6 2009) come from this report.

2.1.3 Eccentric loading

An eccentric load causes variations in contact pressure over the surface, which can cause changes in friction coefficient. Since higher pressures produce less change in CoF than lower pressures, eccentricities tend to mean that friction is increased. Local high pressure also causes increased wear. Dimples in PTFE may be damaged by increased pressure, or the PTFE may be squeezed out of position.

2.1.4 Sliding speed:

Coefficient of friction increases with sliding speed, but approaches a constant value (Campbell and Kong 1989), (Stanton et al. 1999), (Constantinou 1999). The speed at which it reaches a constant value differs for different materials and surface finishes. For conventional unfilled PTFE, and #8 mirror polish SS, that critical speed is much higher than any speed likely to occur in practice. High speed sliding is of interest primarily in seismic isolation systems.

2.1.5 Grit, water, or other contaminants

Contamination of the sliding surface increases the CoF. This is especially true for lubricated PTFE, as the lubrication stops working when contaminated. Campbell and Manning (1993) introduced contamination to dry and lubricated unfilled PTFE in the form of portland cement powder. They found that, though contamination can be introduced before the bearing is put together, it is difficult to introduce contamination once the bearing is in service.

2.1.6 Slide-path:

CoF changes with travel path length. The first few cycles see dramatically decreasing CoF, especially static friction during reversals. Subsequently, CoF may increase slowly with greater travel path, as is the case for #8 mirror polish SS mating surfaces. This is believed to be caused by transfer of PTFE to the mating surface, which causes the interface to mimic a PTFE-PTFE interface, which has a higher CoF.

2.1.7 Breakaway friction

CoF is significantly higher under static conditions than dynamic, such that reversals of motion during cyclic action cause peaks in friction force.

2.1.8 Creep of the PTFE

PTFE exhibits creep behavior under large sustained loads, but normal conditions in bridge bearings will not cause sufficient creep to affect performance. The most common manifestation of creep occurs when high local pressure causes the PTFE to flow out of the recess that is meant to contain it.

2.1.9 Temperature:

The coefficient of friction is not affected at moderate temperatures, but increases with decreasing temperature below 32°F. (Campbell and Kong 1989), Also, low temperatures cause increased wear (Stanton et al. 1999). Constantinou, et al. (1999) introduced property modification factors to allow for the many ways in which PTFE-SS interfaces may perform worse than is documented, including contamination of the interface, long travel paths, and low temperatures. The factor for low temperatures ranges from 1.0 at 20°C to 2.0 at -50°C

3 Experimental Methods

A series of experiments was performed to determine the effects of stainless steel surface finish on friction coefficient. Friction associated with a 2B rolled finish was of greatest interest, so the experiments focused on comparing the behavior of a 2B rolled finish with that of a conventional #8 mirror polished stainless steel. A third material (a relatively rough, hot rolled plate) was originally provided. It was tested as well to provide a broad range of data, even though it is unlikely to be chosen in practice.

3.1 Tests Performed

Eighteen specimen pairs were tested in all. Each specimen was subjected to a series of tests, at different sliding speeds. The same test program was applied to all specimens[1]. The tests were distinguished by the following features:

- Stainless steel surface finish (#8 mirror polished, 2B rolled, and rough rolled).
- Contact pressure (1500, 3000, 4500 psi).
- Sliding speed for long slide-path test (2.5, 3.84, or 10 in/min)
- Cyclic displacement amplitude during long slide path test (±0.05", ±0.25", or ±1")

The stainless steel surface finishes were chosen because:

- #8 mirror polish is the conventionally used surface finish (AASHTO 2009, Campbell and Kong 1989, Constantinou 1999, Stanton et al 1999) so was needed to correlate the data from this study with the findings of other research.
- 2B rolled finish is a possible alternative to mirror that is inexpensive and readily available.
- Rough rolled plates were sent by mistake, but were tested to investigate the effects of a very rough surface finish.

[1] Except R1.45, which was the first specimen tested. This is explained in 3.5.1

The contact pressures were chosen to reflect practice. WisDOT supplied several plans for bridges which use PTFE-SS bearings (WisDOT structures B42-111, B20-168, B51-113). The bearings are sized such that the contact pressure under service loading (dead and live) would be about 1500 psi. Contact pressures up to 4500 psi are allowed by AASHTO. Eccentricities and non-uniform girder loading can cause contact pressures larger than planned.

NHCRP 432 (Stanton et al 1999) used a sliding speed of 2.5 in/min, and AASHTO 18.1.5.2.6 (LRFD Bridge Construction Specifications 2009) uses this speed in the criteria for the testing of bearings, and so it was chosen as a starting point. Other sliding speeds were chosen in the range of thermal movements and traffic vibrations. Thermal movements occur at very slow speeds: a 100' bridge (with a coefficient of thermal expansion of ~5.5E-6 in/in/°F) warming by 100°F will change length by 0.66 inches over the course of 12 hours, or about 0.001 in/min. Tests conducted at this speed would take too long, so a minimum speed of 0.08 in/min was chosen for expedience. The highest speed (at least in the standard tests) of 3.84 in/min was taken from an example bridge calculation done to reflect traffic loading. Unfortunately, it was later found to be slower than the true value. The 10 in/min speed, used in one special test at the end of the program, was chosen so that a very large slide-path could be applied over the course of a few days, as well as to better reflect motion due to traffic vibrations.

Displacements were chosen to relate to AASHTO 18.1.5.2.6 (LRFD Bridge Construction Specifications 2009), which specifies a displacement of ±1.0" for testing. The amplitude ±0.05" was chosen to study the effects of very small, frequent displacements that might occur because of traffic vibrations, and ±0.25" was chosen as an intermediate value.

3.2 Test Specimens

3.2.1 PTFE and carrier

Each PTFE sample consisted of a 3" diameter, 1/8" thick circular piece of PTFE, recessed into a 0.813"x5"x7" carbon steel plate. The plates were surface ground to minimize any irregularities of thickness and to facilitate the measurement of PTFE loss. The circular recess was machined to accept the PTFE discs, which were cut with an

abrasive water jet machine. The PTFE discs were then bonded into their recesses with Caseway B-500 Etched Teflon Adhesive. The bottom surface of the PTFE had been etched by the supplier. A schematic drawing of a typical specimen is shown in Figure 3-1. Assembled specimens are shown in Figure 3-2 and Figure 3-4.

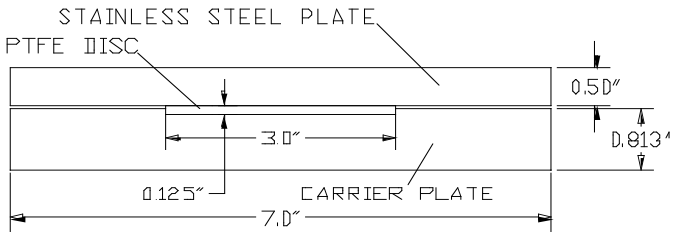

Figure 3-1. Specimen set: PTFE carrier, PTFE disc, and stainless steel plate.

3.2.2 Stainless Steel

The stainless steel specimens were 5"x7", and most were supplied as 0.5" thick plate. Three finishes of stainless steel were used. #8 mirror polished finish is the currently specified finish for PTFE-SS bearings, so was necessary for comparison and to validate the results of this study. It is produced by surface grinding with progressively finer grinding and buffing wheels. Figure 3-2 shows an example of the mirror polish plates and their corresponding PTFE specimens.

Figure 3-2. Mirror specimen before test (M1.45.250.100)

2B rolled finish is an economical, readily available finish which does not require polishing. It is produced by running the material through a set of highly polished rollers. The samples provided were thin sheets (approximately 11 gage), and so were spot welded to

½" backing plates. These welds lie outside of the travel path, and the contact area was protected during welding. Figure shows an example of a 2B rolled plate.

Figure 3-3. 2B stainless steel plate before testing.

Rough rolled finish is a common finish for SS plate, known as No. 1 finish, that was sent by mistake, but provided interesting information about rougher finishes. It is produced by hot rolling, followed by annealing, pickling, and passivation to remove mill-scale and prevent corrosion. Figure 3-4 shows an example of the rough rolled plates and their corresponding PTFE specimens.

Figure 3-4. Rough specimen before testing (R1.30.250.100)

The surface roughness of each plate was measured using a digital profilometer. The results are shown in Table 3-1:

Table 3-1. Profilometer results for the three finishes of SS used.

Finish	**Average Surface Roughness (μin Ra)**
#8 mirror polish	4 (stdev = 0.8)
2B rolled	6.5 (stdev = 1.2)
Rough rolled	190 (stdev = 20)

3.3 Naming Convention and Test Matrix.

The tests were named according to their surface finishes and the tests performed on them. The names consist of the following terms, separated by periods:

- Finish & Batch – **M** for #8 **m**irror polish, **R** for **r**ough or as-rolled, **B** for 2**B** rolled; The first batch was the set of mirror and rough plates provided at the beginning of testing. The second batch was all of the 2B rolled plates, purchased from a Wisconsin materials supplier.
- Contact pressure – the bearing pressure on the PTFE interface in psi/100.
- Sliding speed – sliding speed during the long slide-path test in in/min x100.
- Displacement – one-way displacement during the long slide-path test in inches x100

For example, the first specimen tested, a **r**ough rolled interface from the Batch **1**, which was subjected to **4500** psi contact pressure and a long slide-path test at **2.5** inches per minute and ±**1.0**" cyclic displacement amplitude is called R1.45.250.100. A matrix of the tests and their names is shown in Table 3-2.

Table 3-2. Test Matrix

Sliding Speed:	2.5 ipm			3.84 ipm	10 ipm
Pressure:	4500 psi	3000 psi	1500 psi	1500 psi	1500 psi
#8 Mirror Polished					
±1.0"	M1.45.250.100	M1.30.250.100	M1.15.250.100	•	•
±0.05"	•	•	•	M1.15.384.005	•
2B Rolled					
±1.0"	B2.45.250.100	B2.30.250.100	B2.15.250.100	B2.15.384.100	B2.15.999.100
±0.25"	•	•	B2.15.250.025	B2.15.384.025	•
±0.05"	•	•	B2.15.250.005	B2.15.384.005	B2.15.999.005
Rough Rolled					
±1.0"	R1.45.250.100	R1.30.250.100	R1.15.250.100	•	•
±0.05"	•	•	•	R1.15.384.005	•

3.4 Test Apparatus

3.4.1 Loading Apparatus.

A test rig that had been built for a previous project was adapted for use with the PTFE-stainless steel friction specimens. It is shown schematically in Figure 3-5. It consists of a fixed reaction frame, a set of static rams to provide the normal force across the sliding interface, a servo-controlled actuator that imposes the sliding displacements, and a specimen carrier assembly. The actuator body is attached rigidly to the test frame, with no allowance for pivot or twist. The moving end of the actuator is attached to the moving specimen carrier, shown in detail in Figure 3-5. The PTFE specimens are held by the static plates, which are bolted to the channels which form the uprights of the frame. Hydraulic rams, whose rods pass through the static plates, but run by the moving plates, provide the compressive force on the bearings. They are positioned so that the PTFE specimen is located at the centroid of the compressive force.

.

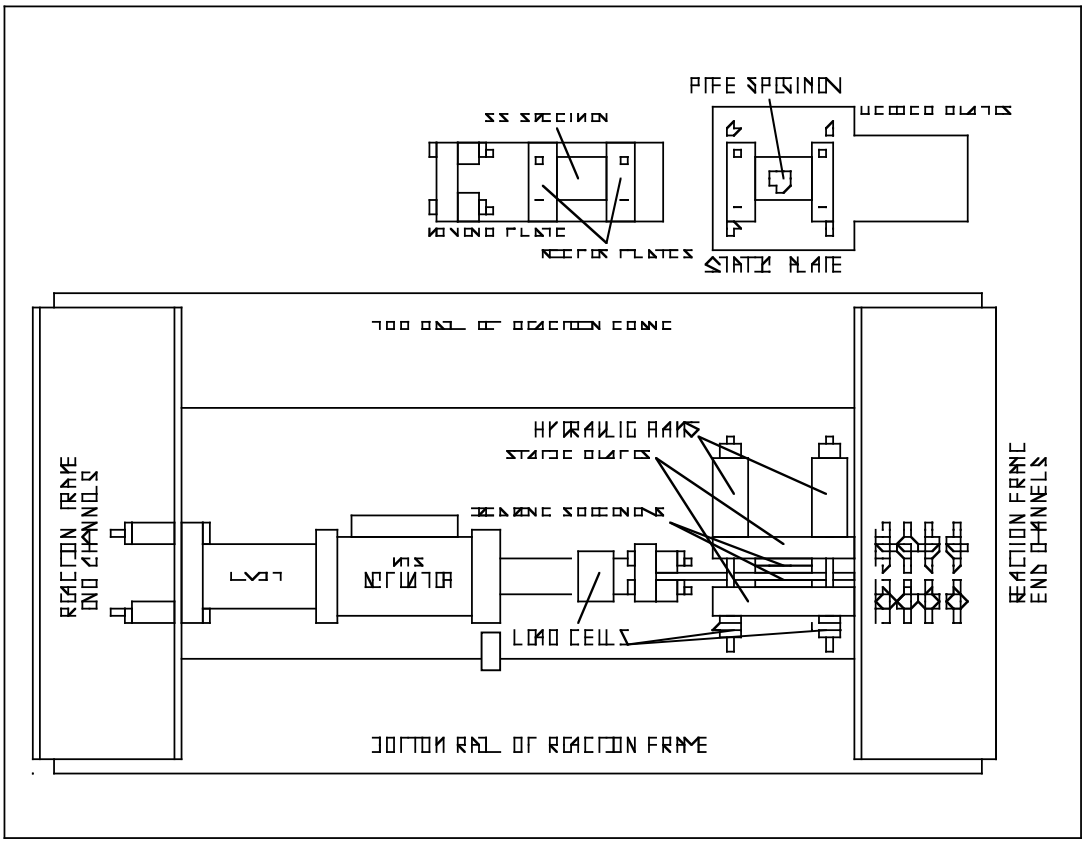

Figure 3-5. Schematic drawing of the testing rig.

The specimens are held in place by ¼" keeper plates, shown in the detail of Figure 3-5. These are bolted to tapped holes in the static plates, or through the moving plate.

Figure 3-6 shows the static plates that hold the PTFE specimens and the four rams that provide the vertical force. The MTS 110k actuator that applied the shear force can be seen on the left.

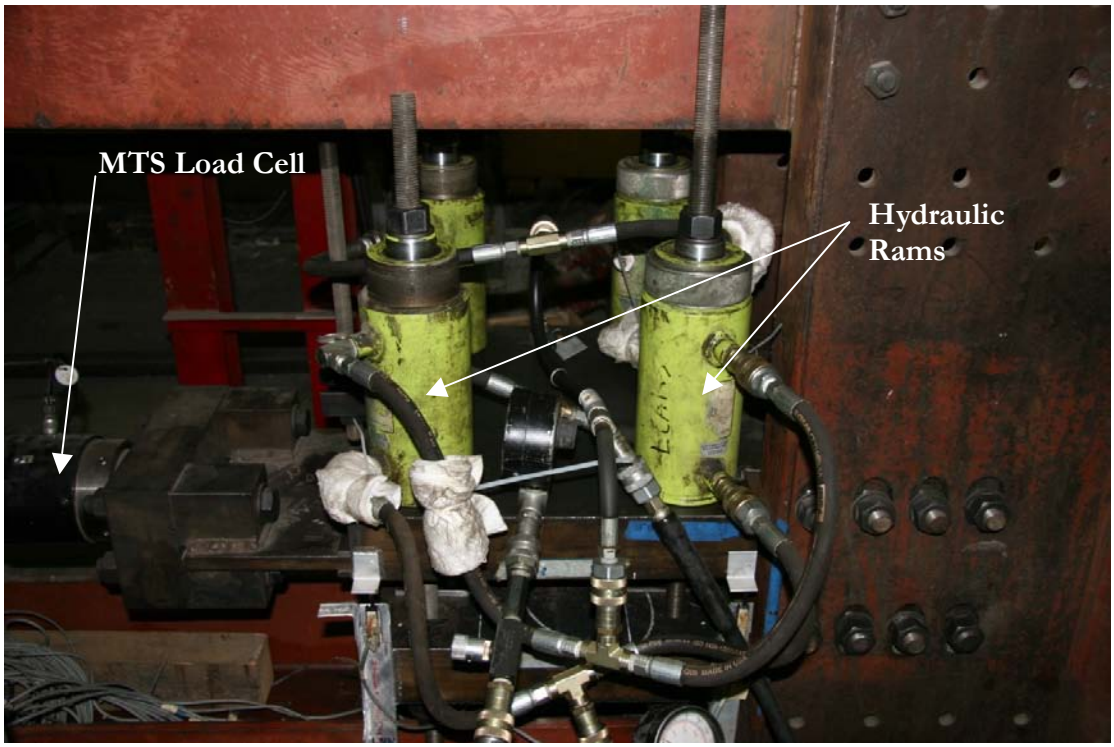

Figure 3-6. Test rig; four vertical rams (center), and horizontal actuator (left).

The four rams were connected via a series of T-connections and a check-valve to a hydraulic pump. This arrangement provided a relatively constant bearing pressure at the two sliding interfaces. Proper alignment and pressure were achieved by first setting the hydraulic pressure in the vertical rams to the desired contact pressure, aligning and bolting down the static plates, then making any final adjustment of the ram pressure.

If there is significant change in the oil pressure in the normal force rams, the static plates would bend slightly, taking some of the force. This would mean that the contact pressure would not be accurately predicted by the oil pressure. If the bolts slip at a small enough force, the oil pressure would again reflect the contact pressure. A brief calculation was performed to determine the change in contact pressure that would cause bolt slip. Based on the torque on the bolts, and the eccentricity of the load, the bolts could withstand a force of 7.8 kips, or a change in contact pressure of 1100 psi at the specimen. Since there were no variations in contact pressure this great, the bolts are predicted not to have slipped. On no occasion were they heard to slip. This means that any difference between

the oil pressure and the contact pressure is taken up in bending of the static plates. An approximate calculation was conducted to determine the relative stiffnesses of the plates in bending (as cantilevers) and the PTFE in compression. The bolted connection was assumed to provide the plates with full fixity against rotation, but the loadpath through the PTFE was found to be 5 times as stiff as that through the plates, so 5/6 of any change in ram force would be transmitted to the PTFE. It is likely that the bolted connection permitted some local flexibility, in which case the proportion of any change in force transmitted through the PTFE would be higher than 5/6.

Because the deformation in the static plates was elastic, the PTFE contact pressure would remain a linear function of the oil pressure in the rams. This is important because later analysis (the correction of CoF data based on variation of pressure, see Section 5.3.1) depends on the oil pressure being related to the PTFE contact pressure by a linear function.

3.4.1 Instrumentation

The compressive and shear loads on the bearings were measured. The compressive load was originally measured using one load cell on each of the four threaded rods (as shown in Figure 3-5). However, the load cells had been designed and fabricated in-house for a previous project, and were found in the first test (R1.45.250.100) to be unreliable. In later tests, hydraulic pressure in the rams was measured using a pressure cell. This provided a much more consistent reading. The load cells remained as a backup.

The shear load was measured using an MTS 110k load cell, model no 661.23E-01, located between the MTS actuator and the specimen carrier assembly.

Displacements were measured using potentiometers. Figure 3-7 shows the locations of the vertical potentiometers. These were intended to record any changes in thickness in the bearings and any tilting due to the loading. Sliding displacements were measured by the LVDT in the MTS actuator. During the first test, R1.45.250.100, in which loads were the highest, the motions of the moving plates and the static plates were measured relative to a common reference (the end channels of the frame to which the static plates are bolted). This was intended to detect any elastic deformation of the rig. The motion of the moving

plate relative to the static plates matched the readings of the LVDT to an RMS error of 8.2E-3 inches during this test. As this was the test with the largest actuator load (high contact pressure, rough rolled, low slide-path), this error was deemed acceptable. The string pots were needed for another test, so were removed.

Later tests were carried out with a cyclic displacement amplitude of ±0.05". For this displacement, and RMS error of 0.0082" would represent 16% of the measured value. Because the displacement amplitude was used in computing the friction coefficient (see Section 4.3), errors in measuring the displacement are important. However, the error of 0.0082" was measured with the highest contact pressure (4500 psi), with the roughest stainless steel, so the forces on the rig, which would cause rig deformation, were at their largest. All of the ±0.05" tests were run at 1500 psi, thus, if friction were independent of pressure, and the same for all surface finishes, the error might be expected to be 16% x 1500psi/4500 psi = 5%. Thus if a friction coefficient was measured to be 5.7%, its true value could be between 0.95 and 1.05 times 5.7%. The error in friction coefficient caused by the displacement measurement is thus likely to be smaller than the inherent scatter in the data.

Figure 3-7. Showing the specimen carriers and pots 4 and 5

The static plates were bolted securely to the frame of the test rig and so were not expected to move appreciably during testing. However, potentiometers were used to detect any unintended movements; in the vertical direction the movements were measured relative to each other, and in the longitudinal direction they were measured relative to the test frame. The maximum measured change during the first test, R1.45.250.100, was 6.3×10^{-4} inches, much smaller than even the smallest cyclic displacement amplitudes. Movement during other tests was likely smaller, as this test saw the largest actuator forces of any test.

3.5 Test Procedure

The test specimens were cleaned, measured and photographed before being loaded into the test rig. The hydraulic rams were then set to the desired contact pressure, compressing the specimen. The thick static plates were aligned parallel to the moving plate and to each other with dial gages. The static plates were then bolted to the reaction frame so that horizontal movements of the bearings would not cause movement of the plates. The

instrumentation and recording was activated, and the servo-controlled horizontal actuator was used to implement the test program. The test was performed over the course of the next 24-72 hours, after which the specimens were removed from the rig, photographed, and measured. Any loose material was brushed off the surface of the PTFE before its thickness was measured

3.5.1 Loading History

The horizontal load was applied under displacement control using a triangular ramp function. This allowed a constant sliding speed throughout the cycle, and a sharp change in direction at the reversal point.

The loading program finally adopted is illustrated in Figure 3-8. It consisted of:

- 20 cycles of "warm-up" movement at 2.5 in/min and ±1.0" displacement.
- A multi-speed test. This consisted of six sets of 3 cyclic displacements in which each set occurred at a different sliding speed, and a displacement of ±1.0". The sliding speeds varied in a geometric progression from 0.08 to 2.5 in/min. The sets were conducted in alternating order to enable the effects of sliding speed to be distinguished from the effects of slide-path, since each test added to the total slide-path experienced by that specimen. This sequence is shown in Table 3-3.
- A long slide-path wear test. 1600 inches of slide-path were applied at a constant sliding speed and displacement amplitude to determine the way in which the friction changed with wear, as characterized by the slide-path.
- A second multi-speed test, identical to the first, to determine the relationship between friction coefficient and sliding speed after the wear test.

Table 3-3. Sequence of sliding speed tests during multi-speed tests.

Test Sequence	Sliding Speed (in/min)
1	2.5
2	0.08
3	1.25
4	0.16
5	0.64
6	0.32

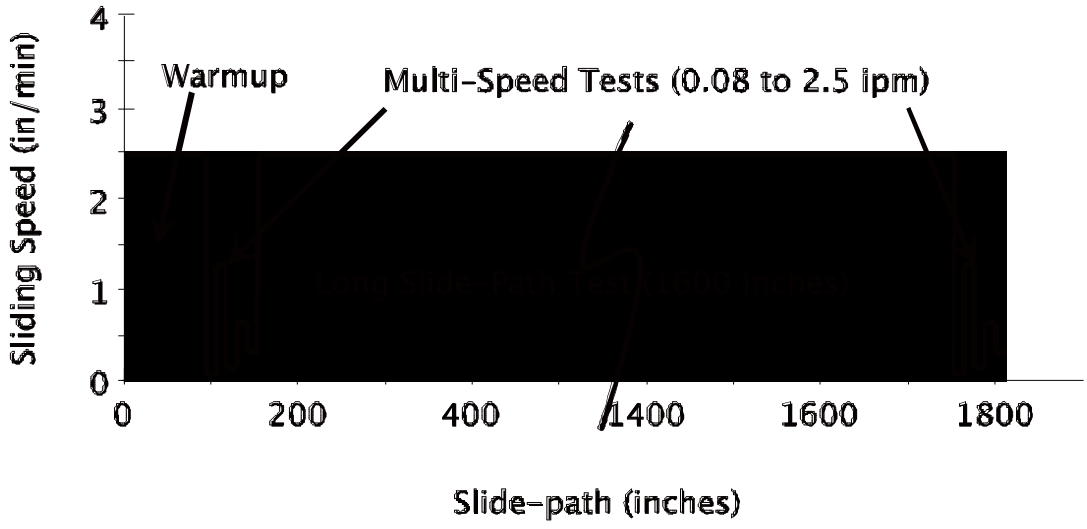

Figure 3-8. Schematic of testing sequence

The warm-up cycles were selected because, especially with the rough stainless steel, the friction changed significantly during the first few cycles. The friction in those first cycles was considered to be less relevant than the subsequent values because:

- Bearings in a real bridge are likely to experience some movement during construction, at which time the full vertical load is not present. During those movements, some PTFE will be transferred to the stainless steel and the friction will change. Even though the friction coefficient may be higher under those circumstances, the friction force, which is the measure of potential damage to the

adjoining elements, is likely not to be critical because the normal force is smaller at that time.

- To conduct a meaningful comparison between different sliding materials, stable friction values are needed. These occur only after a few cycles of displacement have been applied.
- Article 18.1.5.2.6 of the AASHTO Bridge Construction Specification (2009) recommends that the breakaway friction from the sixth through twelfth cycles at 2.5 in/min, ±1.0" displacement should be used for design. The warm-up procedure allows the measurement of these values.

This protocol was followed in nearly all of the tests, with the exception of the first specimen pair, R1.45.250.100. In that test, the warm-up was omitted, and the first of the multi-speed tests was done in descending order of sliding speed, and included an extra speed, 0.04 in/min. The long slide-path test was performed as usual, and then a special large displacement test was performed, to explore the engagement of new, clean stainless steel. For further explanation of test R1.45.250.100, see Section 5.5. After this test, the (rough) plates were flipped over and tested on their opposite sides. A shorter long slide-path test was performed, followed by the speed test as performed in later tests.

In M1.45.250.100, large sideways displacements were detected which affected the friction. The warm-up was extended to study the effect, and then the multi-speed, long slide-path, and second multi-speed tests were performed in the order that they would be in all subsequent tests. The results of the investigation is discussed further in the Appendix A.

Two tests, B2.15.999.100 and B2.15.999.005, were conducted on the 2B material to study the effects of much higher (10 in/min) sliding speeds. After B2.15.999.100 had been subjected to the complete regime of standard tests, an additional 48,000 inches of slide-path were applied. This was done to obtain a better measurement of the rate of wear for the interface.

4 Results

4.1 Observed Results

4.1.1 Temperature

The temperature of the carrier plates at the sliding interface was measured with a laser thermometer pointed at the PTFE carriers from the side. The measurements were made while the test was running, so making contact measurements of the temperature of the PTFE sliding surface itself was not possible.

The temperature at the carrier plates never varied more than 6º F from ambient during any test in which temperature was measured. If any significant heat was generated by the sliding, it was absorbed by the adjoining steel plates.

It was later discovered that changes in the ambient temperature affected the hydraulic pressure in the normal force rams. This is discussed in Section 4.3.

4.1.2 Wear of PTFE

The samples were photographed before and after the test. After the test, the #8 mirror polish plates showed a coating of PTFE, and there were flakes of worn off PTFE around the edges of the PTFE disks. An example is shown in Figure 4-1. The 2B rolled finish plates (Figure 4-2) were visibly polished where they contacted PTFE. Flakes of PTFE were evident on all used 2B specimens. Rough stainless steel plates (Figure 4-3) were found to have been somewhat polished by the PTFE, and the PTFE appeared clean and smooth. Flakes were not seen in the rough specimens.

Figure 4-1. mirror polished specimen after test M1.45.250.100

Figure 4-2. 2B rolled specimen after B2.45.250.100 test

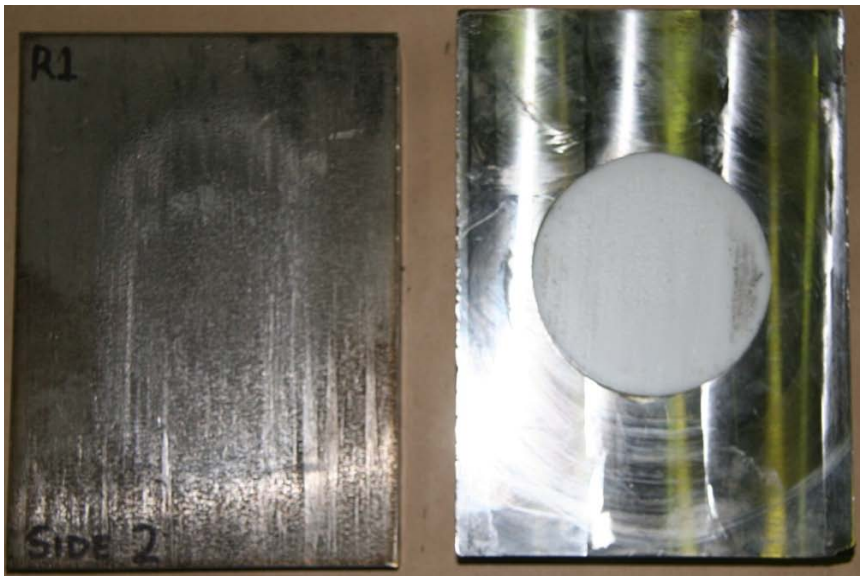

Figure 4-3. Rough rolled specimen after R1.45.250.100 test

Observable wear seemed to correspond to the change in CoF experienced. #8 mirror polished specimens transferred significant amounts of PTFE to the SS surface, and CoF increased during the test. 2B rolled specimens lost some PTFE, and the SS surface appeared polished, but was coated with less PTFE. The CoF rose less than it did for #8 specimens. Lost PTFE was not evident for rough rolled specimens, the SS surface became polished, and no coating of PTFE was visible. CoF decreased for these specimens.

After the tests, the surfaces roughness of rough and 2B rolled specimens was measured, to quantify the degree of polish, if any. The results of this measurement are shown in Table 4-1. At the time these measurements were taken, all the mirror finish plates had been re-used as 2B backing plates, so no data is available for a polish effect on #8 mirror specimens.

Table 4-1. Polishing effect of PTFE Stainless Steel interfaces.

	Before (_in Ra)	**After (_in Ra)**	**Polish Effect**
Rough Rolled:	186.35	160.30833	13.97%
2B Rolled:	5.1125	3.99375	21.88%

4.1.3 PTFE Loss

After the first set of tests (R1.45.250.100 and M1.45.250.100) revealed some unexpected behavior of rough stainless steel interfaces, the thickness of each specimen was measured with a micrometer before and after each test, with the goal of obtaining data on loss of PTFE by wear. Duplicate measurements on any one specimen were found to be repeatable within 2 to 5 thousandths of an inch. Measurements of the loss of PTFE thickness during the testing are given Table 4-2. In all cases the measurements imply some loss of PTFE, presumably through transfer to the stainless steel and flaking off. However, the magnitude of the loss is about the same as the precision of the measurement. Thus, while they indicate that PTFE is being worn away, their usefulness for accurate prediction of long term loss is questionable. Overall, the #8 mirror polish plates suffered PTFE losses similar to those of the rough rolled specimens, and 2B rolled plates suffered very little loss.

The PTFE loss data were collected mostly for tests at 1500 psi contact pressure, so correlation of PTFE loss with contact pressure was not possible.

After the test of B2.15.999.100, the specimens were removed, measured, and re-installed to run for 48000 inches more at 10 in/min and ±1.0" cyclic displacement amplitude. When they were removed, as Table 4-2 shows, they had lost an additional 0.001 inches.

Table 4-2. Measurement of PTFE loss during the tests.

Specimen	PTFE Loss (inches)
M1.15.384.005	0.002
M1.15.250.100	0.006
M1.30.250.100	0.005
B2.15.250.100	0.002
B2.30.250.100	0.000
B2.45.250.100	-0.002
B2.15.250.025	0.001
B2.15.250.005	0.001
B2.15.384.100	0.001
B2.15.384.025	0.000
B2.15.384.005	0.001
B2.15.999.100	0.001
B2.15.999.005	0.005
R1.15.384.005	0.002
R1.15.250.100	0.007
R1.30.250.100	0.009
Mirror Plate Average:	0.004
2B Plate Average:	0.001
Rough Plate Average:	0.006
Extreme Long Path Test:	
B2.15.999.100	0.001

4.2 Recorded Results

The data recorded during the test included:

- The horizontal actuator force and displacement
- The movements of the two static plates in the vertical and longitudinal directions,
- The hydraulic pressure in the rams providing contact pressure (except in tests R1.45 and M1.45, where the force in the rams was measured via load cells on the rods)

Data was collected automatically every 0.5 seconds in most tests. For the slowest tests, this was reduced to once per second. For most of the long slide-path tests, two cycles out of ten were recorded. This section shows examples of the raw data. The processed data are shown and discussed in Chapter 5.

4.2.1 Load-displacement Curves

Figure 4-4 shows some idealized test data. It has the following characteristics: a peak at the "breakaway" point as the bearing begins to slide, and a plateau where friction is constant (and a function of contact pressure and sliding speed). None of the curves generated in this research show such behavior exactly.

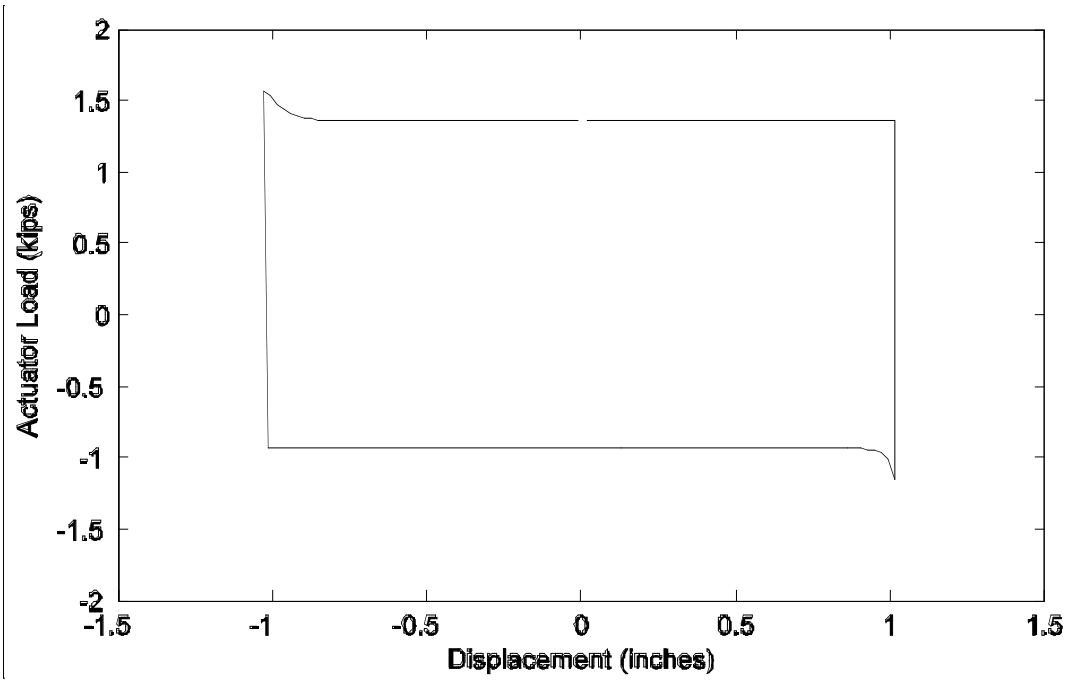

Figure 4-4. Idealized force displacement curve.

Figure 4-5, Figure 4-6, and Figure 4-7 show load-displacement curves that exemplify most of the behaviors observed in the testing.

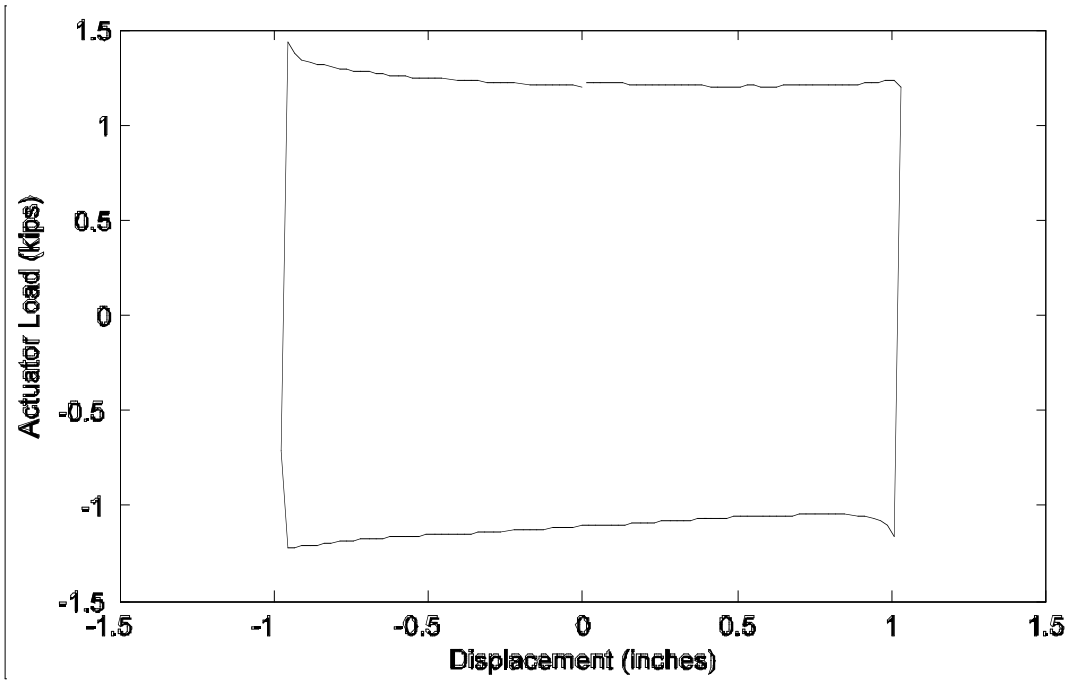

Figure 4-5. Typical load-displacement curve for #8 mirror polish test

Figure 4-5 shows a load-displacement curve recorded during the warm-up to the multi-speed test for Specimen M1.15.250. The sharp peaks at the upper left and lower right show the static friction, or 'stiction', as the actuator reverses direction. The plot shows fairly ideal behavior: small 'stiction' peaks at the beginning of each movement and a fairly constant force thereafter. Note that the figure represents raw data and therefore shows friction force, not friction coefficient. The vertical force varied slightly during each cycle. Thus, when the coefficient of friction was obtained by dividing horizontal force by vertical force, the curves generally became slightly smoother. The variations in friction force are discussed in detail in Appendix A. The load-displacement curve is not exactly symmetric about zero (The positive force is larger in magnitude than the negative force). This occurs because of small offsets in the actuator. The average coefficient of friction during the loop was determined from the loop area, as described in Section 4.3, so it was not affected by this offset.

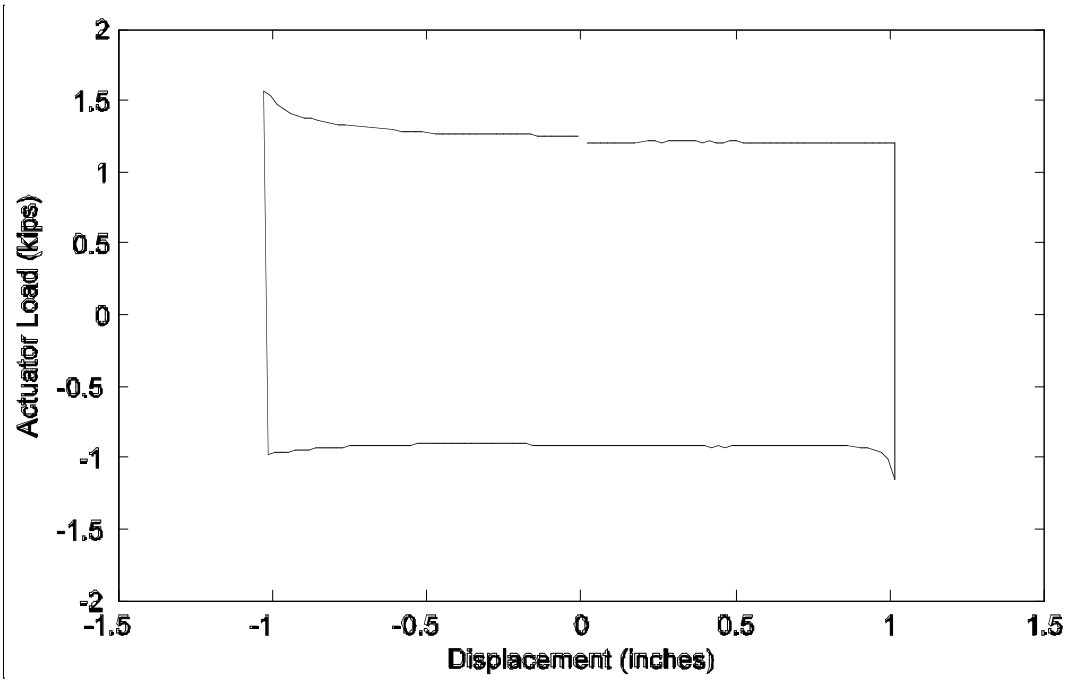

Figure 4-6. Typical load-displacement curve for 2B rolled plate test

Figure 4-6 depicts a load-displacement curve from the warm-up segment of a test on 2B rolled stainless at 1500 PSI. It shows behavior typical of 2B rolled plates: very constant friction during the stroke with a fairly small breakaway peak.

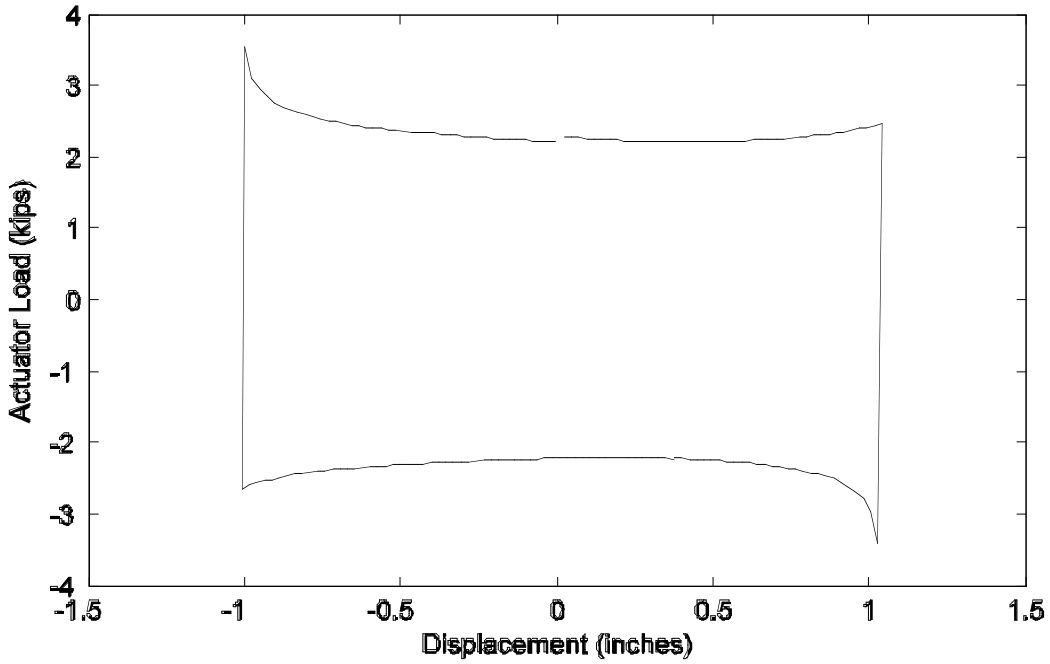

Figure 4-7. Typical load-displacement curve for rough rolled plate test

The load-displacement curve shown in Figure 4-7 was generated by a rough rolled specimen, with 1500 psi contact pressure, and exemplifies the behavior typical of rough rolled interfaces. Instead of a flat plateau, the friction gradually approaches a minimum near the middle of the stroke, then climbs to a small peak just before the reversal point. Some of this effect may also be due to variations in normal force with displacement, which will be corrected in converting the actuator load to coefficient of friction.

A plausible explanation for this behavior is that the CoF of rough stainless steel is very sensitive to slide-path. As shown in Section 5.3.4, the friction coefficient for this steel decreases with slide-path. Every point on the PTFE sample goes through the same slide-path. However, the middle of the plate, which is always in contact with moving PTFE, experiences a longer slide-path than does the edge, and it therefore has the lowest friction coefficient. A short test was done to confirm this hypothesis, in which the specimen R1.45.250.100 was run out to a larger displacement than usual, after the standard series of tests were finished. The trend continued for the larger displacements as predicted, see Section 5.5. Appendix B shows a plot of CoF vs. slide-path for each specimen

4.3 Data Processing

The force-displacement curve for each test was first converted to a curve of coefficient of friction vs. displacement. At each point, the horizontal force was divided by the instantaneous vertical load, which was obtained from a digital pressure gage connected to the four vertical load rams. The result was a value of the instantaneous coefficient of friction at each recording time. Those curves appeared similar, but not identical, to the force-displacement curves because the vertical load varied little during each cycle.

To compare results among specimens, the data were further processed and reduced to a single value of friction for each cycle. This was done by computing the area inside the coefficient of friction vs. displacement loop and dividing by the peak-to-peak displacement. The area was found by numerical integration, using the trapezoidal rule. This procedure results in an average friction coefficient for the conditions of that particular cycle, and allows comparisons with other conditions to be made. Those comparisons are made in Chapter 5.

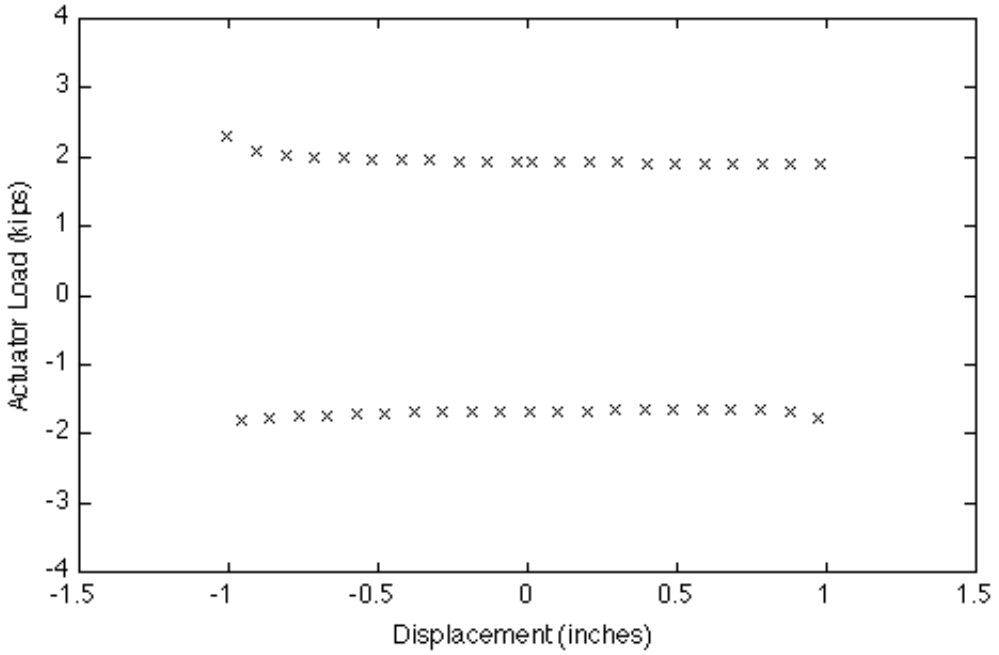

Figure 4-8. Load displacement curve for B2.15.999.100 test showing individual datapoints.

Figure 4-8 shows an example of the individual data points used in analysis. Each of these points represents one reading of actuator force and displacement, as well as hydraulic pressure, pot displacements, etc. The actuator force is first converted to coefficient of friction by dividing by the contact pressure, which is a function of the bearing compression ram pressure. The result is a CoF-displacement curve. To compute the average CoF over the cycle, the area contained by the CoF-displacement curve was divided by the total displacement traveled during one cycle, as measured by the LVDT attached to the MTS actuator (four times the cyclic displacement amplitude). This test was performed at high speed (10 in/min), and so the data-points are somewhat sparse. This resolution is sufficient to calculate the average friction, but the exact breakaway peak is likely not captured. Most tests had much lower speeds, and better resolution of the data.

Some tests could not be analyzed in the standard manner because the sampling rate was insufficient to define the loop well. (This occurred primarily during tests with small displacement amplitudes and high frequency). Figure 4-9 shows an example. The displacement should reach 0.05" on either side, but of the six data points recorded per cycle, the largest had an absolute amplitude of only 0.036".

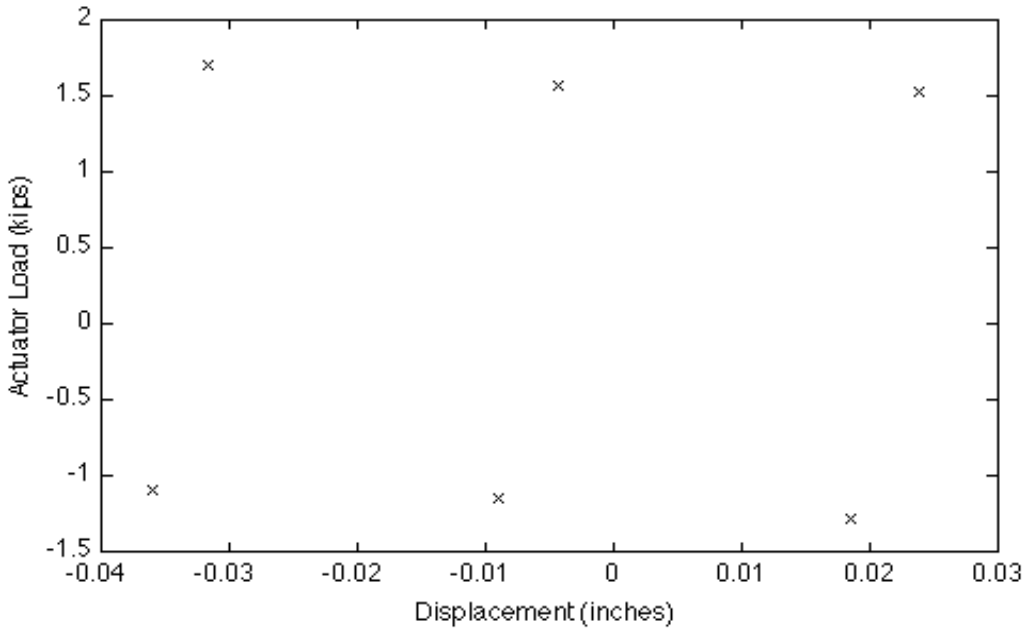

Figure 4-9. Sparse data during the B2.15.384.005 does not adequately represent the cycle.

This data sparsity occurred in tests where the ratio of sliding speed to cyclic displacement amplitude exceeded 10, which included M1.15.384.005, B2.15.384.005, R1.15.384.005, B2.15.250.005, B2.15.384.025, B2.15.999.025 and B2.15.999.005. For these tests, data points from 100 consecutive cycles were sorted by their location on the cyclic path, and treated as one cycle. Figure 4-10 shows an example of this procedure, in which the data from 100 cycles, all distributed randomly but superimposed on the same plot, provide better definition of the loop. The analysis was then completed as usual. The method was verified using borderline cases (where the speed/displacement ratio was between 5 and 10). Both methods produced very similar results. The method is viable if the CoF does not change much over the 100 cycles used to create one composite cycle. Fortunately, the problem occurred only in tests in which the cyclic amplitude was small, which in turn led to very small changes in CoF per cycle.

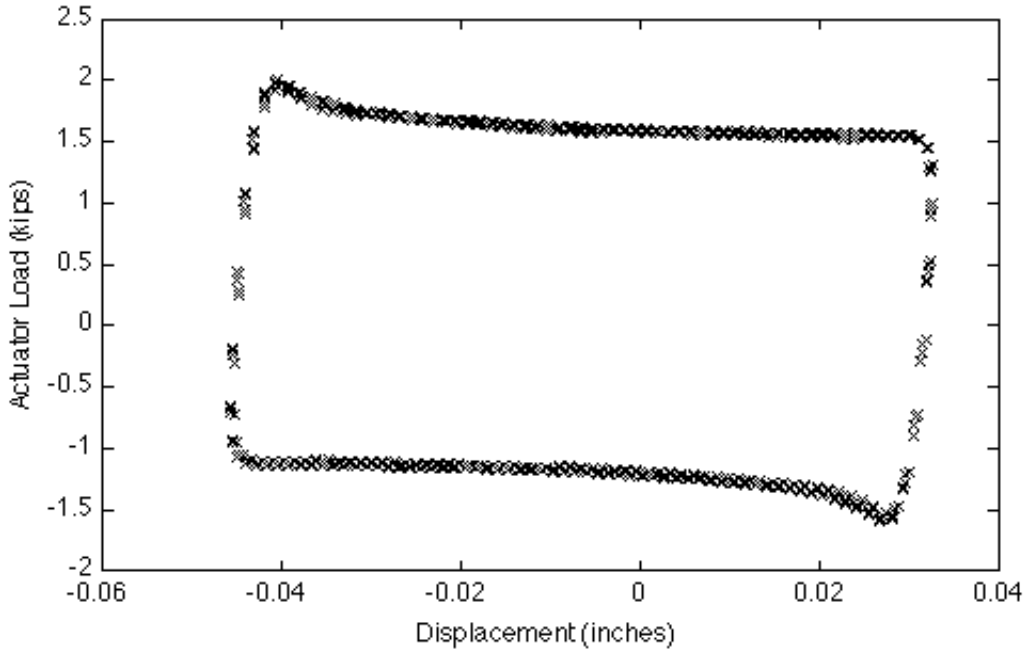

Figure 4-10. Several deficient cycles superimposed reveal a better picture.

The loading and unloading lines on either side of the composite cycle are slightly sloped, which reflects a small amount of elastic deformation of the PTFE. If this deformation is excessive in relation to the displacement of the test, friction would be under-calculated for

small displacement tests. Section 5.3.5 explores this issue in detail. It was found to have a negligible effect on the results.

5 **Analysis & Discussion of Results**

5.1 Introduction

Campbell and Kong (1989) identified the following variables as having an effect on friction coefficient:

- Contact pressure
- Speed of travel
- Roughness of the mating surface
- Length of the travel path
- Dimpling and lubrication
- Eccentric loading
- Temperature
- Creep
- Type of PTFE
- Attachment of the PTFE to the backing plate
- Surface contamination
- Load and travel history
- Specimen size
- Wear

The tests described here were designed to address the first four of these effects (contact pressure, sliding speed, surface finish and slide-path). Because each test conducted on a specimen adds to its cumulative slide-path, there is an inherent difficulty in separating slide-path effects from others. However, this chapter describes the analysis conducted on the data to distinguish the effects of each parameter on the coefficient of friction (CoF). The data were analyzed with the goal of creating an empirical model for CoF based on the four effects tested:

$$CoF = \mu_0 \times f_{(v)} \times g_{(p)} \times h_{(s)} \quad (1)$$

Where:

μ_0 = the basic CoF for one of the three surface finish under reference conditions

$f_{(v)}$ = a function of sliding speed, equal to 1.0 under reference conditions

$g_{(p)}$ = a function of contact pressure, equal to 1.0 under reference conditions

$h_{(s)}$ = a function of slide-path length, equal to 1.0 under reference conditions

Reference conditions are taken as 3000 psi contact pressure, 2.5 in/min sliding speed and zero slide-path. The terms of this equation will be defined as this chapter continues.

Multi-speed test results are described in Section 5.2:

- Section 5.2.1 investigates the effect of speed on the friction coefficient. In all tests, CoF increased with sliding speed.
- Section 5.2.2 investigates the effect of contact pressure on the friction coefficient. In all tests, CoF decreased with an increase in pressure until about 3000 psi. At pressures higher than that, it remained essentially constant.

Long slide-path test results are described in Section 5.3

- Section 5.3.1 explains issues in processing data, and the methods employed in correcting the data.
- Section 5.3.2 investigates the effect of speed on the friction coefficient. As in the multi-speed tests, CoF increased with sliding speed.
- Section 5.3.3 investigates the effect of contact pressure on the friction coefficient. Again, CoF decreased with an increase in pressure until 3000 psi, and was approximately constant at higher pressures.
- Section 5.3.4 investigates the effect of slide-path on friction. In #8 mirror polish specimens, friction increased with slide-path, in rough finish specimens, friction decreased, and in 2B rolled specimens friction increased, but at a rate much lower than that of #8 mirror polish.
- Section 5.3.5 investigates the effect of cyclic displacement amplitude (stroke) on the rate of wear. The rate at which friction increased appeared not to change with different stroke amplitudes.

Warm-up movement results are described in 5.4:

- Effect of slide-path on friction for very small slide-paths.

- Maximum expected breakaway friction.

Results of the extreme cyclic displacement amplitude test are described in 5.5.

Discussion of these results is in section 5.6.

5.2 Short Slide-Path, Multi-Speed, Tests

5.2.1 Effect of Sliding Speed

Previous research shows that higher sliding speeds produce higher friction coefficients (Constantinou et al., 1999). The trend is particularly important for sliding devices used for seismic isolation, although those lie outside the scope of the work reported here. More relevant to this investigation are the different sliding speeds to be expected under thermal and traffic loading. In this section, the results of the multi-speed tests are used to study the effect of sliding speed.

The multi-speed tests were performed in alternating order, with the fastest and slowest tests done first, then the second-fastest and second-slowest, and so on. This order was intended to separate the effects of slide-path from the effects of friction. Figure 5-1 shows artificial CoF vs. sliding speed data. The plot on the left shows how data would look for an interface for which CoF is increasing with slide-path. The plot on the right shows how data would look for an interface for which CoF is decreasing with slide-path.

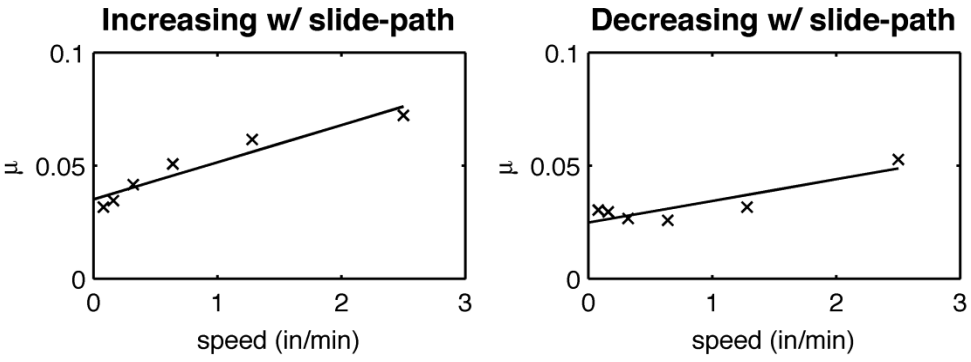

Figure 5-1. Example data showing data increasing or decreasing with slidepath.

In the plots of actual data, there is some evidence of both behaviors, but generally, the CoF remains relatively close to the trendline. The implication is that the sequence of testing in the multi-speed tests was not important after all. It was, however, a predunt precaution.

The coefficients of friction from the multi-speed tests were plotted against sliding speed for each finish of stainless steel in Figure 5-2, Figure 5-3 and Figure 5-4. The plots for before and after the long slide-path test are shown side by side for ease of comparison. In all cases, the friction coefficient used is the average over three cycles.

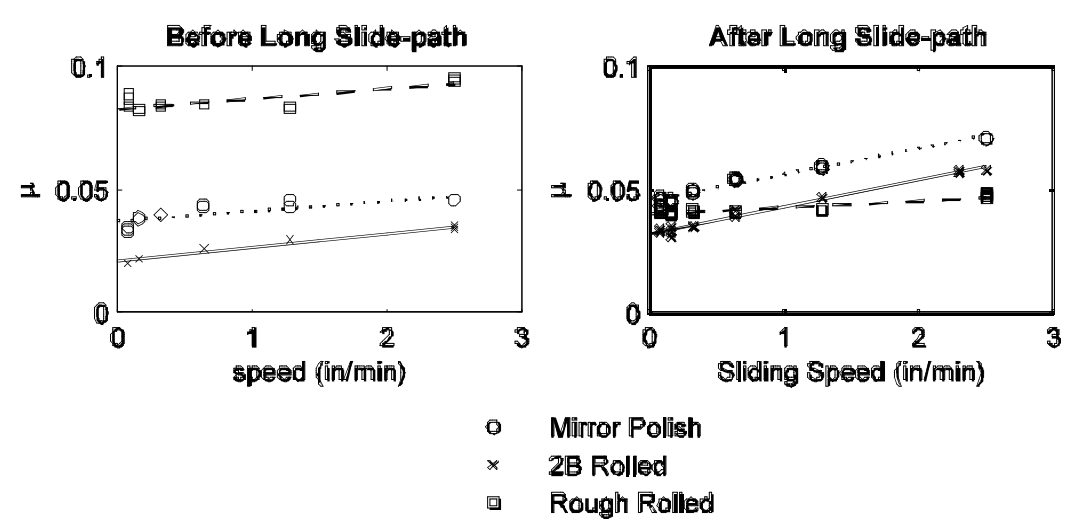

Figure 5-2. Multi-speed test, 1500 psi contact pressure, Long slide-path test at 2.5 in/min, ±1.0" stroke

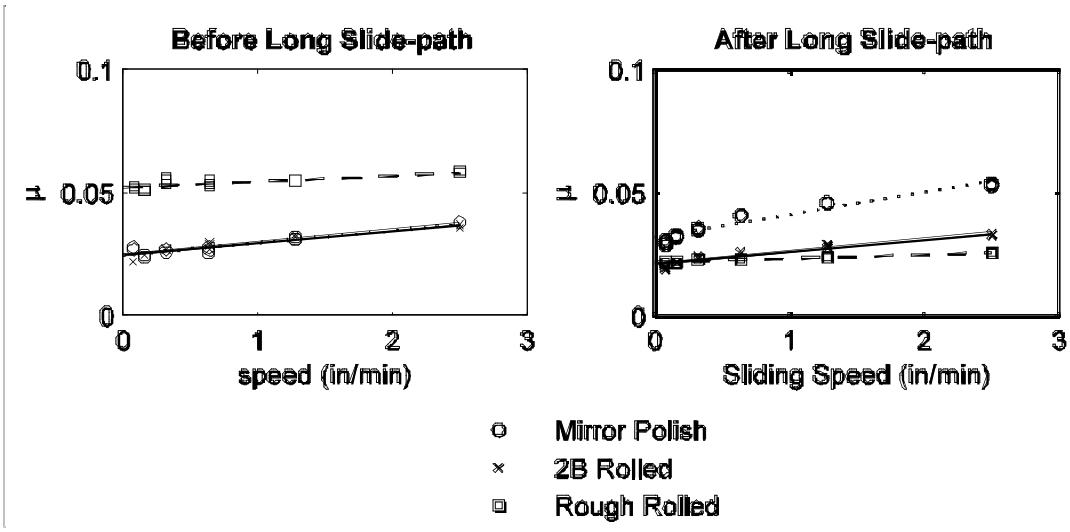

Figure 5-3. Multi-speed test, 3000 psi contact pressure, Long slide-path test at 2.5 in/min, ±1.0" stroke

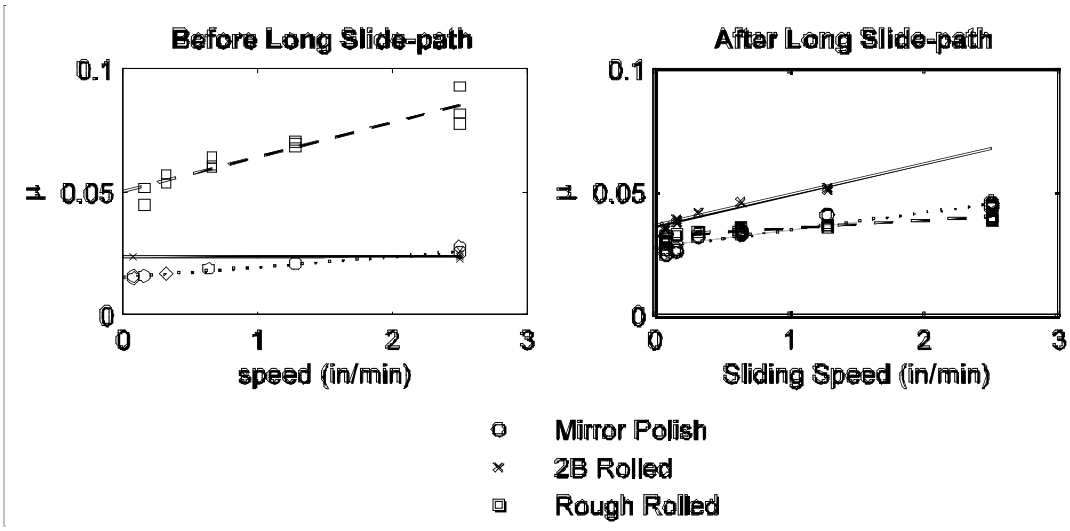

Figure 5-4. Multi-speed test, 4500 psi contact pressure, Long slide-path test at 2.5 in/min, ±1.0" stroke

Several trends are visible from the plots:

- In almost all cases, the CoF increases with sliding speed. The only exception was with the 2B finish at 4500 psi before the long slide-path, when the friction remained constant. However, only a few data points are available from those tests. Contact pressure was found to be unacceptably low for the last several sliding speeds, and those data were thrown out.

- The rough material displayed the highest friction in the tests run before the long slide-path, and among the lowest after the long side-path. This result was unexpected, but it occurred consistently for all rough specimens. Because the tests on different materials were conducted in a somewhat random sequence, the result cannot be a consequence of some unintended change in the test conditions.
- The imposition of a long slide-path loading caused the CoF for #8 mirror polished specimens to rise, while the CoF for rough rolled specimens dropped. The CoF for 2B rolled specimens rose, but less than that of the #8 mirror specimens.
- The 2B material showed a CoF that was in many cases less than that of the #8 mirror polish material.

Figure 5-5, Figure 5-6, and Figure 5-7 show the ratio of 2B CoF to #8 mirror polish CoF. These are useful in determining the suitability of stainless steel with a 2B finish as a substitute for a #8 mirror polished finish at different speeds. They were produced by taking the ratio of the trend-lines, not the data points, because using the individual data points would lead to large scatter in the data. The curves can be thought of as representing the suitability of 2B finish stainless steel as a substitute for #8 mirror polished stainless steel with respect to speed and slidepath. Where the ratio is less than 1.0, 2B steel has superior performance. Where the ratio is larger than 1.0, 2B is inferior.

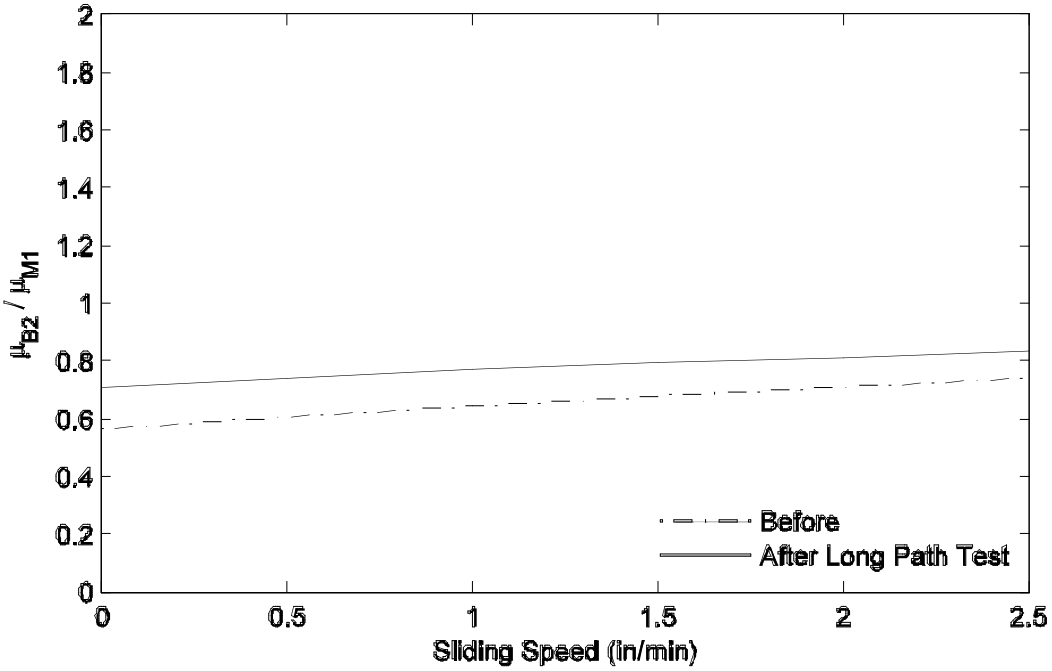

Figure 5-5. Multi-speed test at 1500 psi. Ratio of B2 friction to M1 friction vs. speed before and after the long slide-path test at 2.5in/min and ±1.0" stroke

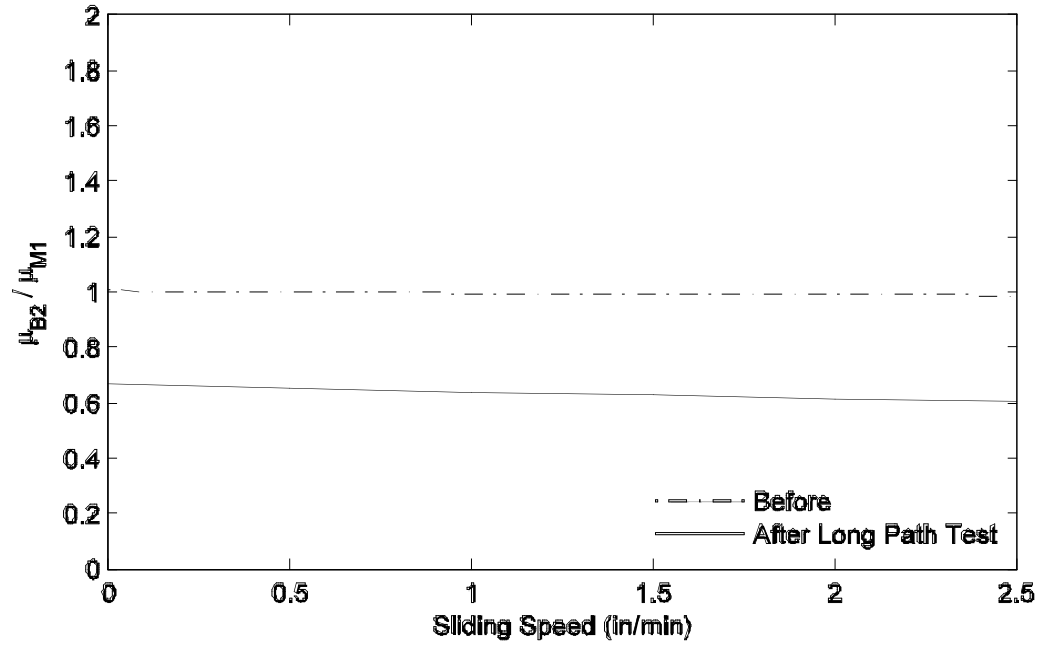

Figure 5-6. Multi-speed test at 3000 psi. Ratio of B2 friction to M1 friction vs. speed before and after the long slide-path test at 2.5in/min and ±1.0" stroke

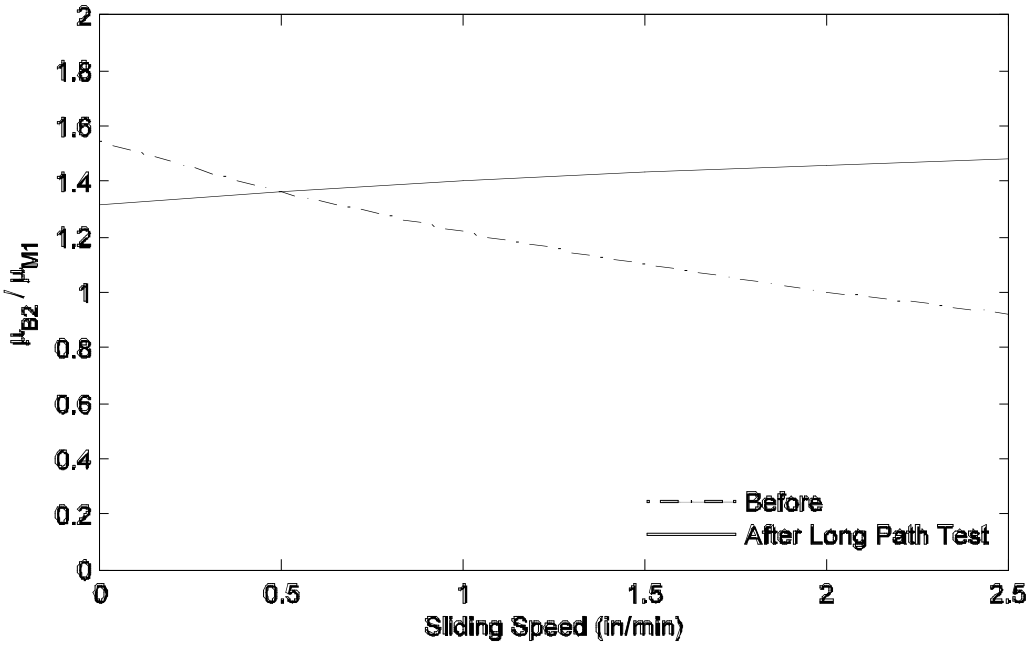

Figure 5-7. Multi-speed test at 4500 psi. Ratio of B2 friction to M1 friction vs. speed before and after the long slide-path test at 2.5in/min and ±1.0" stroke

As can be seen from Figures 5-5 thru 5-7, the CoF for 2B material is lower than that of #8 mirror polished material under all circumstances except a contact pressure of 4500 psi, where 2B rises to about 1.6 times the friction of #8 mirror polished stainless steel.

In order to find an approximate linear function relating CoF to sliding speed for the model in Equation 1, the results of the sliding speed tests from all tests were normalized to the mean of the CoFs from the 2.5 in/min test, so that the factor at the reference condition sliding speed is 1.0. The normalized data are presented in Figure 5-8, along with trend-lines computed for each finish using a linear least squares method.

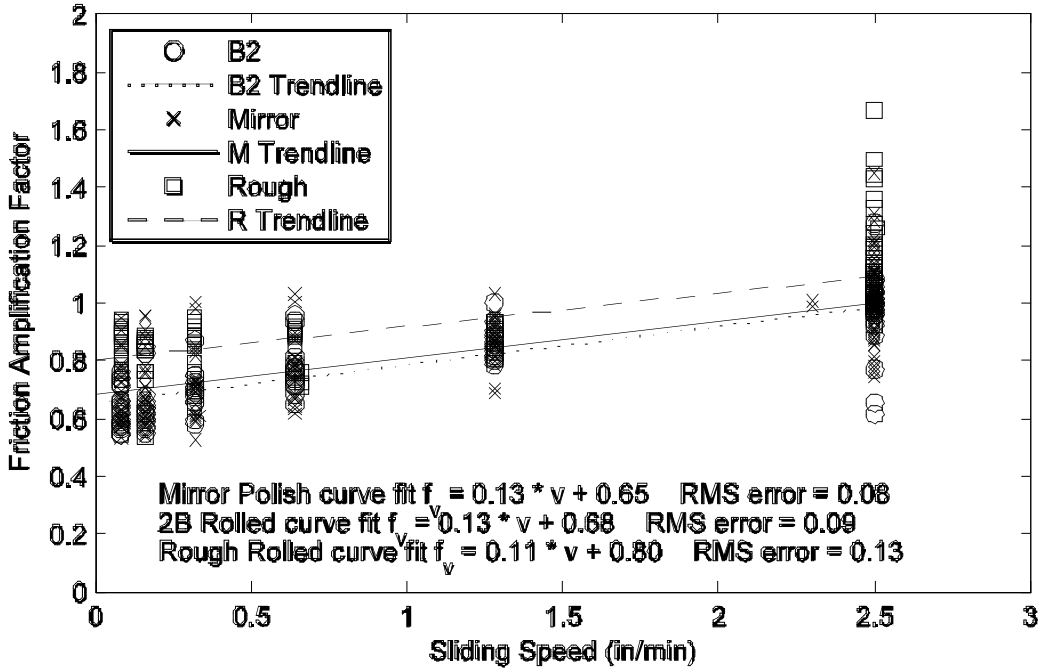

Figure 5-8. All multi-speed tests, before and after a long slide-path test, friction amplification factor normalized to 1 at 2.5in/min for each test.

Figure 5-8 shows that friction amplification factors from all three finishes of stainless steel are about equally sensitive to sliding speed. #8 mirror polished and 2B rolled stainless steel are particularly similar. The function is given by:

$$f_{(v)} = a_v v + b_v \tag{2}$$

Where v is the sliding speed in in/min and the coefficients a_v and b_v are given in Table 5-1.

Table 5-1. Coefficients for the amplification function of sliding speed

	Speed	
	a_v min/in	b_v
Mirror Polish	0.13	0.67
2B Rolled	0.13	0.68
Rough Rolled	0.12	0.71

As can be seen the constants a_v and b_v are nearly the same for all finishes, suggesting that a single pair of constants may provide an adequate representation of the sliding speed sensitivity of all three material pairs.

5.2.2 Effect of Contact Pressure

For each finish and each contact pressure, three points were taken from the multi-speed test at the lowest speed (0.08 in/min) an intermediate speed (0.064 in/min) and the highest speed, (2.5 in/min). Those points were then plotted against the contact pressure. The plots are shown in Figure 5-9, Figure 5-10 and Figure 5-11

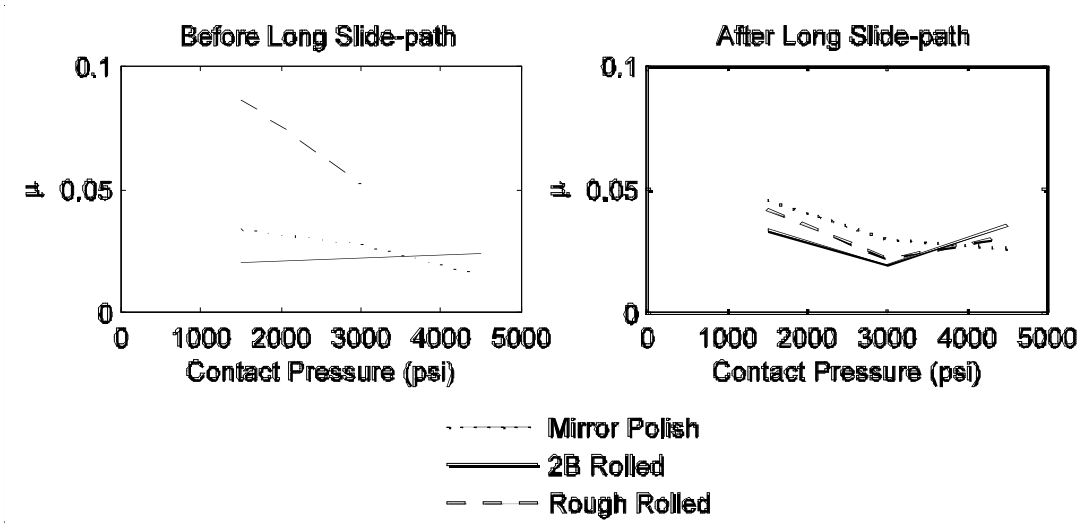

Figure 5-9. CoF vs. contact pressure for 0.08 in/min, before and after long slide-path test at 2.5 in/min and ±1.0" stroke

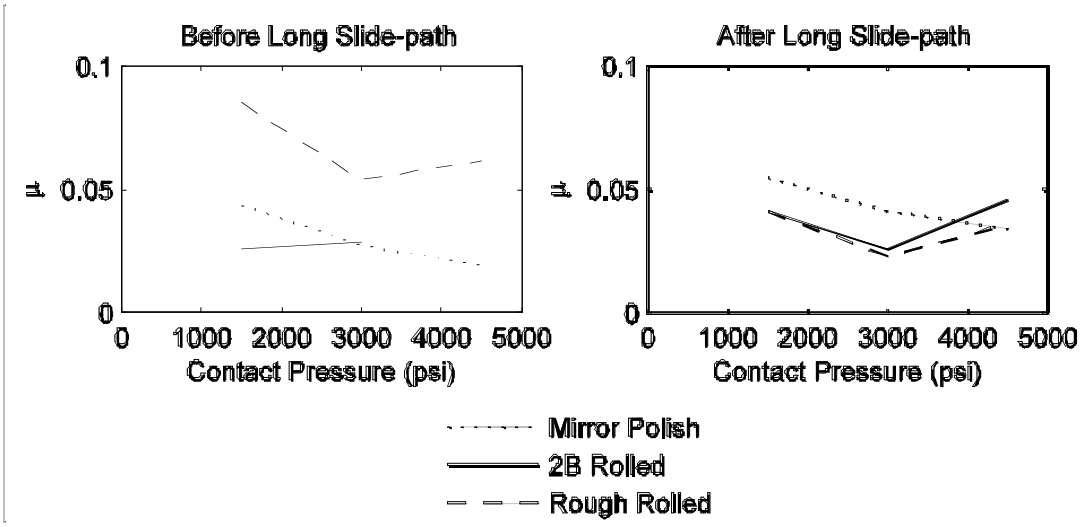

Figure 5-10. CoF vs. contact pressure for 0.64 in/min, before and after long slide-path test at 2.5 in/min and ±1.0" stroke

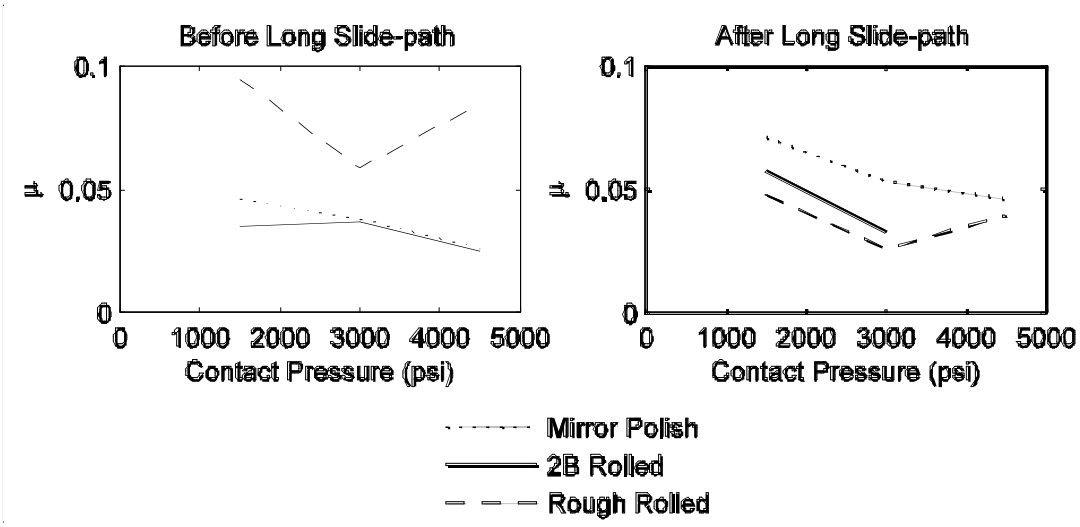

Figure 5-11. CoF vs. contact pressure for 2.5 in/min, before and after long slide-path test at 2.5 in/min and ±1.0" stroke

Figure 5-9, Figure 5-10 and Figure 5-11 show CoF vs. contact pressure at three speeds from the multi-speed tests. The expected behavior is that CoF would be constant between 3000 and 4500 psi, and would increase at lower pressures, and this general trend can be seen in the plots. However, there is too much scatter to make any clear conclusion about the effects of contact pressure from these plots.

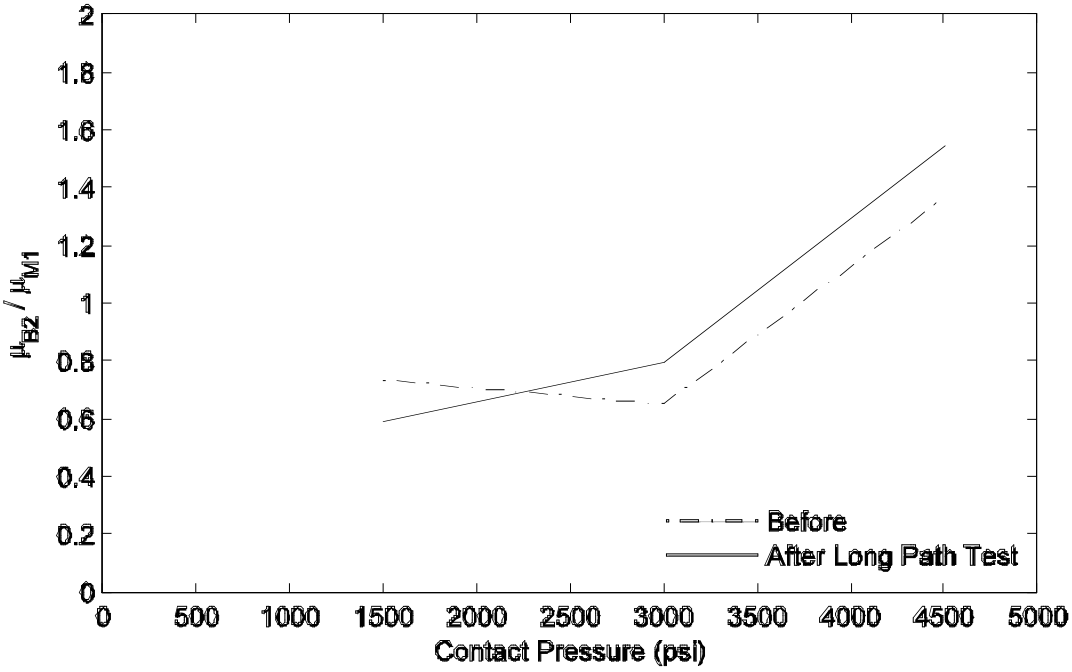

Figure 5-12. Ratio of B2 friction to M1 friction vs. contact pressure before and after the long slide-path test for 0.08 in/min.

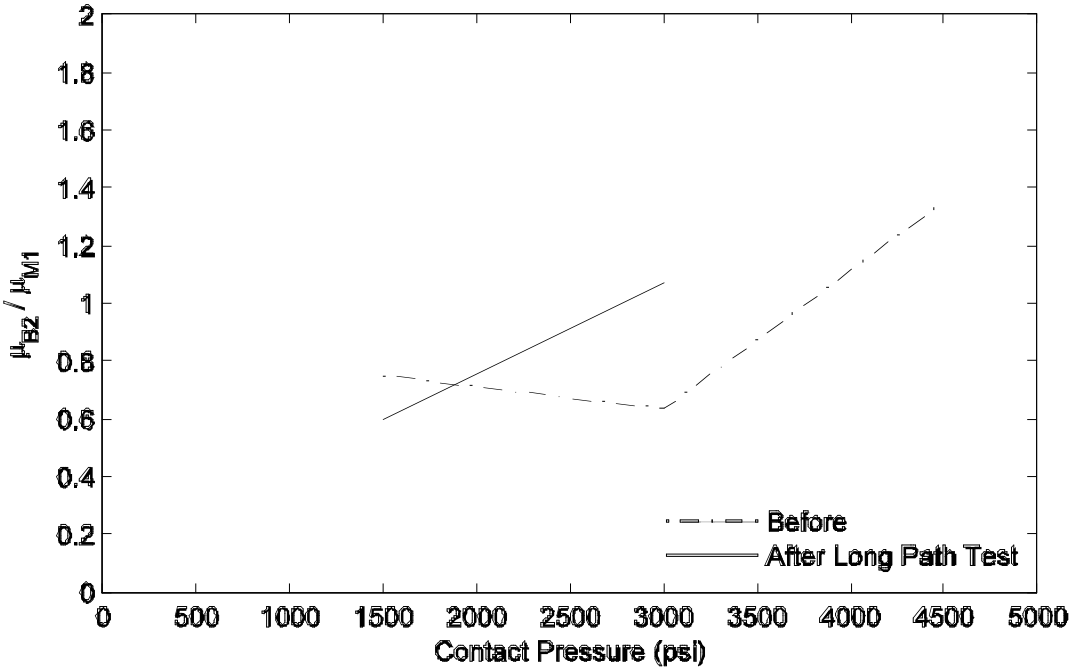

Figure 5-13. Ratio of B2 friction to M1 friction vs. contact pressure before and after the long slide-path test for 0.64 in/min.

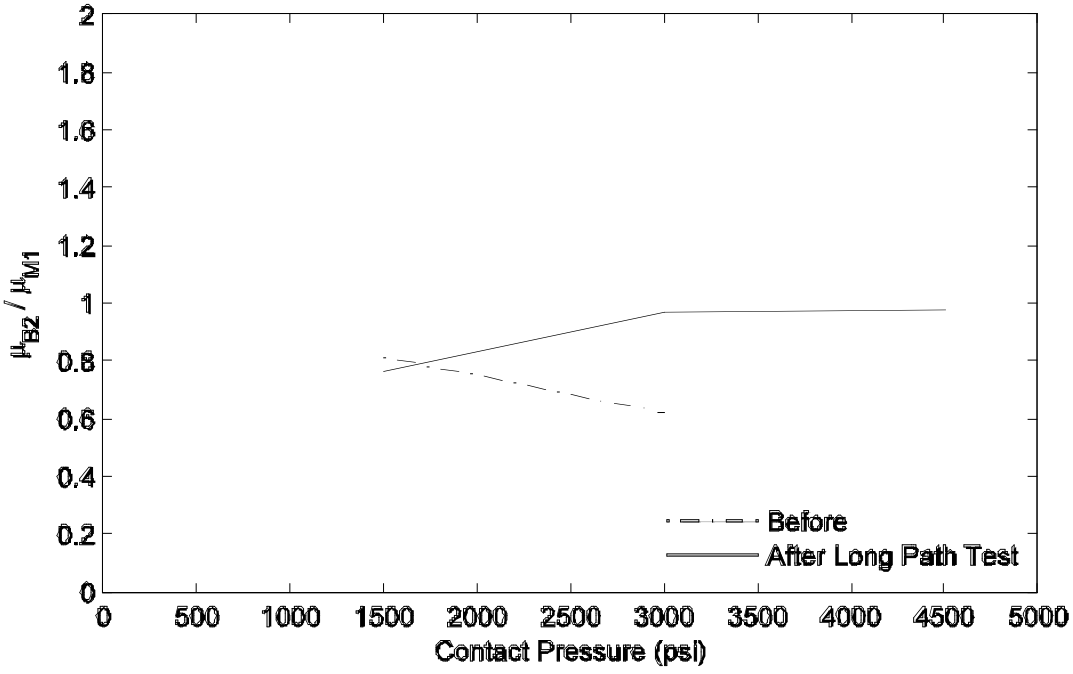

Figure 5-14. Ratio of B2 friction to M1 friction vs. contact pressure before and after the long slide-path test for 2.5 in/min.

Figure 5-12 and Figure 5-14 show the ratio of 2B CoF to Mirror CoF plotted against contact pressure for different speeds. At low pressures, the ratio is less than one, meaning that 2B finish specimens had lower CoFs. At 4500 psi, the CoF for 2B finish was always equal to or higher than that for the mirror polish material.

In Figure 5-12, Figure 5-13, and Figure 5-14, some data points are missing. This is because those data points were found to be spurious due to an accidental pressure drop, and so were omitted (B2.45.250.100, before long slide-path), or escaped recording (due to operator error in B2.45.250.100, after long slide-path). Fortunately, due to the order of the tests, whereby the fastest and slowest tests are completed first, the unaffected data (before the drop in pressure) are usually sufficient to describe the trend. In cases where the first (fastest) cycles were not recorded, there is less certainty, as the next fastest speed was 1.25 in/min, half the speed of the first (2.5 in/min).

5.3 Long Slide-path Tests

5.3.1 Problems with Data and Correction Methods

The resources available for the project did not extend to a servo-controlled hydraulic system for maintaining constant pressure on the normal force rams. Thus a simpler system was used, which resulted in some variation of the normal force during the long slide path tests. It consisted of pumping up the system to the desired pressure, or slightly higher, closing the hydraulic shutoff valves, and re-pumping the system back up to the desired pressure if and when the pressure dropped unacceptably.

The variations in pressure were only detected from the very long slide-path test (2B.15.999.100), which was conducted at the very end of the entire test program. Thus it was assumed that variations had also occurred during the other long-slide-path tests, so all the long slide-path test data was investigated.

If the CoF were independent of contact pressure (which is the common assumption for materials other than polymers), this variation in normal force would be of no consequence. However, because friction between polymers and hard materials, such as stainless steel, is known to be sensitive to contact pressure, an attempt was made to correct the long slide-path data prior to further processing. In the extreme long slide-path test of B2.15.999.100, large, cyclic, fluctuations in CoF were found that showed a negative correlation with the temperature recorded at the nearby Atmospheric Sciences Lab.

Further investigation showed that time variations of the pressure in the normal force rams correlated directly with the temperature. This is shown in Figure 5-15.

It suggested that changes in ambient temperature were causing changes in temperature in the hydraulic system. Because oil has a much higher coefficient of thermal expansion than does steel, heating an isolated ram would cause it to extend. If that extension were restrained (in this case by the threaded rods clamping the specimen carrier assembly together), the pressure in the oil would increase instead of the ram extending. Because, in general, an increase in contact pressure reduces the CoF, higher temperature should be expected to coincide with lower CoF. That is exactly what can be seen in Figure 5-15.

The variations became noticeable only in a test whose duration was longer than one day, which was by definition the period of the daily thermal cycle. The very long slide-path test lasted about 3 days. Most of the "standard" long slide-path tests lasted only about four hours, so the effect in them was smaller and not obvious during the testing. The sudden change in pressure at 2.7 days, visible in Figure 5-15, occurred when the hydraulic system was re-pumped, on the assumption that the low pressure had been caused by oil leaking through the valves.

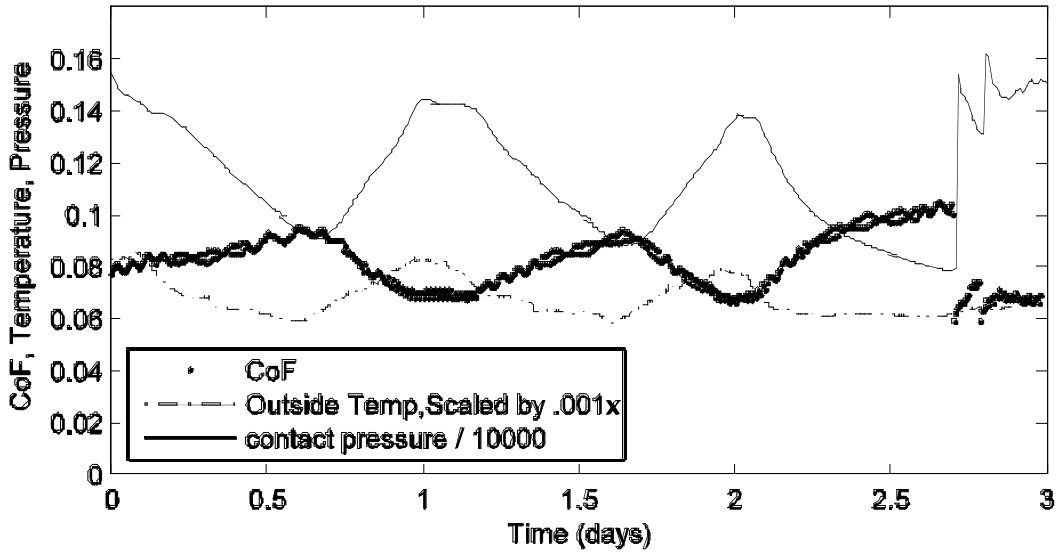

Figure 5-15. Extreme long slide-path test, showing correlation of contact pressure and temperature to friction. Sliding speed was 10.0 in/min, at 1500 psi nominal contact pressure.

The recorded CoF values from Specimen B2.15.999.100 (during the extreme long slide-path test) were compared with the contact pressure using the least squares method. The linear function of pressure, shown in Figure 5-16, correlated well with the recorded data.

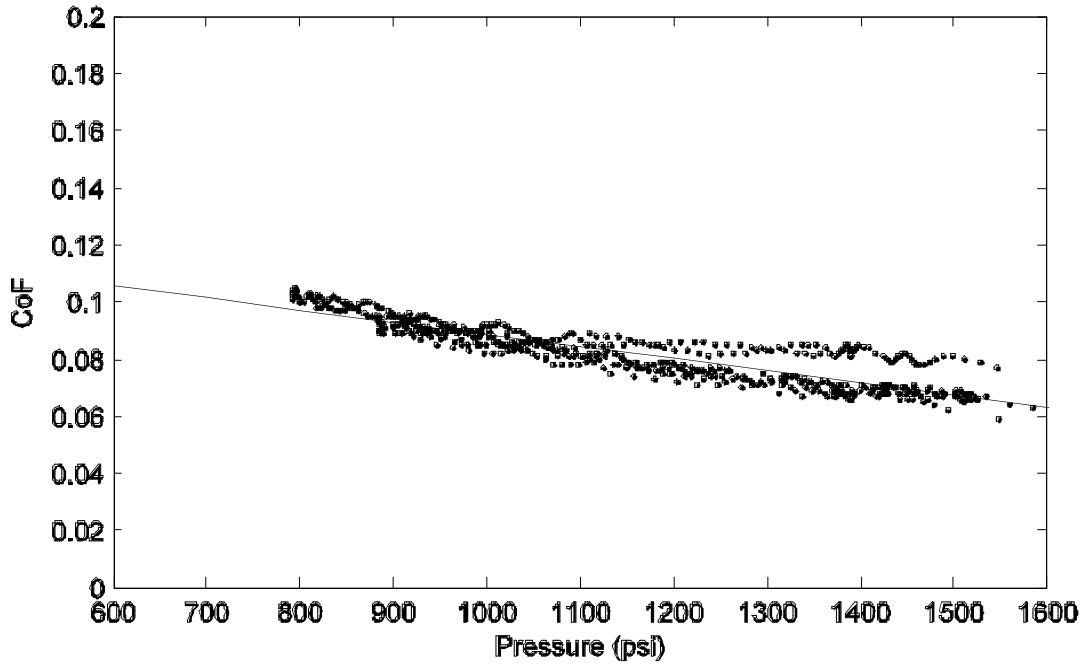

Figure 5-16. CoF and linear function of contact pressure. Sliding speed was 10.0 in/min, at 1500 psi nominal contact pressure.

The correlation of CoF with pressure in this test is much better than in the standard long path tests. In those tests, the slide-path affected the CoF greatly, but in this test, CoF is fairly constant with respect to sliding-path. This is likely because the specimen has already gone through over 1600 inches of slidepath during the standard long slide-path test, so the condition of the interface has stabilized.

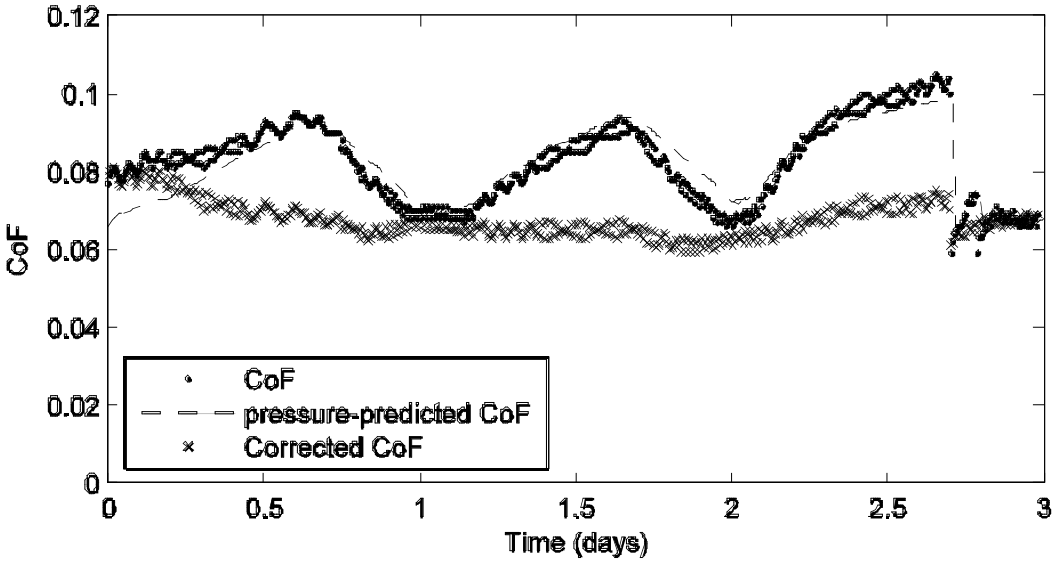

Figure 5-17. Extreme long slide-path test, showing good fit of pressure-predicted CoF, and corrected friction. Sliding speed was 10.0 in/min, at 1500 psi nominal contact pressure.

Figure 5-17 shows the recorded CoF along with the CoF predicted by the linear function of pressure. The remaining error between these must be due to other variables, such as slide-path. To create a curve that represents as closely as possible the one that would have been measured if the pressure had remained constant, the following steps were taken:

- Define the best fit linear relationship between pressure and CoF

  $$\mu_{(p)} = c_1 p + c_2 \quad (3)$$

  Where:

  c_1 = Response of CoF to an increase in contact pressure

  c_2 = friction at hypothetical zero contact pressure

  p = contact pressure

- Create the baseline constant μ curve for the nominal pressure:

  $$\mu_{(t)} = c_1(1500psi) + c_2 \quad (4)$$

  from the least squares fit.

- Add the error term $e_{\mu(t)}$ where:

  $$e_{\mu_{(t)}} = \mu_{meas(t)} - c_1 p_{(t)} + c_2 \quad (5)$$

which accounts for variations in CoF from sources other than contact pressure (PTFE wear, contamination, etc.)

The temperature in the lab was not recorded. However, the lab is a large, enclosed, space in which the temperature varies less than it does outdoors. The friction coefficient between PTFE and stainless steel is known to change with temperature, (Stanton et al. 1999), but it was assumed that the temperature changes of the PTFE were too small to have any direct effect on the CoF, and that the change of pressure was the only important consequence of the changing temperature in all of the tests.

Figure 5-18 shows the variation in CoF with temperature taken from AASHTO's design CoF values for #8 mirror polish stainless steel and unfilled PTFE. If linear interpolation is used between the tabulated data, the variation of temperature in this very long slide path test would cause a change of friction of 0.04. However, the linear interpolation is not likely, since continuing along it would lead to zero friction at about 110°F. A curved interpolation is more likely, with nearly constant CoF after 68°F. This would mean that during the range of temperatures in this test, CoF would not change much.

For this reason, the changes in the CoF were assumed to be attributable to changes in pressure alone, and the technique was applied to all of the long slide-path tests, using a least squares fit of the long slide-path tests done at varying pressures. The data used in this correction is detailed in Section 5.3.3.

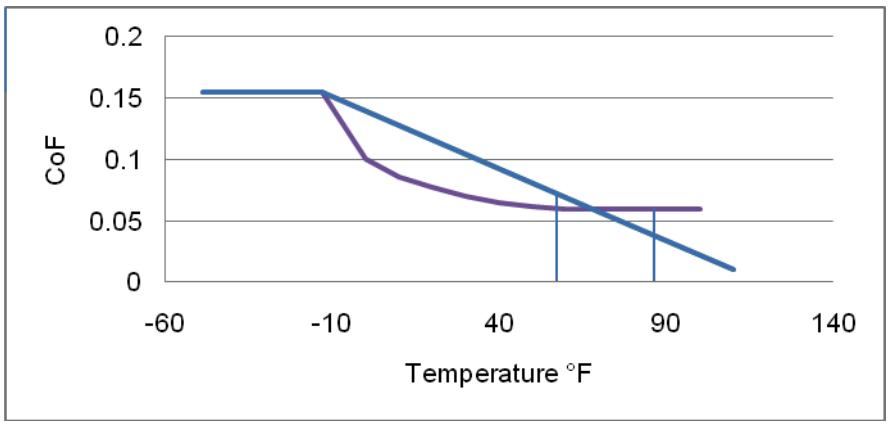

Figure 5-18. AASHTO design CoFs for #8 mirror polish

5.3.2 Effect of Speed

In Section 5.2.1, the effects of sliding speed were investigated using only the multi-speed test data from the short slide-path test. Additional information can be gleaned from the long slide-path tests at different sliding speeds. To provide the best comparison, groups of tests should be used in which the only variable that changes is the sliding speed. Table 3-2 shows that the most extensive comparison is possible with the 2B material, 1500 psi contact pressure and ±1.0 in. amplitude, tested at sliding speeds of 2.5, 3.84 and 10 in/min. Those data are shown in Figure 5-19. Also shown are the data from the short slide-path multi-speed tests, previously shown in Figure 5-2.

A similar comparison, but with cyclic amplitude of ± 0.05 in. instead of ± 1.0 in., is shown in Figure 5-20. As stated earlier, this data has been corrected according to the method shown in Sections 5.3.1 and 5.3.3.

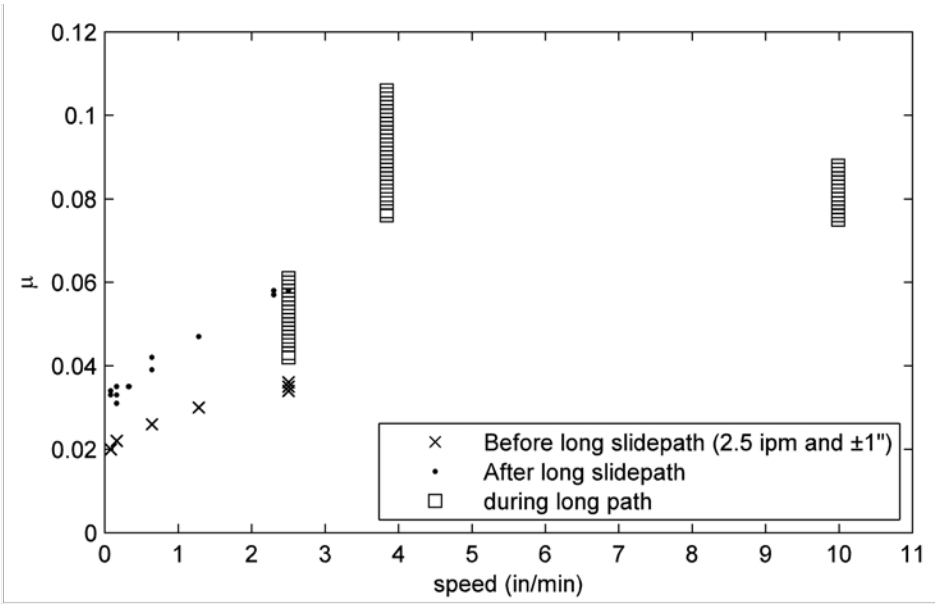

Figure 5-19. CoF for B2 long slide-path tests at ±1.0" and 1500 psi, all speeds, and multi-speed test for B2.15.250.100.

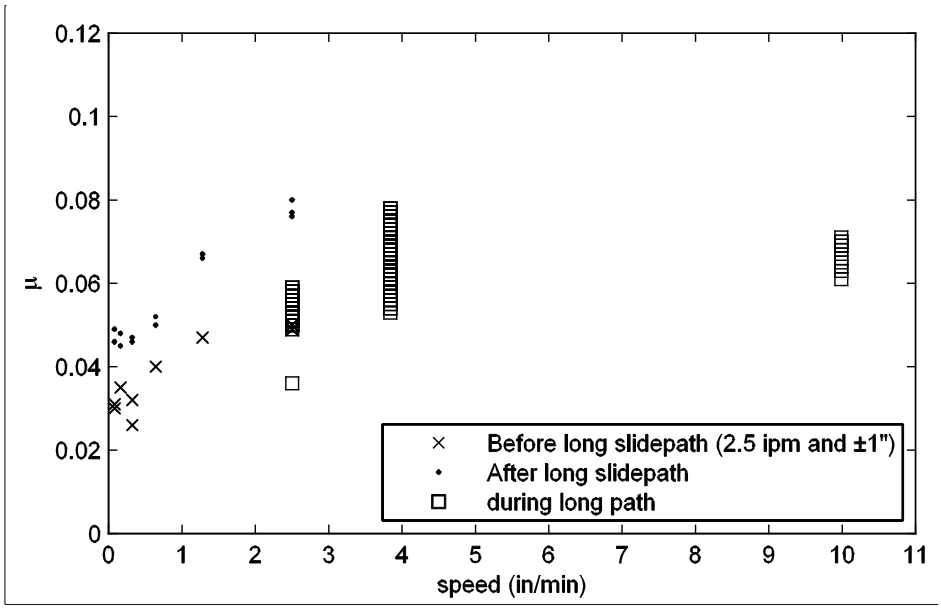

Figure 5-20. CoF for B2 long slide-path tests at ±0.05" and 1500 psi, all speeds.

In Figure 5-19, the data from the long slide-path test matches well with the data from the comparable short slide-path tests, thereby adding credibility to the complete set of measurements.

Constantinou et al. (1999) performed tests at greater speeds than these. In that report, friction was shown to increase from 0.025 to 0.085 between about 0 and 25mm/s (59 in/min) for specimens at 20.7 MPa (3000 psi), in a softening curve. Those numbers demonstrate the same trends as the data measured here, although the very different speed ranges and the higher contact pressure make precise comparison difficult.

CoFs from B2 and M1 long slide-path tests were compared with respect to speed. A ratio of μ_{B2} to μ_{M1} was calculated from the mean CoF during 10 cycles of long path data from the beginning, middle, and end of the test, as well as from the mean CoF over the entire test. This was done for the tests at 2.5 in/min, ±1.0" stroke, and 3.84 in/min, ±.05" stroke. The results are shown in Figure 5-21. The lines on this plot stretch from tests done at 2.5 in/min and ±1.0" amplitude to tests done at 3.84 in/min and ±0.05". No tests were done on #8 mirror polished stainless steel at 3.84 in/min and ±1.0", so a comparison in which all variables other than sliding speed were held constant was not possible.

The data show that in all cases the 2B finish leads to a CoF lower than that for the mirror polish finish. The effects of the change in displacement and sliding speed are not distinguishable, but the data discussed in Section 5.3.5 suggest that cyclic displacement amplitude does not have a significant effect on friction.

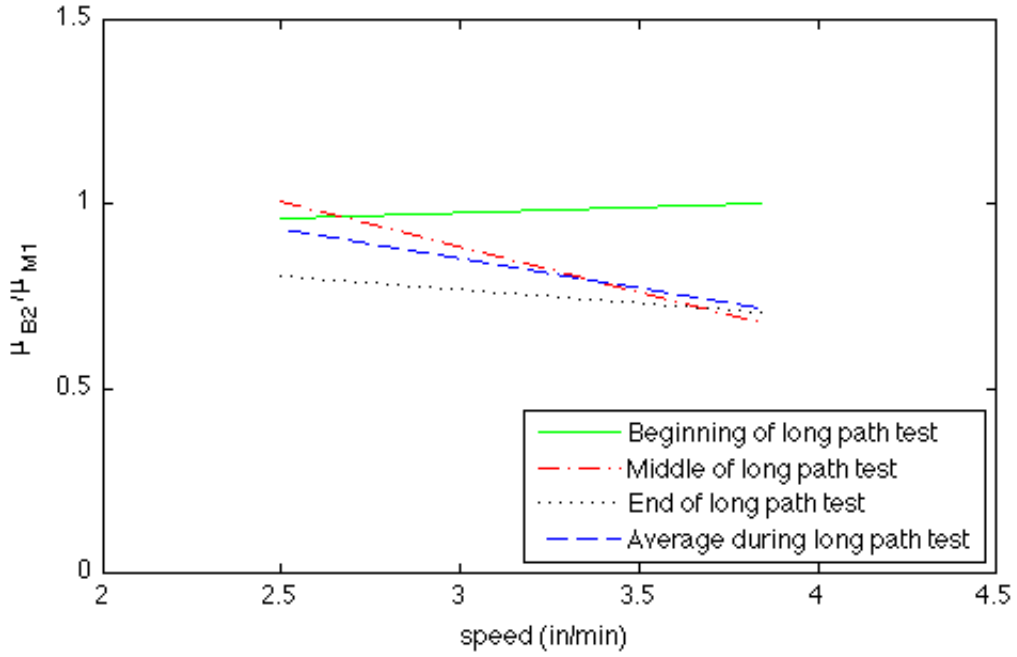

Figure 5-21. Ratio of mu_{B2} to mu_{M1} during long slide-path tests at 2.5in/min, ±1" stroke and 3.84in/min, ±.05" stroke.

Figure 5-21 suggests that higher speeds increase the difference in the rate of change of CoF with slide-path between 2B rolled and #8 mirror polished finishes. At low speeds, the friction from the two tests remained similar throughout the test. At the higher speed, friction in the #8 mirror polished specimen increased much more than it did for the 2B rolled specimen.

5.3.3 Effect of Contact Pressure

Previous work has shown that, for PTFE-stainless steel friction interfaces, friction increases at lower pressures (Stanton et al. 1999). The AASHTO LRFD Specifications (18.1.5.2.6) suggest that CoF is inversely related to pressure from zero up to 3000 psi, after which the CoF becomes constant with respect to pressure.

In this study, the intention was to keep pressure constant over the course of each test. As described in Section 5.3.1, the hydraulic system was locked off after being pumped up to the desired pressure. However, minor leakage in the valves caused the pressure to drop over the course of the test, and it also fluctuated with the ambient temperature. This meant that the pressure did not in fact remain constant. Therefor, the following procedure was used to develop the relationship between friction and contact pressure.

- For each finish of SS, take the three tests done at 2.5 in/min, ±1.0" displacement and different pressures, and combine them as if they were done on the same sample. This was done to facilitate the calculation of a linear function to relate pressure to CoF. The sequence and the implied slide-path have no influence on the result, so the fact that they are artificial is irrelevant. An illustration of this step is shown in Figure 5-22. The vertical scale shows the CoF. The pressure is also shown, and should be read using the vertical scale multiplied by 10,000 to give psi. The horizontal scale serves an organizational purpose only.
- Reduce all pressures above 3000 psi to 3000 psi, in conformance with the implication by AASHTO that pressures above 3000 psi cause no change in CoF. (The validity of this step is evident from the plots of CoF vs. contact pressure, which show that friction for pressures above 3000 psi is fairly constant.)
- Perform a least squares analysis of CoF vs. contact pressure for each finish, resulting in an equation for the relationship for pressures below 3000 psi for each finish of SS.

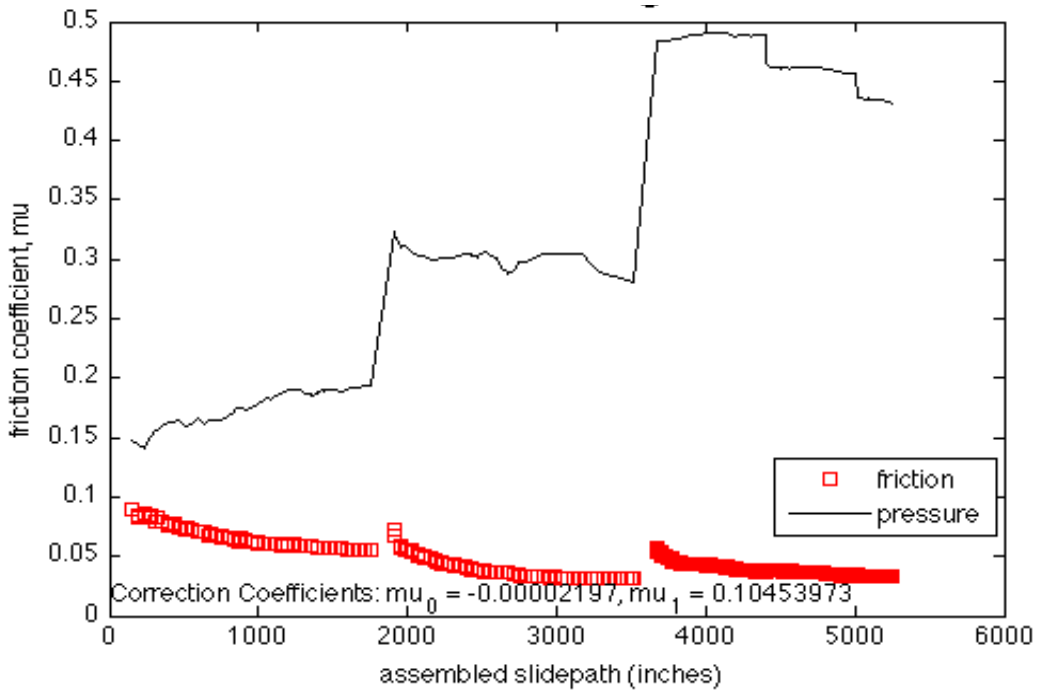

Figure 5-22. Concatenation of CoF vs. slide-path curves. Rough plate, 2.5 in/min.

The result of this process is shown in Figure 5-23. As suggested, friction decreases with increasing pressure until around 3000 psi. The abrupt change in the fit curves at exactly 3000 psi is a consequence of the choice of curve shape described above, but the trend is consistent.

The data show considerable scatter. At any nominal contact pressure, such as 1500 psi, the data extend over a considerable range of CoF values. Most of this scatter is due to the effects of slide-path, as discussed in Section 5.3.4. As the long slide path test progressed (at a nominally constant contact pressure) the CoF changed, although not always in the same direction. For example, at 1500 psi contact pressure, the Mirror data start at a low CoF (about 4%) and increase with slide path to about 8.5%, whereas the Rough data do the opposite.

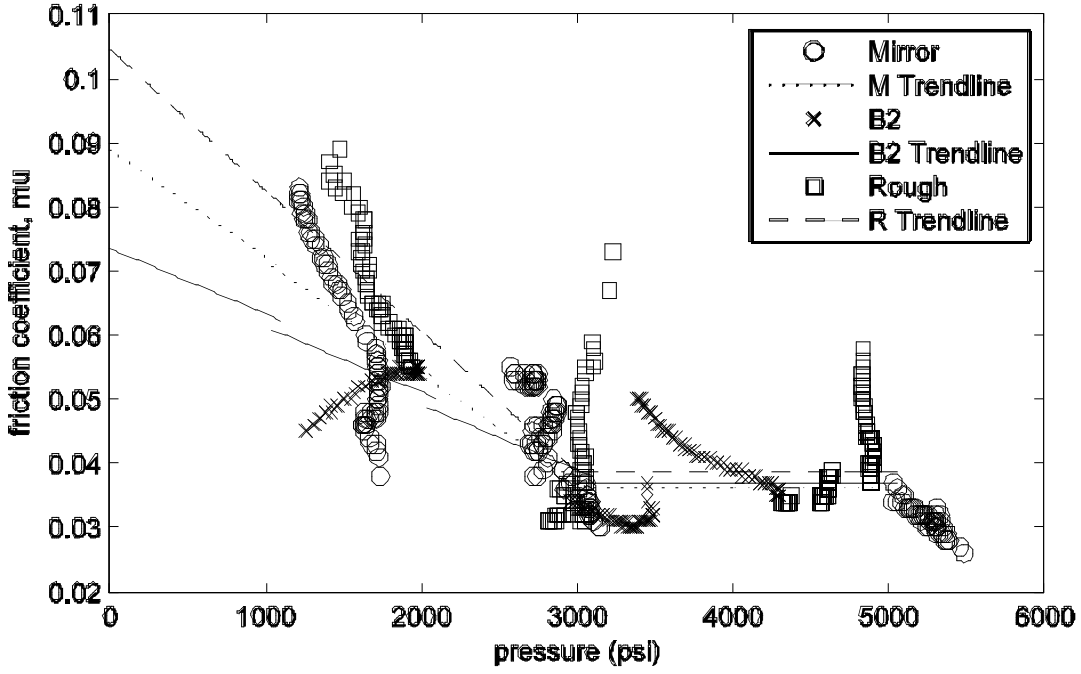

Figure 5-23. CoF vs. Pressure for the three 2.5 in/min tests done on each of the finishes of SS, showing trend-lines and 95% Confidence Interval. (CIs are the higher lines)

These results will be used to determine coefficients for the linear model. First, the results of this process were used to correct all of the long path data according to the equation:

$$\mu_{corrected} = (Ap_{nom} + B) + (\mu_{meas.} - Ap_{meas.} - B)$$

Where $\mu_{corrected}$ is the new, corrected friction for a given cycle, p_{nom} is the nominal contact pressure (1500, 3000, or 4500 psi), $\mu_{meas.}$ is the uncorrected, measured friction for a given cycle, and $p_{meas.}$is the corresponding measured contact pressure. The coefficients, A and B are given in Table 5-2. These values are not yet normalized to reference condition for use in the linear model of friction, given by Equation 1.

Table 5-2. Pressure correction coefficients for the three finishes of SS for 2.5 in/min sliding speed

	A (psi^{-1})	B
#8 mirror polish	-0.000018	0.089
2B Rolled	-0.000012	0.074
Rough Rolled	-0.000022	0.10

Note that the value of these coefficients defined for 2B material in Table 5-2 differs from that shown in Figure 5-16 because the sliding speeds are different in the two cases.

In order to conform to the linear model for CoF shown in Equation 1, the function of pressure must produce a value of 1.0 at the reference condition of 3000 psi. The coefficients used to correct the data, therefore had to be normalized against CoF at reference conditions.

$$CoF = \mu_0 \times f_{(v)} \times g_{(p)} \times h_{(s)} \quad (1)$$

The amplification function for pressure is given by:

$$g_{(p)} = a_p p + b_p \quad (6)$$

Where p is the contact pressure in psi, and the coefficients a_p and b_p, as well as the coefficients for sliding speed are given in Table 5-3.

Table 5-3. Coefficients for the amplification function of sliding speed and contact pressure

	Speed		Pressure (≤3000 psi)	
	a_v	b_v	a_p	b_p
	min/in		10^-3/psi	
Mirror Polish	0.13	0.67	-0.48	2.50
2B Rolled	0.13	0.68	-0.33	2.00
Rough Rolled	0.12	0.71	-0.57	2.70

5.3.4 Effect of Slide-path

Figure 5-24 shows the friction coefficient vs. path length for the #8 mirror polished surface. As expected, friction decreases with higher contact pressure, and is approximately constant after 3000 psi. At all pressures, the CoF increased with slide path, but it increased faster in the 1500 psi test than in the 3000 psi test.

Figure 5-25 shows a similar plot of the 2B rolled data. Again, CoFs in the 4500 psi and 3000 psi tests are very similar. Friction in the 1500 psi test increased early in the test, then approached a stable value, above those from the tests at higher contact pressures

Figure 5-26 plots the corresponding data for rough plates at different contact pressures. The variation with pressure is as expected, but the finding that the CoF diminished consistently with slide path was unexpected, because it is the opposite of the behavior for

other finishes found in this study and others (Stanton et al. 1999). However, the trend occurred consistently with all the Rough rolled specimens. The data presented here has been corrected according to the method in Sections 5.3.1 and 5.3.3.

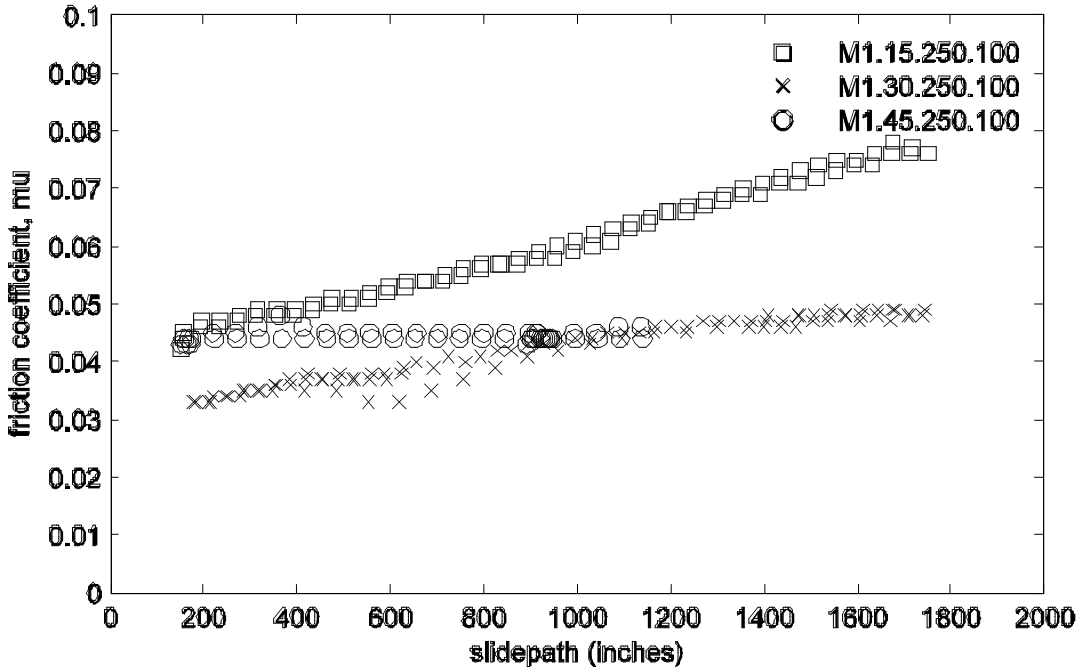

Figure 5-24. Coefficient of friction vs. path for different contact pressures on #8 mirror polish specimens at 2.5 in/min

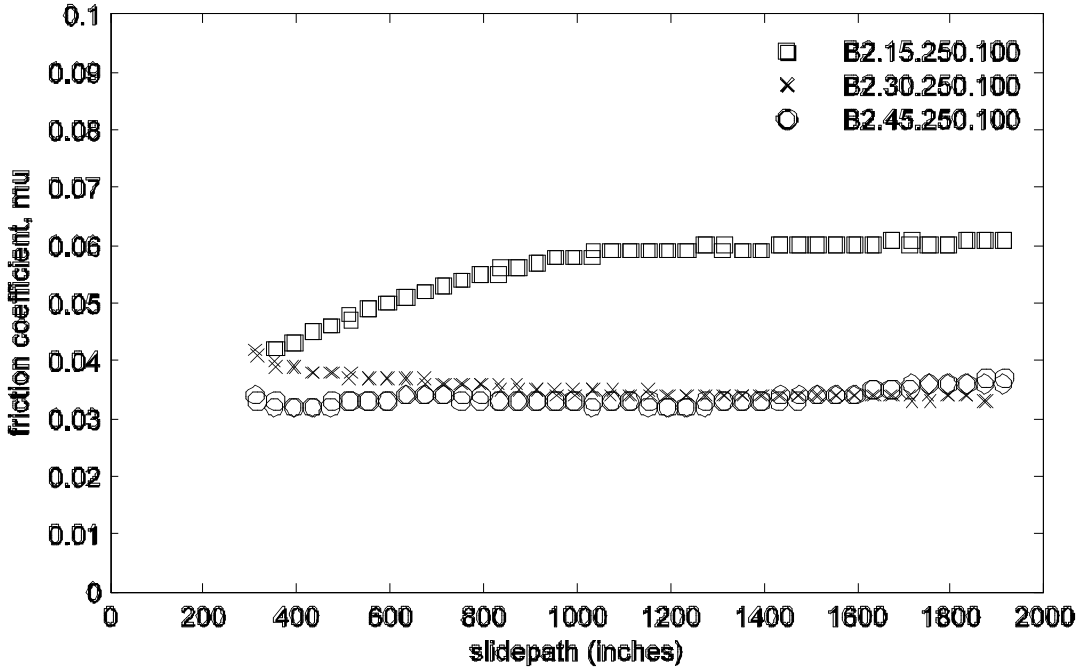

Figure 5-25. Coefficient of friction vs. path for different contact pressures on 2B Rolled plates at 2.5 in/min

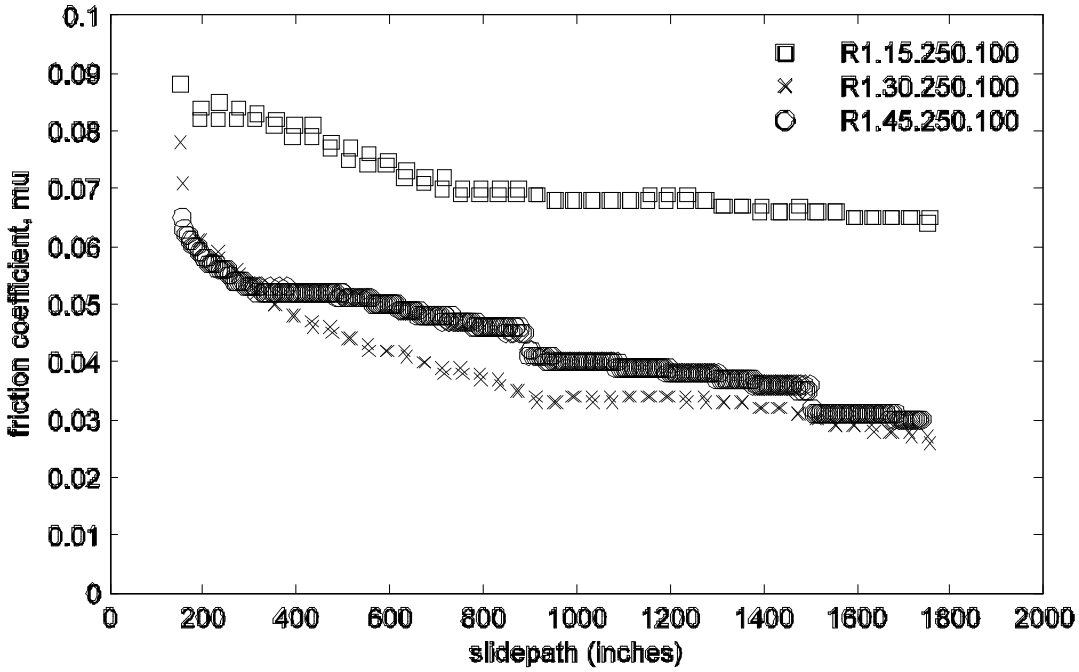

Figure 5-26. Coefficient of friction vs. path for different contact pressures on rough rolled specimens at 2.5 in/min

Change in COF with slide path has traditionally been attributed to wear, and the associated roughening, of the two surfaces, and to transfer of PTFE (Campbell and Kong 1989, Stanton et al. 1999). The rate of wear is also believed to be related to the contact pressure (Campbell and Kong 1989). The above plots do not strongly suggest that pressure has an effect on the rate of change of CoF of PTFE, but there is some trend in the mirror and 2B tests that lower pressures caused CoF to increase faster with slide-path. For the #8 mirror and 2B rolled specimens, CoF increased more during tests at 1500 psi than it did for the high pressure tests. For the rough rolled tests, CoF decreased most for the two higher pressure tests.

Figure 5-27 shows the results for all interfaces loaded to 4500 psi contact pressure. (The curves are the same as the three 4500 psi curves in Figure 5-24, Figure 5-25, and Figure 5-26). The CoF of the rough specimen changed rapidly at the start of the test, then approached a stable value. This suggests that the physical mechanism that lay beneath the change was most active while slide-path was small.

By contrast, the rate of change of CoF for the #8 mirror polished and 2B rolled specimens are fairly constant. The result is that, at end of the slide-path, the CoF in the rough rolled specimens is the lowest of the three.

Figure 5-28 shows comparable information for a contact pressure of 3000 psi. The 2B specimen experiences very little change in friction during this test, while the CoF in the #8 mirror polish increases and that of the Rough finish plate decreases. By the end of these tests, both rolled specimens display significantly lower friction than the #8 mirror polished specimen. The friction for the rough rolled specimens again decreased rapidly at first, while the friction on the #8 mirror polish specimen increases slowly and more uniformly with travel path.

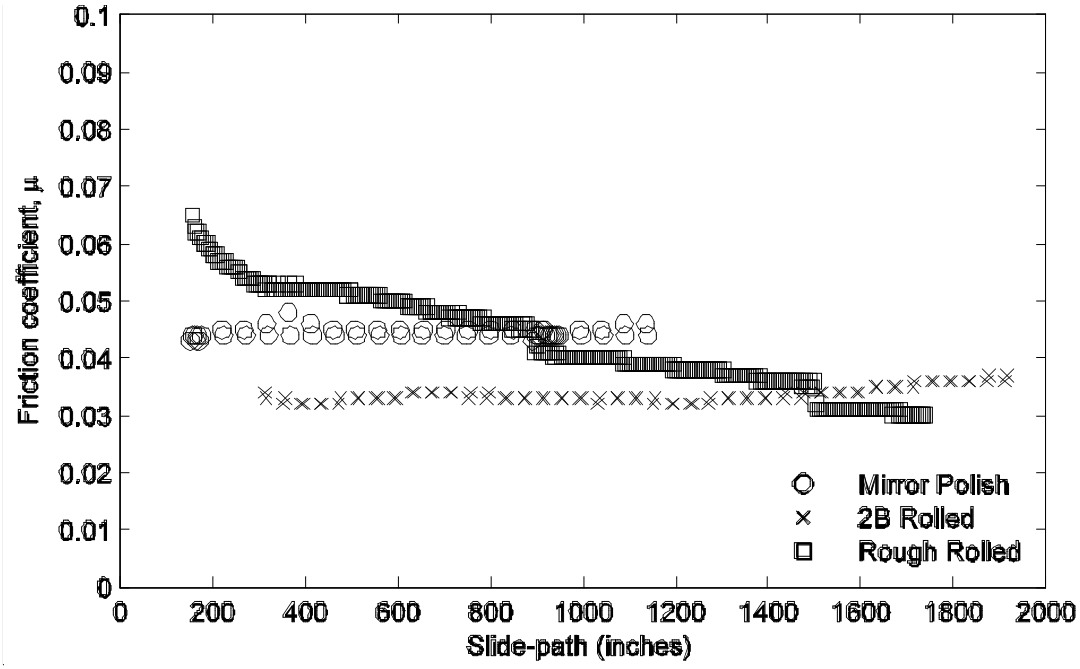

Figure 5-27. CoF v. Path for all finishes during long slide-path test (4500 psi, 2.5 in/min, ±1" stroke)

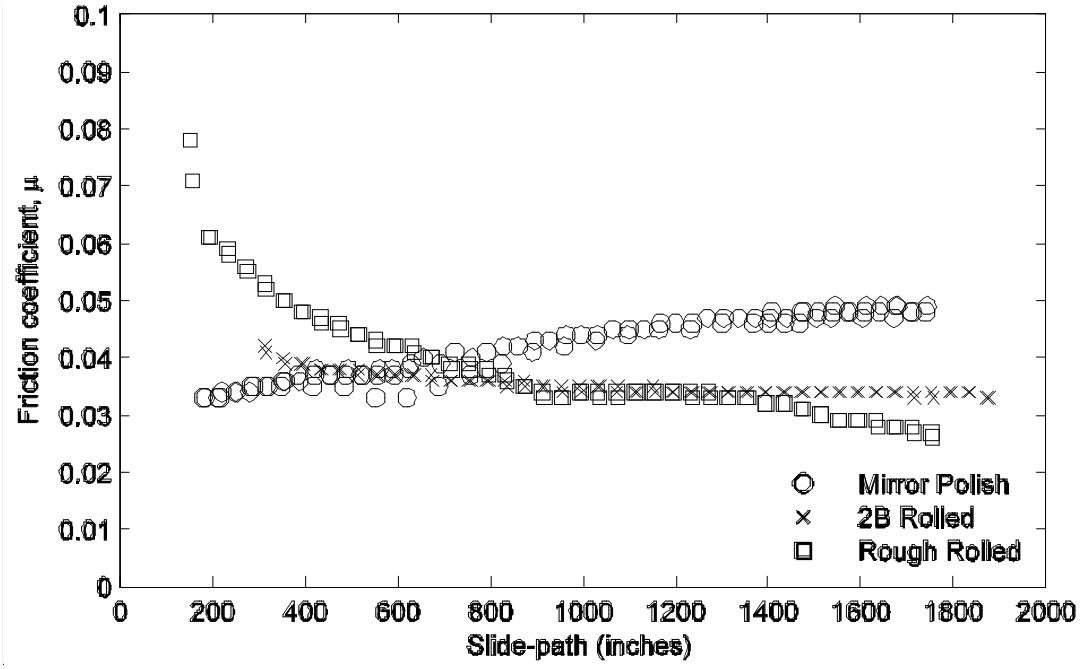

Figure 5-28. CoF v. Path for all specimens during long slide-path test (3000 psi, 2.5 in/min, ±1" stroke)

Figure 5-29 shows the same plot for contact pressures of 1500 psi. The behavioral trends are very similar to those of the tests at higher pressures, except that CoF in the rough rolled specimen decreases more uniformly. For the 2B specimen, friction initially follows the rate of the #8 mirror polish, but stops increasing after 1000 inches. At the end of the slide-path, in the rolled specimens, friction is similar, and is significantly lower than that of the #8 mirror polish specimen.

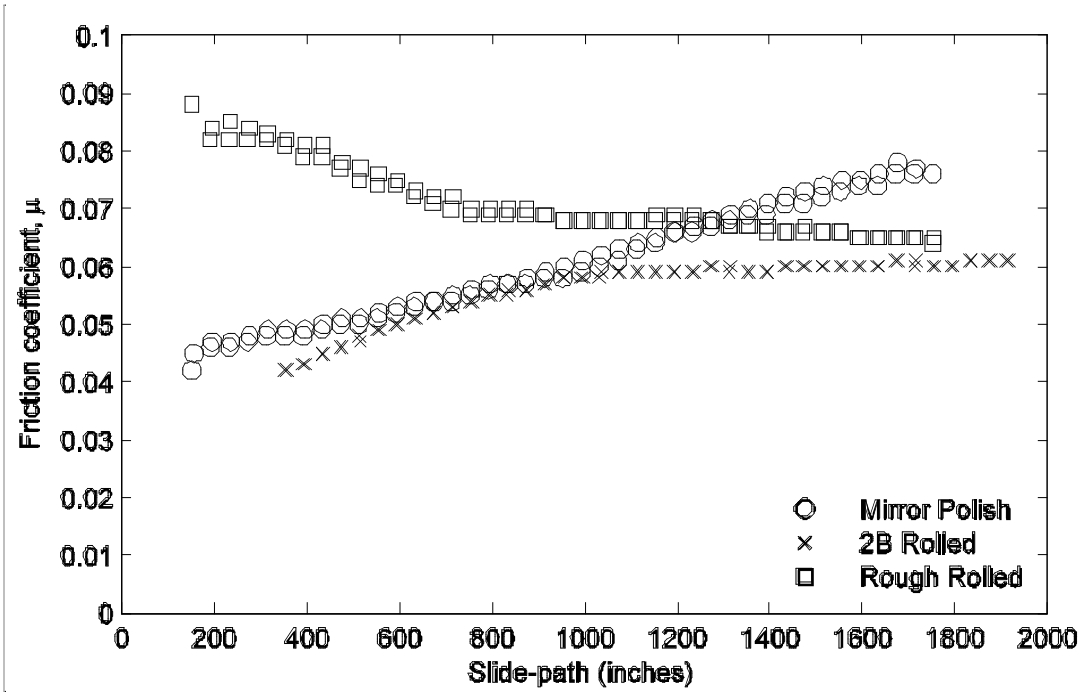

Figure 5-29. CoF v. Path for all specimens during long slide-path test (1500 psi, 2.5 in/min, ±1" stroke)

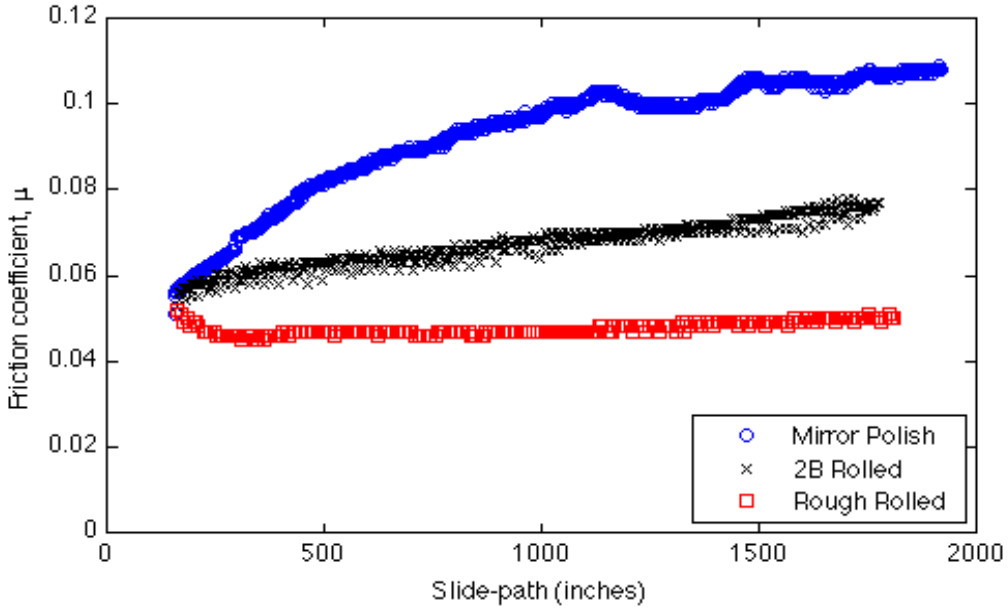

Figure 5-30. CoF v. Path for all specimens during high speed, low displacement test (1500 psi, 3.84 in/min, ±0.05" stroke)

During the high speed, small displacement test, shown in Figure 5-30, friction was initially almost the same for all three specimens, but it then increased significantly for the #8 mirror polish specimen, increased slightly for the 2B rolled specimen, and remained fairly low and nearly constant for the rough finish specimen. Shortly after the beginning of the test, the friction on the rolled specimens had already dropped below that of the #8 mirror polished specimen.

At all contact pressures except 4500 psi, the CoF of the #8 mirror polish specimens almost doubled during the slide path, ending up at values at least 1.5 times those given by the AASHTO LRFD Design Specifications.

From the long path tests at 3000 and 4500 psi, reference condition CoFs were taken for each finish. These are given in Table 5-4. They are based on a linear fit of the data projected back to zero slide-path. These values are used in Equation 1:

$$CoF = \mu_0 \times f_{(v)} \times g_{(p)} \times h_{(s)} \quad (1)$$

Table 5-4. CoF at reference conditions (3000 psi contact pressure, 2.5 in/min, zero slide-path)

	μ_0
Mirror Polish	0.034
2B Rolled	0.039
Rough Rolled	0.060

To permit comparison of the effects of slide-path on CoF for the three finishes without the effects of pressure, the CoF vs. Path data were normalized against their value for the first 20 cycles of the test. Figure 5-31 shows the normalized CoF for the tests done at 1500, 3000, and 4500 psi, at 2.5 in/min and ±1.0" cyclic displacement amplitude. The trend lines shown will be used to determine the amplification function for slidepath, to be used in Equation 1. It appears that the CoF in many of the tests reaches a plateau, so extrapolation beyond the slide-paths used in this research may not be accurate. This was also done for the extreme long slide-path test on 2B rolled plate, at 1500 psi, 10 in/min and ±1.0" cyclic displacement amplitude, shown in Figure 5-32. The trendline from this test is shown in Figure 5-31 as a dashed line, for comparison. The CoF for the extreme long path test is nearly constant, which suggests that the CoF reaches a plateau after significant slide-path is applied. This appears to be true for the other finishes, but longer slide-path data are needed for certainty.

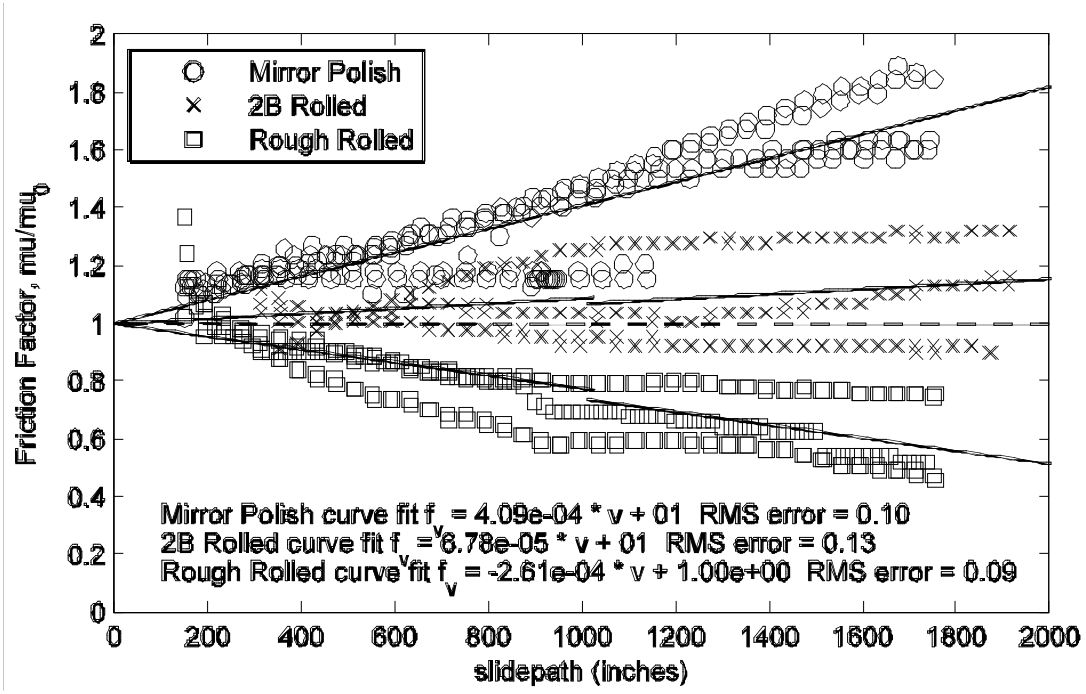

Figure 5-31. Normalized CoF vs. Path for tests done at 2.5 in/min and ±1.0" cyclic displacement.

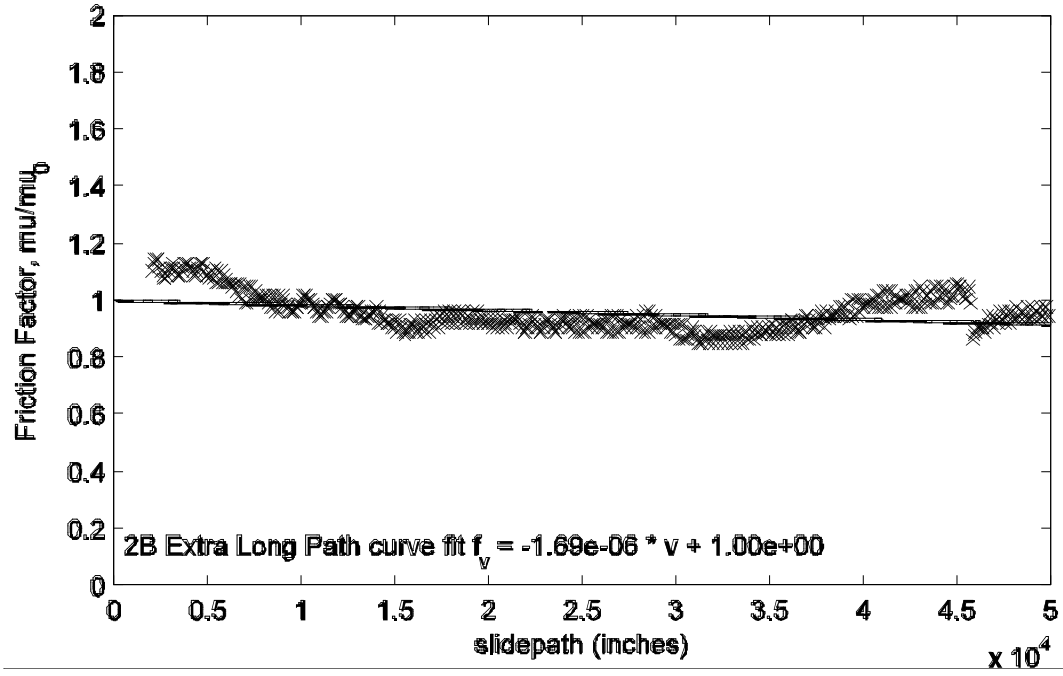

Figure 5-32. Normalized CoF for extreme long path test at 1500 psi, 10 in/min and ±1.0" cyclic displacement.

The linear trendlines generated here comprise the amplification function for slide-path, given by:

$$h_{(s)} = a_s s + b_s \quad (7)$$

Where s is the slide-path in inches, and the coefficients a_s and b_s, as well as the coefficients for sliding speed and contact pressure are given in Figure 5-8

Table 5-8. Coefficients for modifying reference CoFs for different conditions.

	Speed		Pressure (≤3000 psi)		Slide-path	
	a_v	b_v	a_p	b_p	a_s	b_s
	min/in		10^-3/psi		10^-3/inch	
Mirror Polish	0.13	0.67	-0.48	2.50	0.41	1
2B Rolled	0.13	0.68	-0.33	2.00	0.07	1
Rough Rolled	0.12	0.71	-0.57	2.70	-0.26	1

5.3.5 Effect of Cyclic Displacement Amplitude

The study also investigated the possibility that, for a given slide-path length, a large number of small displacement cycles may be more damaging to a PTFE-SS interface than a small number of large displacements. For the tests done on 2B stainless steel, all at 1500 psi contact pressure but with different speeds and displacements, the plots of CoF vs. path were compared to plots of CoF vs. number of reversals. Figure 5-33 through Figure 5-35 show groups of tests conducted at 2.5, 3.84 and 10 in/min respectively. Each plot shows the results of three tests, all done at the same sliding speed, but using different cyclic displacement amplitudes. Since all of the tests used the same total slide-path, tests done with smaller cycles experienced more reversals.

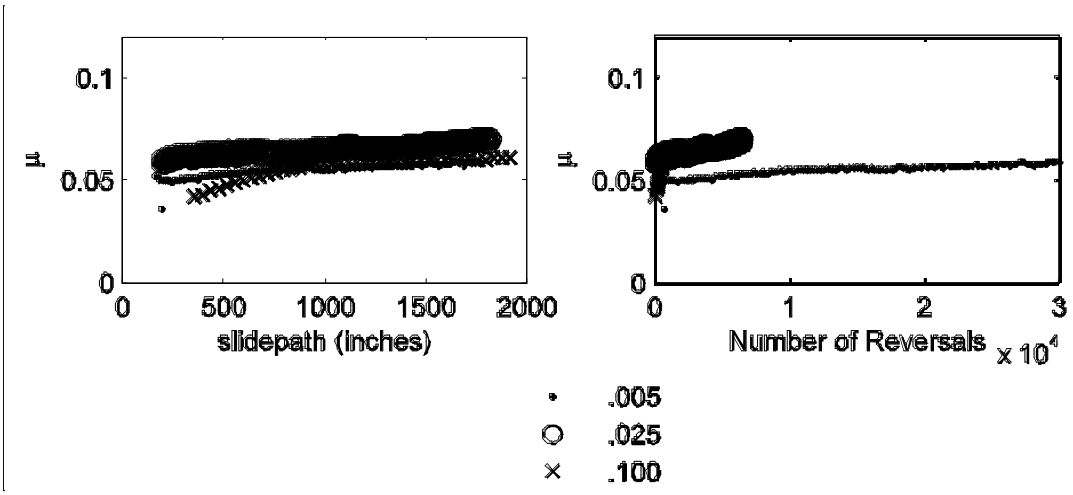

Figure 5-33. Long slide-path test on 2B Rolled Plates at 1500 psi and 2.5in/min, different displacement amplitudes.

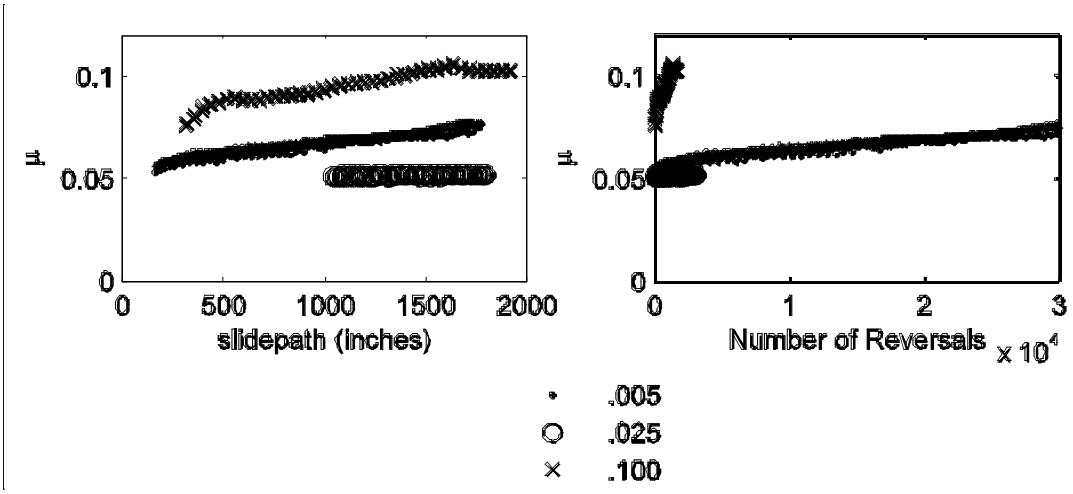

Figure 5-34. Long slide-path test on 2B Rolled Plates at 1500 psi and 3.84in/min, different displacement amplitudes.

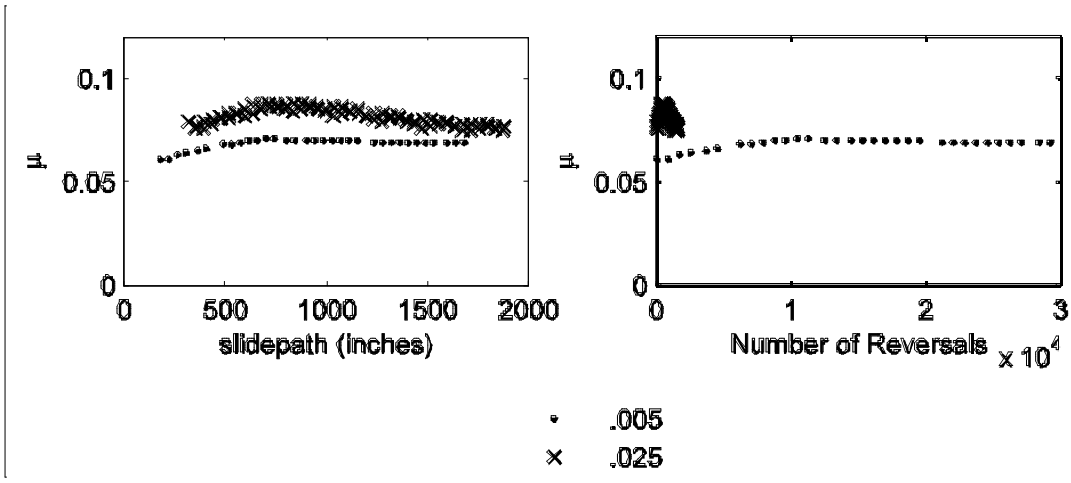

Figure 5-35. Long slide-path test on 2B Rolled Plates at 1500 psi and 10in/min, different displacement amplitudes.

The plots of CoF vs. number of reversals show the different tests progressing at dissimilar rates. Specifically, CoF changes faster in tests done at larger displacements (fewer reversals during the test) than in tests done at smaller displacements (more reversals). The plots of CoF vs. slide-path show the different tests progressing at similar rates. This suggests that the CoF is better predicted by slide-path than by number of reversals. In Figure 5-34, the first half of the test at ±0.25" was performed with inadequate pressure, which could not be corrected. The spurious data was omitted.

The possibility that some of the sliding displacement might be accommodated by deformation of the PTFE, rather than by true sliding at the interface, was also investigated. Because any shear deformation would be independent of the cyclic displacement amplitude, this behavior might be expected to be most influential in tests with small cyclic displacement amplitudes.

If the elastic shear deformation of the PTFE were significant, the true total slide path would be shorter than the intended one, the wear would be reduced, and the change of CoF would be slower than that associated with larger displacements. If the elastic deformation in the ±0.05" tests were significant, the CoF of these small displacement tests would be consistently lower, because of the technique used in the integration process used to obtain the CoF.

To find the average CoF over a cycle, the area of the CoF vs. displacement is divided by the total displacement path of the loading head, which includes any shear deformation of the PTFE. A slide-path longer than the true one would lead to a CoF that was smaller than the true one. As seen in Figure 5-33 through Figure 5-35, the ±0.05" tests fall within the range of scatter between specimens, so elastic shear of the PTFE cannot have caused a significant difference in the slide-path.

This conclusion was confirmed by an independent calculation. The shear modulus, *G*, of PTFE is approximately 30 ksi. At a contact pressure of 1500 psi and a μ of at most 0.1, shear stress ( ) is less than 150 psi, the length (*L*) of protrusion of the PTFE is 1/16", the deformation, $\Delta = \tau \frac{L}{G}$ = (150 psi)(1/16")/(33.4 ksi) = 0.00028 inches. This is about 0.5% of the total displacement of ±0.05", and so for practical purposes is negligible.

5.4 Warm-up Segment and Breakaway Friction

Prior to the first multi-speed test, each specimen was subjected to a 20 cycle warm-up loading at 2.5 in/min and ±1.0" stroke. This was done to allow friction to stabilize before the test. The warm-up procedure was introduced after Test R1.45.250, because of the large variation of CoF in the first few cycles. These initial values are often the largest friction coefficients that occur, and are particularly relevant during the construction of a bridge. It should be noted, however, that a high CoF during construction is not necessarily cause for concern. The friction force is the most important characteristic, because it provides an upper bound on the force that will be experienced by the adjoining elements, such as anchor bolts, columns and abutments. The friction force is the product of CoF and normal force. During the early stages of construction, before the bearings have been through any cycles of thermal displacements, the normal force is likely to be lower than its lifetime maximum value. Thus the friction force may be less than the value obtained from the design CoF and the maximum contact force. Furthermore, if construction occurs during the summer months, as is usual, considerable daily movement may be expected when the girders alone are in place prior to casting the deck, because the thermal mass of the girders is small and the day-to-night temperature range is large. These movements

during construction will play the same role in the field as the "warm-up" cycles in the test program, and will reduce the CoF from its initial value.

The CoF under static conditions is generally larger than the CoF under sliding condition. This effect is called breakaway CoF, and average values from all of the tests are shown in Table 5-5. During the warm-up segment for each of the tests, the maximum CoFs for both directions of motion during the sixth through twelfth cycles were recorded. The mean value of these maximums is shown. When multiple tests were performed at a single contact pressure, the breakaway CoFs from the tests were averaged together. For R1.45.250.100, the value given is from the second long path test at 2.5 in/min, after the stainless steel plates were flipped to their unused sides.

Table 5-5. Breakaway CoF from cycles 6 through 12 of the warm-up test, all at 2.5 in/min, ±1.0" displacement

	Contact Pressure (psi)		
	1500	3000	4500
Finish			
Mirror Polish	0.056	0.034	0.033
2B Rolled	0.068	0.053	0.031
Rough Rolled	0.15	0.10	0.07

Figure 5-36 through Figure 5-38 are plots of the CoF against the slide-path for the first 20 cycles administered. These are averages over the cycle, so should not be confused with the breakaway CoF shown Table 5-5.

The CoFs reported in AASHTO are based on breakaway friction, whereas the values from this study are based on average friction. In Appendix B, data for all the tests is plotted. These plots show values of the coefficient of friction uncorrected for pressure variations, so the contact pressure is also shown. The plots show average CoF as well as breakaway. Breakaway friction is difficult to measure without very fast data collection, as the peak may fall between data points. For this reason, where the graph of breakaway friction varies widely, the locus of the peaks will give the best estimate of the real peaks. The difference between average CoF and breakaway CoF appears to be fairly constant with respect to slide-path, and the breakaway CoF ranges from 5% to 30% greater than the average CoF. The difference was greatest for rough specimens, and was about the same for 2B and mirror finish specimens.

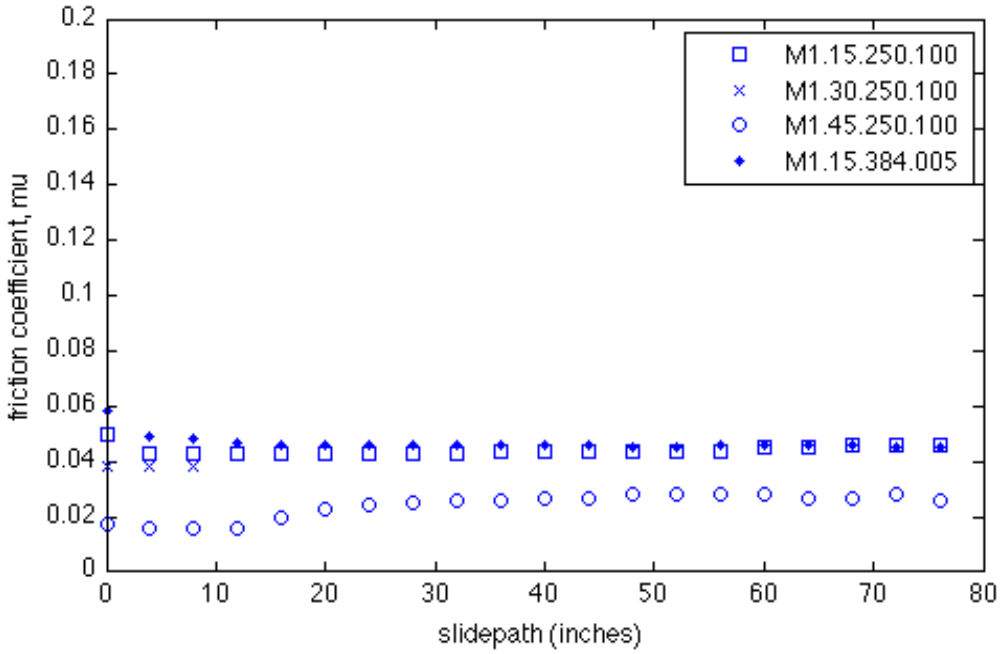

Figure 5-36. CoF vs. path during warmup cycles for #8 mirror polish specimens. Sliding speed is 2.5 in/min and stroke is ±1.0" except for M1.15.384.005, where sliding speed is 3.84 in/min and stroke is ±0.05"

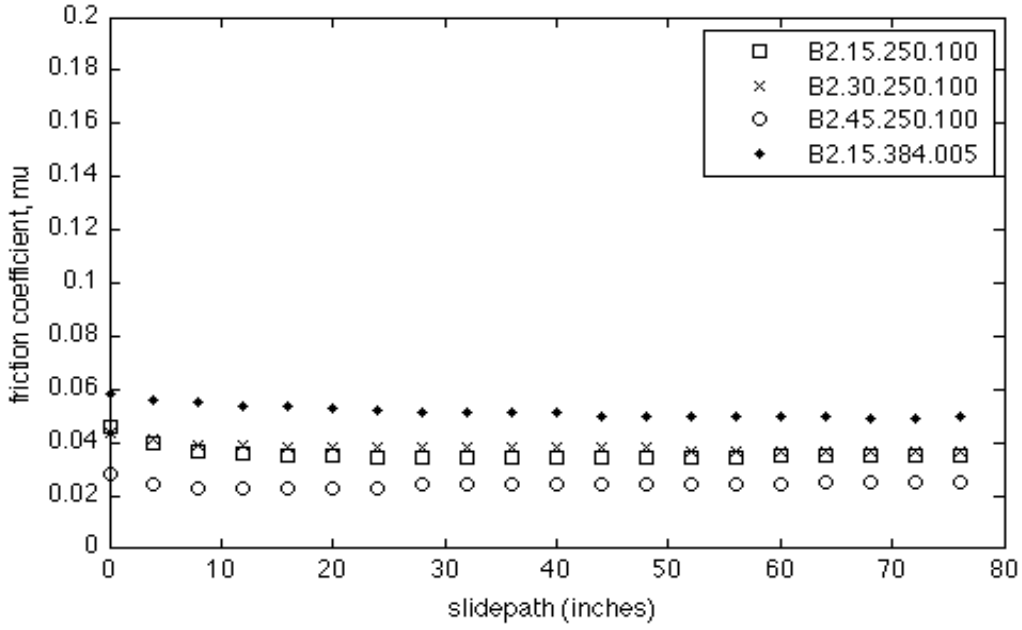

Figure 5-37. CoF vs. path during warmup cycles for 2B rolled specimens. Sliding speed is 2.5 in/min and stroke is ±1.0" except for M1.15.384.005, where sliding speed is 3.84 in/min and stroke is ±0.05".

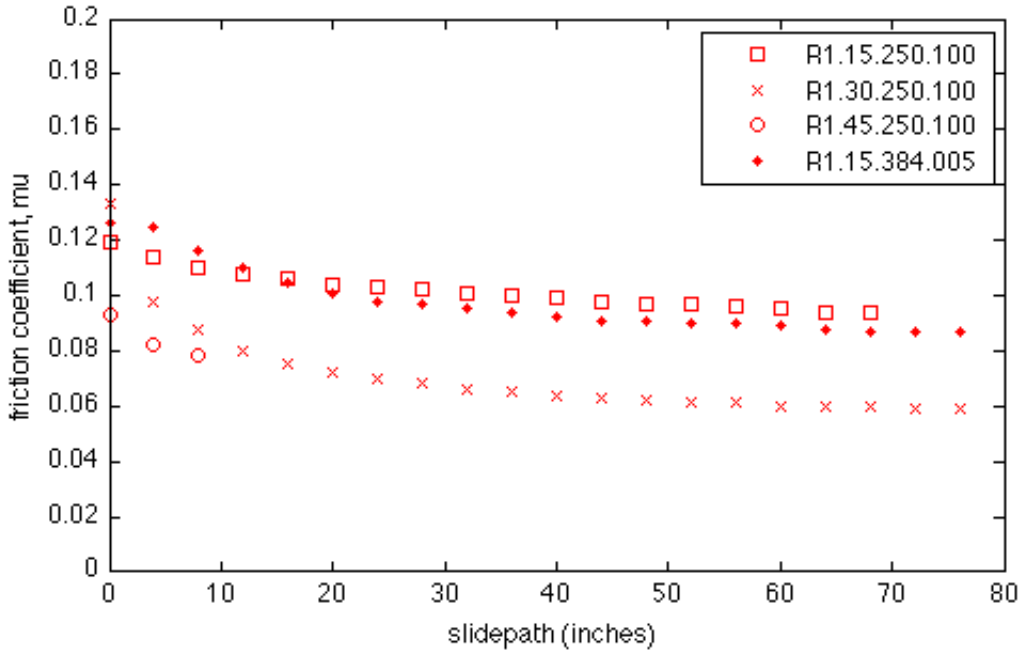

Figure 5-38. CoF vs. path during warmup cycles for rough rolled specimens. Sliding speed is 2.5 in/min and stroke is ±1.0" except for M1.15.384.005, where sliding speed is 3.84 in/min and stroke is ±0.05".

5.5 Extreme Cyclic Displacement Amplitude Test

During any one cycle, the contact pressure, temperature and slide-path completed remained essentially constant. Therefore the CoF was expected to be constant, except for the effect of breakaway at the reversal points. However, this was not the pattern observed. Particularly in the rough plate tests, the CoF was found to be lower at the middle of the stroke and higher towards the ends (see Figure 4-7). A hypothesis was formulated to explain this behavior.

The hypothesis was that the concave shape of the displacement loop (with lower friction in the middle of the stroke) was due to the dependence of CoF on slide path. The middle of the stainless steel experiences longer contact with PTFE, and therefore a longer slide-path, than do the extremes. In all of the standard tests, the radius of the disc was larger than the displacement amplitude, so that, during a normal cycle, a central area of the stainless steel was always in contact with PTFE, whereas the outer regions were in contact only at the extremes of the cycle. The center therefore experienced a longer slide-path, and

consequently lower friction, than the outer edges, because the CoF decreases with slide-path for the rough finish stainless steel (see Section 5.3.4).

To investigate this behavior exhibited by rough rolled specimens, the first specimen (R1.45.250.100) was subjected to an extra test in which the cyclic displacement amplitude was increased to ±1.75". In this special test, friction (shown in Figure 5-39) continued to increase along the same curve in the first pass over new SS and was lower in subsequent passes. This is consistent with the hypothesis.

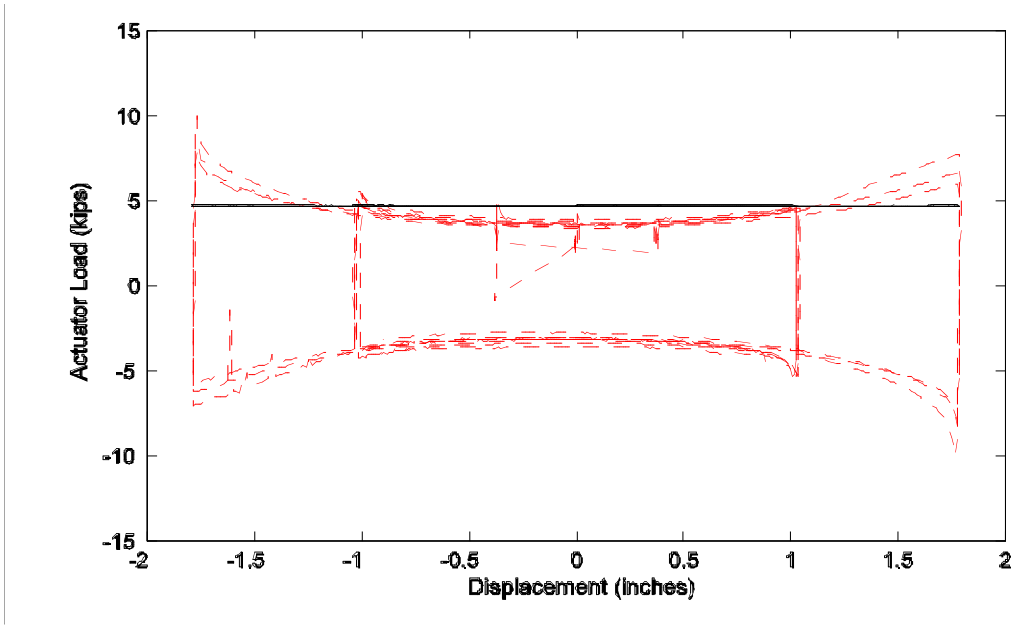

Figure 5-39. Extreme cyclic displacement amplitude test, showing force and contact pressure.

Figure 5-39 shows that the CoF increased at the ends of the stroke. The possibility that this was caused by a change in contact pressure was considered. The contact pressure was calculated from the oil pressure in the rams. However, because of the sequence of clamping of the fixed plates, (see Section 3.5) and because the rams inevitably have some internal friction, variations in contact pressure could occur without showing a proportional change in oil pressure. However, the CoF decreased with each subsequent excursion to the extreme displacement. If some geometric effect had caused contact pressure to be greater at the extremes, the CoF would remain high at these displacements.

The measured change in friction force must therefore be a result of a change in CoF based on the varying slide-path along the stainless steel.

5.6 Discussion of Results

The results of these tests suggest that:

- The coefficient of friction varies significantly with surface finish, contact pressure, sliding speed and slide-path. There is also considerable scatter between individual specimens.
- In all tests, friction increased with sliding speed. The CoFs of 2B rolled stainless steel and #8 mirror polished stainless steel with respect to sliding speed were very similar.
- In all tests, the coefficient of friction decreased with an increase in contact pressure until about 3000 psi. At pressures higher than that, it remained essentially constant. Friction coefficients in 2B rolled specimens were lower than those of #8 mirror polished specimens at low pressures, and similar at high pressures. Rough rolled specimens were more sensitive to changes in pressure, with higher friction at low pressures, and CoFs comparable to the other finishes at high pressures.
- #8 mirror and 2B rolled specimens exhibited similar CoFs at low values of slide-path, with friction in #8 mirror polished specimens slightly lower.
- The change in coefficient of friction with slide-path was characterized by a rapid increase for #8 mirror polished specimens, a slow increase for 2B rolled specimens, and a decrease for rough rolled specimens.
- The rate at which friction changed with slide-path was found to be unaffected by the amplitude of the cyclic displacement. Total slide-path is the better predictor of the increase in friction with wear.
- Measurements of wear provided inconclusive evidence about rates of wear and dependence on contact pressure or sliding speed. The measured wear was of the

same order of magnitude as the measurement error, about 0.002", even with the longest slide-path (48,000 inches).

- Observable wear seemed to correspond to the change in CoF experienced. In #8 mirror polished specimens, the CoF increased with wear, and significant amounts of PTFE were transferred to the stainless steel surface. In the two rolled surface finishes, the SS surface became polished with wear, and less PTFE was deposited. The CoF either remained almost constant (2B finish) or decreased (rough finish) with slide-path.

In particular, 2B stainless steel has friction properties that are similar to, and in many cases better than, those of mirror polish material; they change little with slide-path; and PTFE loss by wear is very low. These characteristics make it a suitable choice for use in PTFE-SS sliding bearings.

Table 5-6 shows design CoF values for #8 mirror finish bearings from AASHTO at 68°F alongside values from this study. For the latter, two separate values are given: the reference value (at 3000 psi, 2.5 in/min sliding speed and zero slide-path) and values corresponding to the worst case slide-path used in the tests (zero or 1600 inches). As can be seen, the existing AASHTO values are about the same as the reference values obtained in these tests, but about half of the worst case slide-path values. This suggests that the AASHTO values are too low. The extent to which they are too low depends on the estimated slide-path of the bearing.

Table 5-6. Comparison of CoF between AASHTO and this study

	Pressure (psi)	500	1000	2000	<3000
AASHTO		0.08	0.07	0.05	0.03
This Study, Reference Case		0.076	0.069	0.052	0.034
This Study, Worst Case		0.14	0.12	0.090	0.070

The model developed in this chapter was defined by Equation 1:

$$CoF = \mu_0 \times f_{(v)} \times g_{(p)} \times h_{(s)} \quad (1)$$

Substituting the linear amplification functions, Equation 1 becomes:

$$CoF = \mu_0 (a_v v + b_v) \times (a_p p + b_p) \times (a_s s + b_s) \quad (8)$$

It expresses the average coefficient of friction during a cycle, , as a function of sliding speed, *v*, contact pressure, *p*, and accumulated slide-path, *s*. The best fit values for the constants are given in Table 5-7 and Table 5-8. The limits of equation (8) are:

$0 < v < 5.0 \frac{in}{\min}$

$0 < p < 3000\ psi$ (For higher pressures, set p = 3000 psi)

$0 < s < 1600\ inches$

Table 5-7. CoF at reference conditions (3000 psi, 2.5 in/min, ±1.0")

	_o
Mirror Polish	0.034
2B Rolled	0.039
Rough Rolled	0.060

Table 5-8. Coefficients for modifying reference CoFs for different conditions.

	Speed		Pressure (≤3000 psi)		Slide-path	
	a_v	b_v	a_p	b_p	a_s	b_s
	min/in		10^-3/psi		10^-3/inch	
Mirror Polish	0.13	0.67	-0.48	2.50	0.41	1
2B Rolled	0.13	0.68	-0.33	2.00	0.07	1
Rough Rolled	0.12	0.71	-0.57	2.70	-0.26	1

Equation 8 can be evaluated at specific pressures to give suggested CoF values for all three surface finishes. They are given in Table 5-9 and correspond to 68°F, 2.5 in/min sliding speed and the worst case slide-path (1600" for mirror and 2B finishes, zero for rough rolled). These values suggest that the design values presently in the AASHTO LRFD specifications should be reviewed for possible change. It should be noted that the values from this study do not address behavior at low temperature.

Table 5-9. Suggested CoF at 2.5 in/min and worst-case slide-path.

Surface Finish	Pressure (psi)	500	1000	2000	3000
Mirror		0.16	0.15	0.11	0.077
2B Rolled		0.083	0.075	0.061	0.046
Rough Rolled		0.14	0.13	0.094	0.059

One of the objectives of this study was to determine the suitability of 2B finish stainless steel as a substitute for #8 mirror finish. The global characteristics of the two are compared here, with reference to the coefficient of friction averaged over each cycle, rather than the breakaway value.

Reference coefficient of friction, μ_0. μ_0 = 0.034 and 0.039 for #8 mirror polish and 2B rolled respectively. Thus under reference conditions, the 2B finish leads to a higher CoF.

Effect of slide-path. The CoF increases significantly with slide-path for #8 mirror polish, and very little for 2B finish, up to 1600" of slide-path. At that slide-path, the CoF of the mirror finish was about twice that of the 2B, so any initial advantage offered by the #8 mirror finish had by then evaporated. No mirror finish tests were carried out at longer slide-paths. One 2B finish specimen was tested to 48,000 inches, although only at 1500 psi constant pressure. By the end of that test, the CoF had decreased from 0.08 to 0.07, a decrease of 12%. This result suggests that, if a long slide-path is envisioned, the 2B finish would be a better choice than the #8 mirror finish.

Effect of sliding speed. The change in CoF with sliding speed were nearly identical in 2B and #8 mirror materials.

Rate of wear. Campbell and Kong (1989) studied friction for bearings with stainless steel surface roughnesses of 1.18 and 13.4 micro-inches. (in this study, #8 mirror specimens were 3-4 micro-inches, and 2B specimens 4-6 micro-inches). In that study, which used dimpled and lubricated PTFE, CoFs as low as 0.002 (0.2%) were measured for the mirror polished stainless, and 0.01 for the rougher material. This difference is much larger than that found in this study between mirro polished and smooth rolled materials. Evidently,

surface roughness plays a much larger role in the CoF of lubricated bearings than in dry ones.

The foregoing comparisons suggest that 2B finish stainless steel is an acceptable substitute for #8 mirror polish in PTFE-stainless steel bearings, at least under the conditions tested here. The tests focused on three variables (sliding speed, contact pressure, and slide-path). Temperature is also known to have a significant effect on both CoF and wear rates but could not be investigated within the scope of this project. Conducting tests on 2B finish at low temperature would be desirable before deploying it for use in the field.

6 Bearing Life

A PTFE bearing will cease to function properly when the PTFE is worn sufficiently to cause the steel carrier plate to come into contact with the stainless steel. In this chapter, an attempt is made to estimate the life of a PTFE-stainless steel bearing using wear rates obtained from the test program. The calculation has two components. The demand, i.e. the slide-path to be expected in the field, is addressed in Section 6.1. The capacity, i.e. the ability of the PTFE to withstand wear caused by slide-path, is addressed in Section 6.2.

Because of the low level of certainty associated with the measurement of PTFE loss during the tests, the predictions made here are also quite uncertain, but can be improved if better wear data become available. Wear rates in practice are likely greater than those shown here; bearings are often located near expansion joints, which afford them plentiful sources of potential contamination. Also, bearings that cannot accommodate sufficient rotation may experience load eccentricity, which can exacerbate ingress of contamination and increases contact pressure locally . However, the methodology outlined here is believed to capture the important aspects of the behavior.

6.1 Slide-path Expected in the Field.

6.1.1 Thermal Movements.

Bridges expand and contract with changes in temperature. An increase in temperature will cause a bridge to lengthen, and vice-versa. Sun on the top of the deck causes a temperature gradient, which causes a change in curvature. The following process is outlined for an idealized, symmetric, single span bridge with both ends set on PTFE sliding bearings, and equal and opposite displacements at each end. However, the process can easily be extened to other conditions.

6.1.1.1 Seasonal Motion

Over the course of a year, temperature may vary by around 90°F in Seattle, or 110°F in Wisconsin (AASHTO 2009). The amplitude of this motion is given by:

$$u_{long} = L \times \Delta T \times \alpha \tag{9}$$

Where:

L = length of bridge

ΔT = change in temperature

= Coefficient of thermal expansion = $6x10^{-6}$ for both steel and concrete

For a 120' span, this motion would amount to 0.94". This motion occurs twice a year, and is dwarfed by the sum of the faster motions caused by daily fluctuations in temperature and traffic loading.

6.1.1.2 Daily Motion

In addition to longtitudinal length change, bridges often experience temperature gradients though the deck structure, resulting in a change in camber. This is usually a result of sun shining on the top of the deck. Both the elongation and the camber must be accounted for in evaluating the daily movement of the bearings.

If the gradient is not linear, mechanical strains will result. The total strain is the sum of environmental (temperature) strain and mechanical strain:

$$\varepsilon_{tot} = \varepsilon_e + \varepsilon_m = \varepsilon_e + \sigma / E \tag{10}$$

The total strain can also be defined by the strain at an arbitrarily chosen origin, and the curvature:

$$\varepsilon_{tot} = \varepsilon_0 - \phi y \tag{11}$$

Where:

ε_0 = total strain at the origin

ϕ = curvature

y = vertical coordinate, measured positive downwards from the origin

Combining equations 10 and 11 leads to:

$$\sigma = E(\varepsilon_0 - \phi y - \varepsilon_e) \tag{12}$$

Axial force equilibrium requires:

$$0 = \int \sigma dA = \int Eb(\varepsilon_0 - \phi y - \varepsilon_e)dy \tag{13}$$

Moment equilibrium requires:

$$0 = \int y\sigma dA = \int yE(\varepsilon_0 - \phi y - \varepsilon_e)dA \tag{14}$$

From these equations, the deformation from any temperature change can be calculated, given the temperature gradient and the properties of the bridge. The result is a combination of longitudinal elongation from the increased average temperature of the bridge, and camber due to the gradient of that temperature increase.

Using the method from AASHTO Design Specification, Article 3.12.3 a design temperature gradient can be calculated for a bridge in one of four zones, built of either concrete or steel. For a steel bridge in "Zone 3", the gradient would be characterized by:

At deck surface: $\Delta T_1 = 41°F$

4" below surface: $\Delta T_2 = 11°F$

16" below surface to bottom flange: $\Delta T_3 = 0°F$

A spreadsheet was devised which calculated the bearing slip based on a given geometry and temperature gradient using equations 10 through 13. The spreadsheet calculates the total strain throughout the depth of the girder, including at the bottom, which controls the bearing slip, and includes the effects of longitudinal elongation and camber. Assuming a 120' steel bridge with a total superstructure depth of 8' and neutral axis depth of 33", This temperature gradient would cause a bottom strain of -14 microstrain, or 0.02 inches inward for a 120 ft span. This movement would occur daily during the summer months. The value is small because the outward movement due to girder elongation is almost completely cancelled out by the inward movement due to the girder end rotation resulting from camber.

An upper bound on the thermal motion of a bridge can be produced by assuming that the bridge has zero thermal mass. This would mean that all of the deformation would be longitudinal, because such a bridge would heat and cool uniformly (and instantly), so there would be no temperature gradient. The elongation would then be given by Equation 9.

Assuming again an arbitrary simple span of 120' and using temperature data from Seattle during 2008, (UW Atmospheric Sciences Department), the resulting cumulative slide-path, from January 1, 2008 till January 1, 2009 would be 1084 inches. Again, since bridges have thermal mass, and therefore experience less temperature change than the air around them, this number represents an upper bound on the amount of thermal motion that can be expected for a bridge in Seattle. Annual slide paths for bridges located in more extreme climates would be proportionately larger.

6.1.2 Traffic Movements.

In a heavily traveled bridge, the total bearing slip due to many small traffic-induced movements may be larger than the total thermal movement.

The amount of slip experienced when a truck crosses the bridge can be found by summing the components of the movements. The following process is outlined for an idealized, symmetric, single span bridge with both ends set on PTFE sliding bearings, and equal and opposite displacements at each end. However, the process can easily be extened to other conditions.

6.1.2.1 Girder End Displacement.

In most girder bridges, the girders are made composite with the deck so the neutral axis is high. This means that when the girder deflects, end rotation causes significant longitudinal movement of the bottom flange relative to the support. The bearing experiences this movement as slip. This effect is illustrated in Figure 6-1.

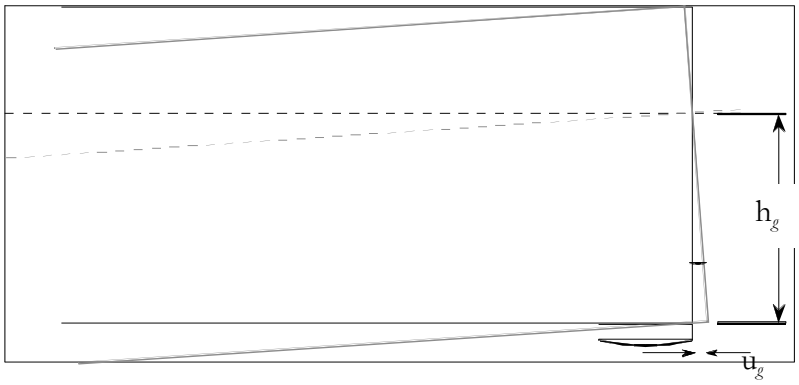

Figure 6-1. Girder end rotation causing bearing slip

The bearing slip, u_g is given by:

$$u_g = \Delta\theta h_g \tag{15}$$

where

Δ = end rotation due to truckpassage.

h_g = vertical distance between bearing interface and girder neutral axis.

6.1.2.2 Rocker rotation

If the sliding surface is placed on top of a rocker, the top face of this rocker moves towards midspan of the bridge when the truck passes over the bridge and the rocker rotates. Sample rocker dimensions taken from WisDOT structure B51-113 are a height of about 3" and a radius of about 24". This bearing slip adds to the one due to Girder End Displacement, and is given by:

$$u_r = \Delta\theta h_r \tag{16}$$

where

ϑ = end rotation due to truck passage.

h_r = height of rocker.

6.1.2.3 Neutral Axis Shortening

As a bridge deflects under load, the neutral axis suffers no strain so its length is unaltered. However, the camber changes, so, even though the length along the curved neutral axis

remains the same, the chord length changes and adds to the bearing slip. For simplicity, the camber is considered here to be parabolic. The the length along the curve, S, is related to the chord length, L, by

$$S \approx L\left(1+\frac{8}{3}\left(\frac{c}{L}\right)^2\right) \tag{17}$$

where

c = camber.

L = chord length.

S = length of bridge span along neutral axis.

Thus the difference in length between the curved path and the chord is

$$S - L \approx L\left(\frac{8}{3}\left(\frac{c}{L}\right)^2\right) \tag{18}$$

A change in camber, Δc, causes a change in length along the curve, ΔS, if the chord length L remains constant. It can be obtained by differentiation as:

$$\Delta(S-L) \approx \frac{16c}{3}\frac{\Delta c}{L} \tag{19}$$

If the change in the curved shape of the girder is also parabolic, the quotient $\frac{\Delta c}{L}$ is related to the girder end rotation by

$$\Delta\theta = 4\frac{\Delta c}{L} \tag{20}$$

So $$u_{NA} = \Delta(S-L) \approx \frac{4c}{3}\Delta\theta \tag{21}$$

Equation 21 is based on the assumption that the sign of the girder camber remains the same during the live load deflection but its magnitude changes. That is, if the girder shape is an upwards camber when no live load acts, the camber is reduced by the truck load, but it remains upward nonetheless.

6.1.2.4 Total Longitudinal Displacement

The total slip is given by adding the components:

$$u_{tot} \approx \Delta\theta\left(h_g + h_r + \frac{4c}{3}\right) \tag{22}$$

The magnitudes of the three components are evaluated here for a girder bridge, assuming arbitrarily a simple span of 120 ft, a neutral axis height of 63 inches (total depth 8 ft), a rocker height of 3 inches, and an initial (upwards) camber of 4 inches. Then

$$h_g = 63in$$

$$h_r = 3in$$

$$\frac{4c}{3} = 5.3in$$

The girder end rotation accounts for the great majority of the slip and, unless special cirumstances prevail, it alone could reasonably be used to represent the total displacement.

The bearing displacement is expressed in Eq. 22 as a function of end rotation. It can be related to the mid-span deflection. If the deflected shape is parabolic,

$$\Delta\theta = 4\frac{\Delta c}{L} \tag{23}$$

If the shape is instead caused by a uniform load or a point load at mid-span, the form of equation 23 remains the same, but the constant 4.0 becomes 3.2 or 3.0 respectively. The AASHTO LRFD Design Specifications limit the live load deflection to L/800, for which the corresponding end rotation is 3.2/800, or 0.004 radians if the deflection is caused by uniform load. This process leads to an upper bound to the end rotation, and hence to the longitudinal movement at the bearing.

$$u_{tot} \le \Delta\theta\left(h_g + h_r + \frac{4c}{3}\right) = 0.004 \times (63 + 3 + 5.3) = 0.29in \tag{24}$$

6.1.2.5 Effect of Column Stiffness.

The foregoing estimates of the bearing slip are based on the assumption that the column supporting the bearing is rigid. If it is not, it will deflect longitudinally under the friction force from the bearing, and some or all of the movement will be accommodated by column bending rather than bearing slip. The extent of the column bending is of interest, because it may reduce the slide–path experienced by the bearing.

If the girder end movement is caused by the superstructure vibrating, the problem becomes dynamic and assumptions are needed about the column inertial mass, the CoF of the PTFE under high-speed sliding, etc. Values for these are not available, so no attempt is made here to analyze that behavior.

A truck traveling at 60 mph takes about 1.3 seconds to cross the 120' span bridge, and this is long enough to eliminate almost all inertial effects associated with non-vibratory motion. Under those circumstances it is possible to estimate the critical column stiffness that will prevent slip of the bearing. It is given by

$$K_{cr} = \frac{F_{slip}}{u_{tot}} \tag{25}$$

where

$F_{slip} = \mu N$, the force required to initiate slip in the bearing

N = the normal force on the sliding surface

u_{tot}= the sum of the individual displacement components

If the column stiffness is less than K_{cr}, all of the longitudinal motion will be absorbed by column bending, so the bearing will not slip. For higher column stiffness, some slip will occur. Since sliding friction is lower than the breakaway friction, it is possible that some rebound will occur after slip starts, and that the proportions of the total movement attributable to bearing slip and column bending will differ from the values obtained by static analysis. For this reason, it would be conservative but prudent to assume that all longitudinal motion is absorbed by bearing slip if the column stiffness exceeds K_{cr}.

If the superstructure consists of a number of continuous spans of approximately equal length, the largest rotations are likely to occur at the abutment, where the girders are simply supported. There, the longitudinal stiffness of the support is that of the abutment itself. Because the abutment is likely to be very stiff, as well as to have a high inertial mass, that bearing is likely to experience the largest rotation and the longest slide-path. It is therefor fortunate that bearings at abutments are geneally more accessible and easeir to inspect for wear than those on the intermediate columns.

6.1.2.6 Total Slide-Path Length

Provided data are available on the frequency of traffic sufficient to cause slip (that is, where the column or abutment is stiffer than K_{cr}. for that loading), the amount of slide-path expected in a year can be calculated as:

$$u_{year} = u_{tot} \times N_{year} \tag{26}$$

Where:

N_{year} = number of times the slip causing load occurs in one year.

6.2 Bearing Slide-Path Capacity

In Section 4.1.3, the wear from about 48000 inches of slide-path at 10.0 in/min on a 2B rolled finish specimen caused a loss of 0.001 inches of PTFE. If this is representative of the normal rate of wear of PTFE against a 2B rolled plate, then it should take 3,000,000 inches (50 miles) of slidepath to wear down a 1/16" projection of PTFE down to the surface of the carrier plate. However, wear rates in the field are likely much higher. Observation of bearings in-situ is recommended to obtain more useful values of the wear rate. Also, cold temperatures have been shown to increase wear rate significantly (Stanton, Roeder and Campbell 1999)

If the 120' span used above were a flexible steel bridge, it might experience the maximum permissible deflection of L/800 with some regularity. By Equation 24, this would cause a bearing slip of 0.23 inches. If it were to experience this 500 times per day, the bearing

should last about 56 years. These arbitrary numbers are for explanatory purposes, but application of this method to any particular situation is possible.

The estimated life of the sliding interface clearly depends on the asumptions underlying the calculations. Most steel bridges deflect less than the maximum permissible L/800, even under maximum load, and concrete bridges are generally stiffer than steel ones. Lateral load distribution also causes load sharing between girders that is likely to reduce further the deflection of an individual girder. Therefore the foregoing estimate of PTFE life is likely to be conservative.

However, the greatest uncertainty lies with the wear rate for PTFE. Wear could not be measured with great accuracy in this research. In NHCRP 432, (Stanton et al. 1999) a wear rate of about 0.01 in/mile of slide-path was reported, which is about 7 times higher than that reported here. The methods of measurements and the total slide-paths were different in the two studies, so comparisons are difficult. For example, in the NCHRP 432 work, the specimens were secured in the carrier plate by reccessing alone, without bonding, whereas in this study, they were bonded. This procedure made accurate measurement (by weight) simpler, but it could have exposed the specimens to higher levels of wear. In this study, measuring the PTFE loss by weight would have been impossible, since the weight of the carbon steel carrier plate would have dwarfed the weight of the lost PTFE. (The weight of PTFE lost in the worst case would only amount to $1/100^{th}$ of a percent of the total weight).

7 Summary and Conclusions

7.1 Summary

Most sliding bridge bearings consist of a stainless steel surface sliding on a PTFE surface, because that pairing leads to low friction. The AASHTO LRFD Design Specifications provide design values for the coefficient of friction only for the most highly polished type of stainless steel – #8 mirror polish – but it is expensive and sometimes difficult to obtain. The purpose of this research was to investigate the friction properties of other stainless steel surfaces with the goal of providing design values for an alternative surface finish that is more economical and more readily available than the #8 mirror polished finish.

Tests were performed on eighteen PTFE-stainless steel specimen pairs. They included three surface finishes: #8 mirror polished finish, 2B rolled finish, and a rough as-rolled finish. Four pairs of specimens in each finish were subjected to a series of standard sliding tests. Special tests were then conducted on six other specimen pairs. Each specimen consisted of two interfaces, which were tested back to back in the test rig to achieve symmetry. The complete set of test parameters included surface finish of the stainless steel, sliding speed, contact pressure, total slide-path and cyclic displacement amplitude.

For the standard tests, the specimen pair was subjected to several warm-up cycles, a multi-speed test, a long slide-path to mimic the long term behavior of a bridge, and then a second multi-speed test. This test program enabled the experiment to show the relationship between sliding speed and friction both when the materials were new and after significant wear, and also showed the progression of this change. The multi-speed tests consisted of three cycles at each of six different sliding speeds, intended to determine the instantaneous Coefficient of Friction without adding significantly to the total slide path. The sets of cycles were alternated between slow and fast tests, so that the relationship between slide-path in the multi-speed tests and friction did not disguise the relationship between sliding speed and friction.

During the long slide-path tests, three of the pairs were tested at different nominal contact pressures, with all other parameters unchanged, and the fourth pair was tested at the

lowest of the three contact pressures (1500 psi) but at a higher sliding speed and smaller displacement amplitude during the long slide-path test, in order to mimic the effects of traffic induced vibrations.

The special tests were conducted only on the 2B specimens, and explored different sliding speeds and displacements, all at the lowest contact pressure.

7.2 Conclusions

The following conclusions were drawn from the testing:

1. Variations in Friction Coefficient. The Coefficient of Friction (CoF) of stainless steel sliding against PTFE is not a fixed value. It varies with many parameters, including all of those used in the test program. It also displays considerable scatter from one sample to the next. Any single value used for design is necessarily an approximation.

2. #8 Mirror polished stainless steel. For this material, the frictional behavior showed the same trends as have been found by previous researchers. The CoF for virgin material is low (about 4% at 3000 psi, and sliding speeds below 2.5 in/min), but increases significantly with increasing slide path, higher sliding speed and lower contact pressure. The agreement between the trends found in this and previous studies suggests that the experimental techniques used here were appropriate.

3. 2B rolled finish stainless steel. For the 2B material, the behavior was quite similar to that of the #8 mirror polished material, except that the CoF was initially slightly higher, and it changed little with slide-path. After a long slide-path (1600 inches), the CoF of the 2B material was lower than that of the comparable #8 mirror polish material. 2B rolled finish appears to be a suitable alternative to #8 mirror polish stainless steel for the conditions tested here (e.g. no lubrication, moderate ambient temperature, etc).

4. For the rough stainless steel, the results were unexpected but consistent across all specimens. The initial CoF was, as anticipated, considerably higher than that of the #8 mirror polish material, but the wear imposed by the long slide path tests caused the friction to decrease. At the end of each of the long slide path tests, the CoF of the rough stainless steel was lower than that of the #8 mirror polish material tested under

comparable conditions. Campbell and Kong, (1987) referenced a similar trend in unlubricated 'standard finish' stainless steel vs. mirror finish

5. Effect of Cyclic Displacement Amplitude. Many small cycles and few large ones were found to cause about the same change in CoF when the total slide path was the same in both cases. Thus, slide-path appears to be the best single indicator of the effects of long term wear.

6. Wear of PTFE. The estimated loss of PTFE thickness during the long slidepath tests was of the same order of magnitude as the precision of the measurements (about 0.003 in). This was true even for the very long slidepath test (48,000 inches). The results showed that PTFE wear in all 2B specimens was the same as, or less than, that in comparable #8 mirror polish specimens. The conditions in the lab are likely much cleaner and more temperate than those under most bridges. Contamination, cold weather, and other effects not tested are likely to cause wear in the field greater than that observed here.

7.3 Recommendations.

7.3.1 Recommendations for Implementation

This research suggests that the use of 2B rolled stainless steel in PTFE-stainless steel sliding interfaces is acceptable, provided that other applicable bridge components are designed to accommodate friction that is slightly higher than that published in AASHTO specifications for #8 mirror polish stainless steel. The proposed CoFs for various situations are given in Table 5-9. They correspond to the slidepath value, within the range of those tested, that gives the highest coefficient of friction. They also represent a friction coefficient that is the average through out the cycle, rather than the initial breakaway value.

It would be prudent to monitor the wear of the PTFE bearings in a few installations, both because the wear rates for 2B finish specimens measured in this study were smaller than those measured previously for #8 mirror polish, and because field conditions are likely to be more aggressive than those experienced in the laboratory. Also, since no tests were performed at cold temperatures, which have been shown (Stanton, et. al. 1999) to cause

much higher wear rates, tests should be done at cold weather to determine the CoF of 2B finish under those conditions, as well as measuring the wear rate

Table 5-9. Suggested CoF at 2.5 in/min and worst-case slide-path.

	Pressure (psi)	500	1000	2000	3000
Surface Finish					
Mirror		0.16	0.15	0.11	0.077
2B Rolled		0.083	0.075	0.061	0.046
Rough Rolled		0.14	0.13	0.094	0.059

7.3.2 Recommendations for Further Research.

This research suggests that the coefficients of friction for #8 mirror polish stainless steel published in the AASHTO LRFD Specifications are slightly too low, especially after significant slide-path has been accumulated. Further testing at long slide-paths should be done to obtain better design values of friction.

This research did not cover the wearing of PTFE in depth. This aspect of behavior should be investigated further, using more precise measuring tools and larger slide-paths. In addition, more investigation of the rate of slide-path accumulation in actual bridges would help determine the true demand and the estimated life of the bearing.

Bibliography

AASHTO (2009a). *AASHTO LRFD Bridge Construction Specifications*. 2nd ed. 2004, with Interim Revisions.

AASHTO (2009b). *AASHTO LRFD Bridge Design Specifications*. 2nd ed. 2004, with Interim Revisions.

Bondonet, G. and Filiatrault, A. (1997). "Frictional Response of PTFE Sliding Bearings at High Frequencies." *ASCE Jo. Bridge Eng.* 2(4), pp. 139-148.

Campbell, T. Ivan, and W. L. Kong. (1987)*, TFE Sliding Surfaces in Bridge Bearings.* Report No. ME-87-06, Ontario Ministry of Transporation, Downsview, Ontario, Canada. 58 p.

Campbell, T.I, and W.L. Kong. (1989). *Laboratory Study of Friction in TFE Sliding Surfaces for Bridge Bearings.*. Report No. MAT-89-04, Ontario Ministry of Transporation, Downsview, Ontario, Canada. 65 p.

Campbell, T.I., Fatemi, M.J. and Manning, D.G. (1993). "Friction in Bridge Bearings with Contaminated TFE Slide Surface." ASCE *Jo. Str. Eng.* 119(11) pp. 3169-3177.

Constantinou, M.C., A. Mokha, and A. Reinhorn. (1990). "Teflon Bearings in Base Isolation. II: Modeling." *ASCE Jo. Str. Eng.* 116(2) pp. 455-474.

Constantinou, M.C., Caccese, J., and Harris, H.G. (1987). "Frictional Characteristics of Teflon-Steel Interfaces under Dynamic Conditions". *Earthquake Engineering And Structural Dynamics*, 15(6), pp. 751-759.

Constantinou, M.C., Tsopelas, P., Kasalanati, A. and Wolff, E.D. (1999). *Property Modification Factors for Seismic Isolation Bearings.* Report No. 99-0012 MCEER Buffalo, NY: MCEER, 1999.

Dolce, M., D. Cardone, and F. Croatto. (2005). "Frictional Behavior of Steel-PTFE Interfaces for Seismic Isolation." *Bulletin of Earthquake Engineering*, 3(1), pp.75-99.

Campbell, T.I. and Fatemi, M. J.(1989). *Further Laboratory Studies of Friction in TFE Slide Surface of a Bridge Bearing*. Report No. MAT-89-06, Ontario Ministry of Transporation, Downsview, Ontario, Canada. Oct. 25 p.

Rheault, J. T. (1992). *Frictional And Wear Characteristics of Different Types of PTFE*. MSCE Thesis, Queen's University, Kingston, Ontario, Canada, March. 77 p.

Stanton, J. F. (2009). "Effects of Shrinkage and Temperature." *CEE 511 Advanced Concrete Design Notes* . Seattle, WA. Oct.

Stanton, J. F., Roeder, C.W. andCampbell, T.I. (1999). *High-Load Multi-Rotational Bridge Bearings*. NCHRP Report 432: National Academy Press, Washington, D.C.

Appendix A, Problems During Testing

Though nearly all of the tests went smoothly, there were a few problems, which are discussed here.

A.1 Sideways Displacement

For most of the tests on #8 mirror polish specimens, the moving specimen carrier moved sideways during its motion, in a pattern not quite in phase with the extension of the actuator. The sideways movement was limited to ±0.16". Methods of preventing this motion, such as guides, were initially rejected because they would introduce additional forces that would contaminate the results. For this reason, and further that the problem conveniently vanished or decreased in amplitude during the warmup phase of the tests, it was decided to do nothing about the problem. The problem persisted throughout the tests and was most severe for specimen M1.30.250.

Figure A-1 shows the friction force during this period. Large variations in force resulted, particularly when, for a few cycles, the specimen carrier came into contact with the side of the rig.

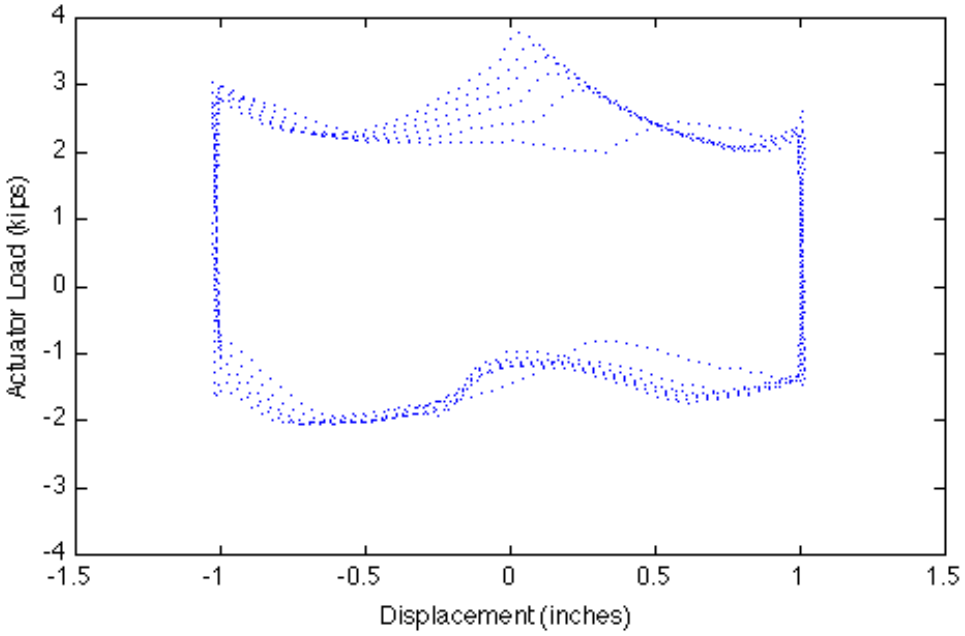

Figure A-1. Force-Displacement curve for three cycles during lateral specimen movement

Testing of the 2B rolled plates also exhibited sideways motion, and it was decided to install guides to limit the deflection so that contact with the fixed frame of the rig could not occur. The guides were mounted on the bottom static plate, and incorporated a lubricated PTFE surface bearing on a strip of #8 mirror polished stainless steel welded to the edge of the moving plate.

An approximate upper bound was obtained to the additional friction force introduced by contact with these guides. The stiffness of the actuator was obtained from a simple pull test. That value was multiplied by the peak sideways displacement (0.16") observed up until that time to give a peak sideways force. That force was then multiplied by the assumed upper bound CoF of the lubricated PTFE (3%) to give the additional longitudinal force. That force was two orders of magnitude smaller than the primary friction force, so it was ignored.

A.1 Spikes in Data

During the first tests, (Specimen R1.45.250), the load reading was inconsistent, and on the force-displacement loops, there were large spikes in the data. This was attributed to contamination in the hydraulic lines, which was corrected for the second specimen (M1.45.250). The problem did not re-occur.

A.2 Pressure Malfunctions

During some tests, the hydraulic system used to maintain contact pressure did not function as planned, either because of temperature changes or accidental release of the valve. In the analysis section, data associated with small differences in pressure due to temperature changes were corrected, as shown in Section **Error! Reference source not found.**. In tests where the pressure was released, or otherwise wildly out of range, the corresponding data have been omitted. All data is shown in Appendix B.

Appendix B, Data Plots

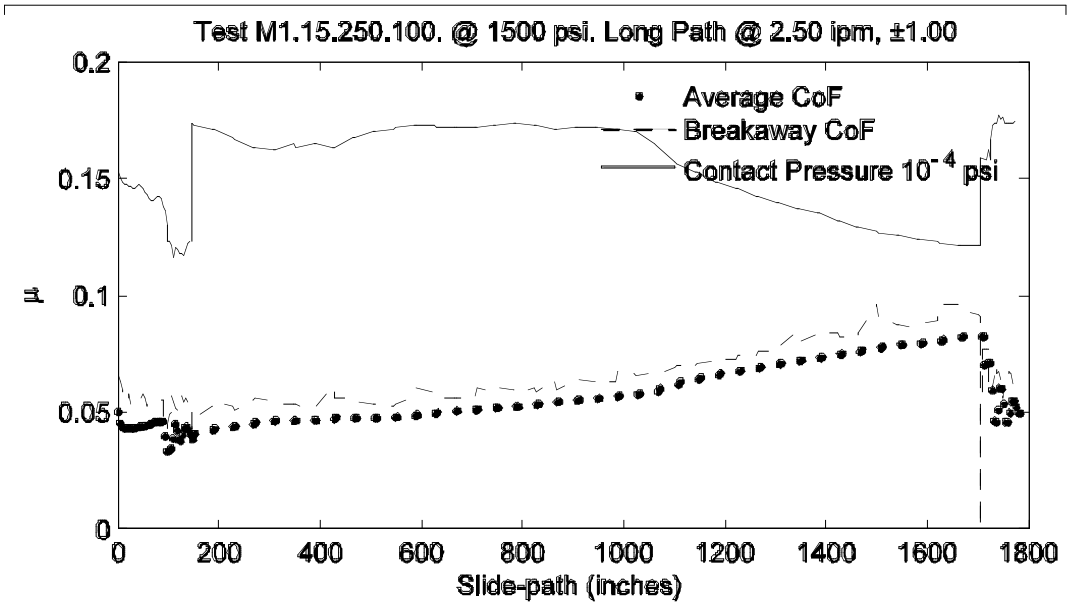

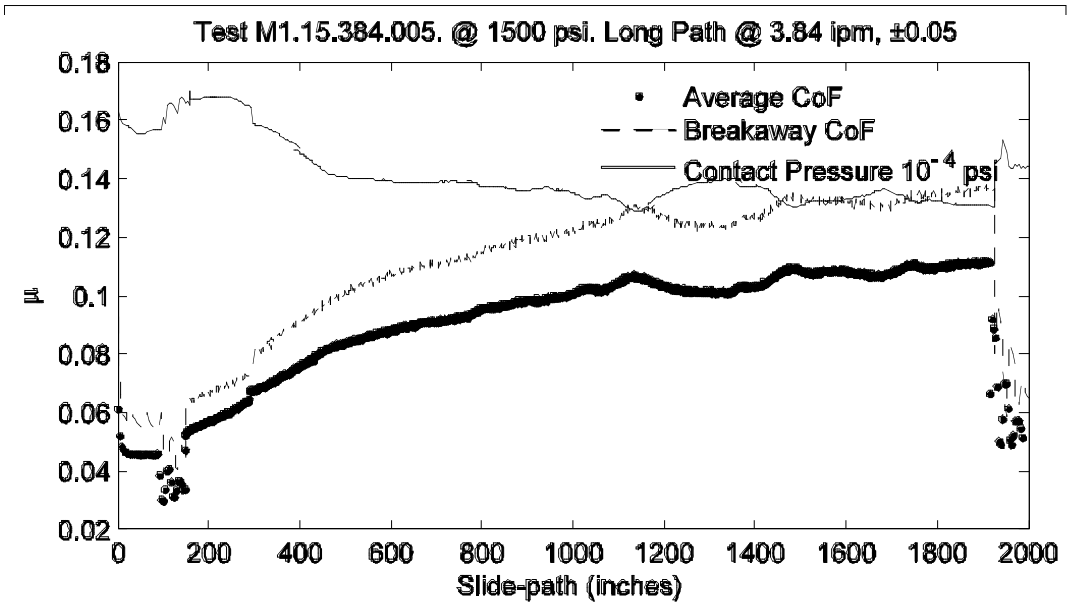

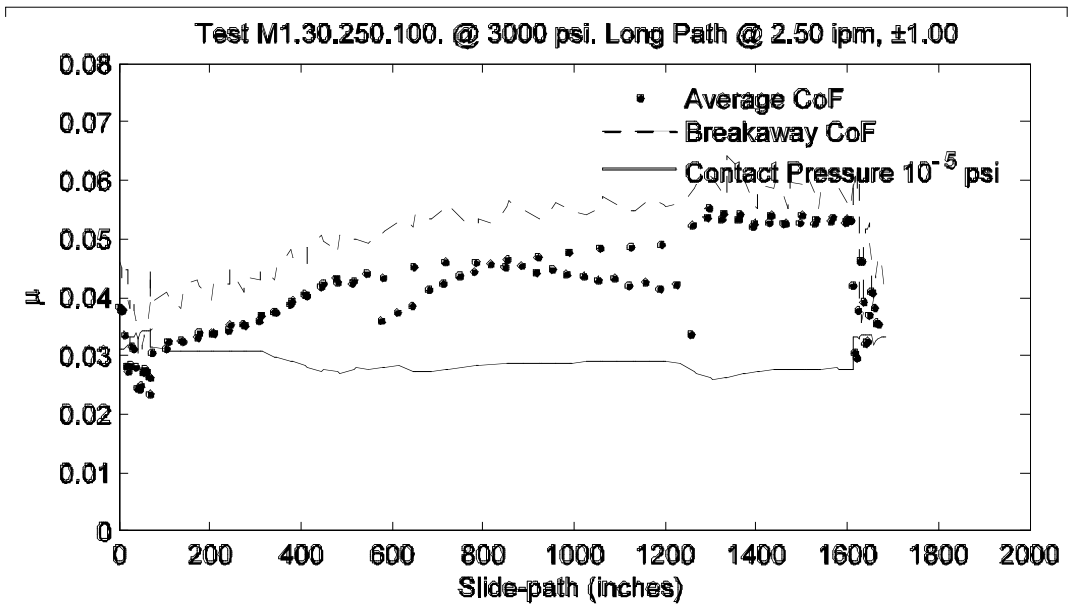
Test M1.30.250.100. @ 3000 psi. Long Path @ 2.50 ipm, ±1.00
Average CoF
Breakaway CoF
Contact Pressure 10^-5 psi
μ
0.08
0.07
0.06
0.05
0.04
0.03
0.02
0.01
0
0
200
400
600
800
1000
1200
1400
1600
1800
2000
Slide-path (inches)

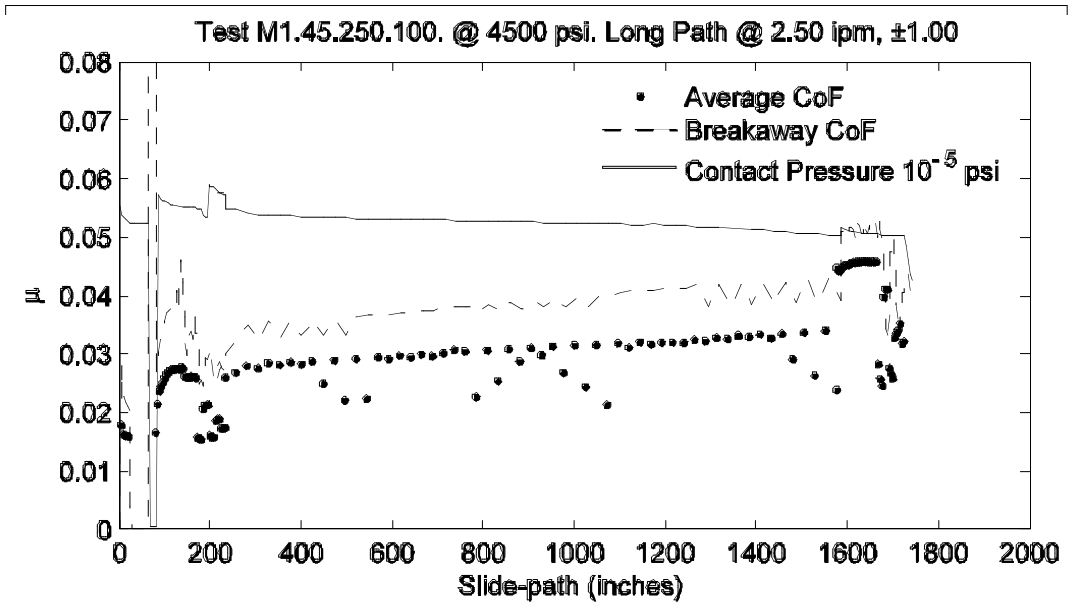
Test M1.45.250.100. @ 4500 psi. Long Path @ 2.50 ipm, ±1.00
Average CoF
Breakaway CoF
Contact Pressure 10^-5 psi
μ
0.08
0.07
0.06
0.05
0.04
0.03
0.02
0.01
0
0
200
400
600
800
1000
1200
1400
1600
1800
2000
Slide-path (inches)

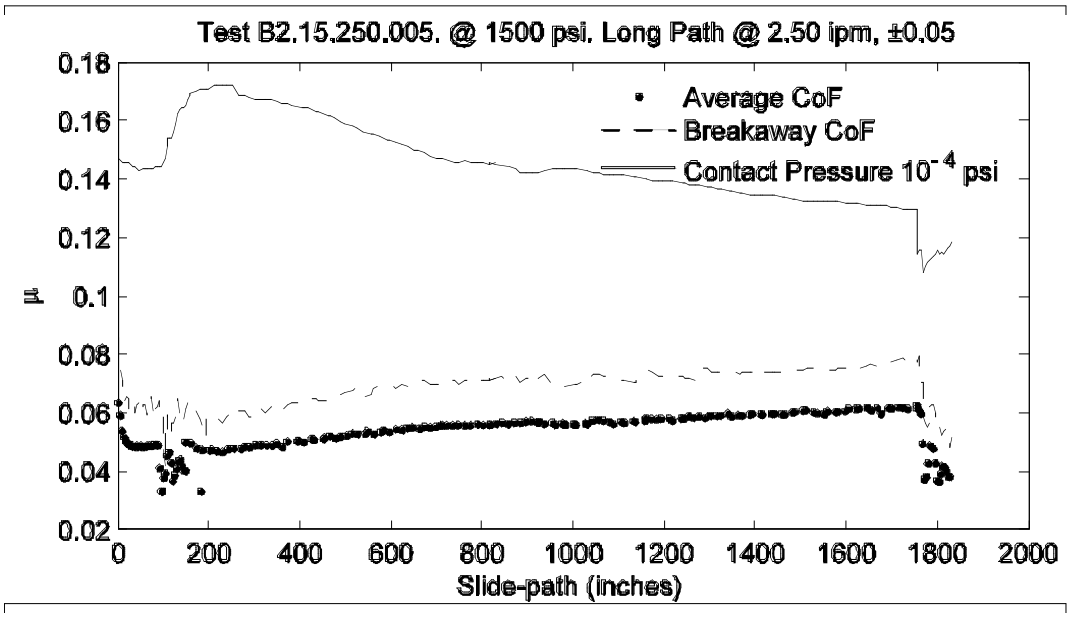
Test B2.15.250.005. @ 1500 psi. Long Path @ 2.50 ipm, ±0.05
Average CoF
Breakaway CoF
Contact Pressure 10^-4 psi
μ
0.18
0.16
0.14
0.12
0.1
0.08
0.06
0.04
0.02
0
200
400
600
800
1000
1200
1400
1600
1800
2000
Slide-path (inches)

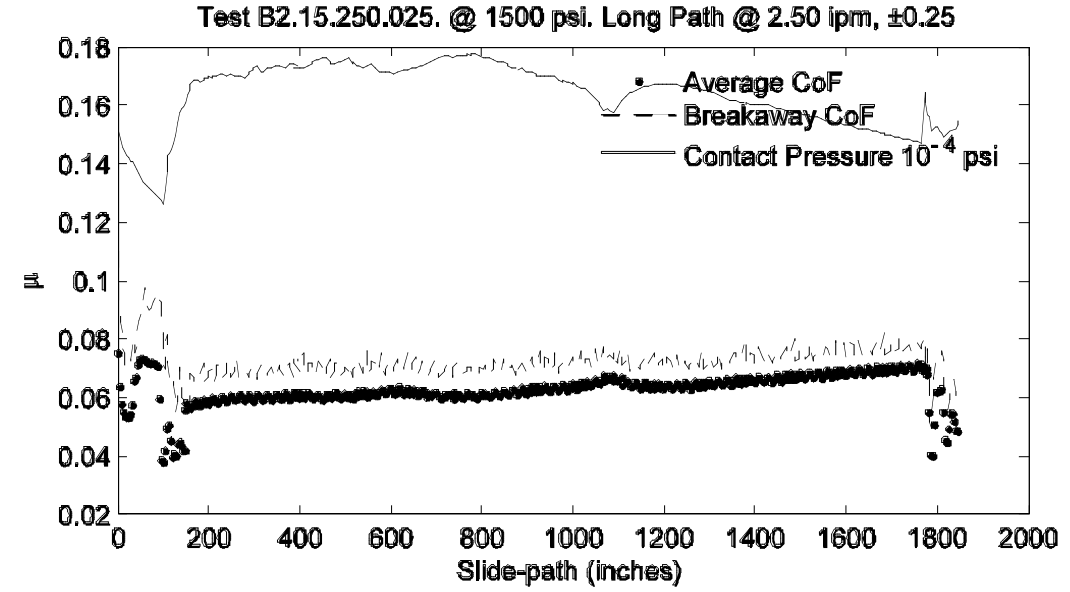
Test B2.15.250.025. @ 1500 psi. Long Path @ 2.50 ipm, ±0.25
Average CoF
Breakaway CoF
Contact Pressure 10^-4 psi
μ
0.18
0.16
0.14
0.12
0.1
0.08
0.06
0.04
0.02
0
200
400
600
800
1000
1200
1400
1600
1800
2000
Slide-path (inches)

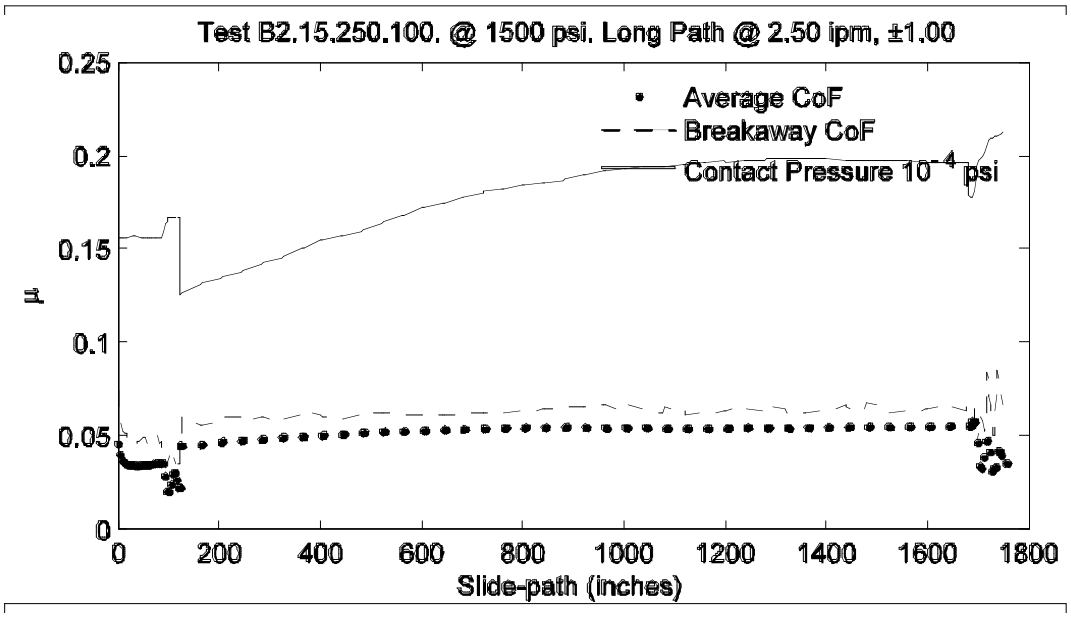
Test B2.15.250.100. @ 1500 psi. Long Path @ 2.50 ipm, ±1.00
Average CoF
Breakaway CoF
Contact Pressure 10^-4 psi
μ
0.25
0.2
0.15
0.1
0.05
0
0
200
400
600
800
1000
1200
1400
1600
1800
Slide-path (inches)

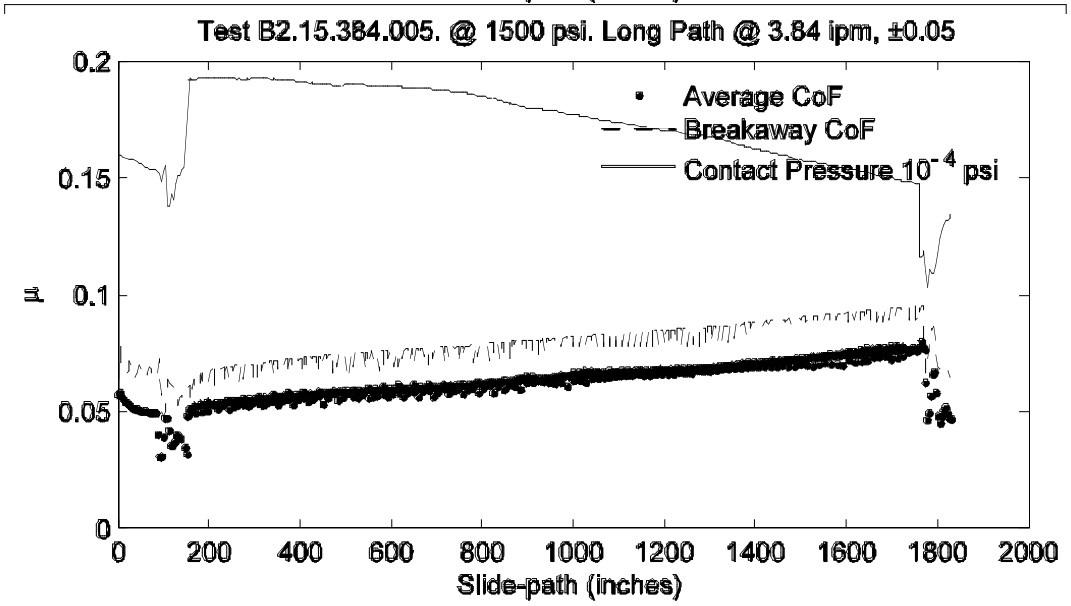
Test B2.15.384.005. @ 1500 psi. Long Path @ 3.84 ipm, ±0.05
Average CoF
Breakaway CoF
Contact Pressure 10^-4 psi
μ
0.2
0.15
0.1
0.05
0
0
200
400
600
800
1000
1200
1400
1600
1800
2000
Slide-path (inches)

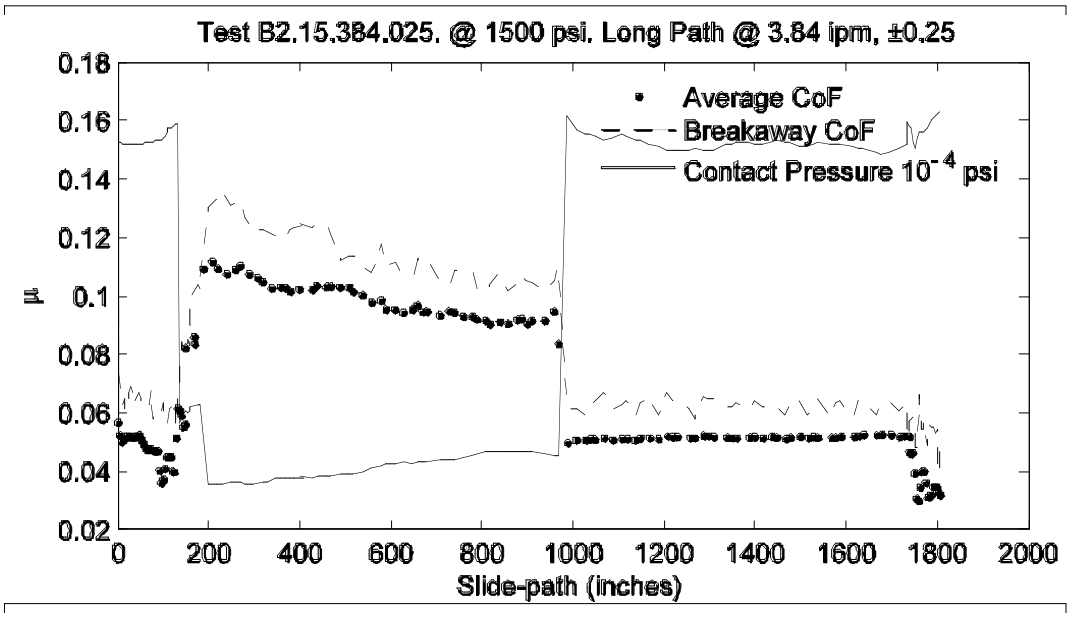
Test B2.15.384.025. @ 1500 psi. Long Path @ 3.84 ipm, ±0.25
Average CoF
Breakaway CoF
Contact Pressure 10^-4 psi
μ
Slide-path (inches)
0.18
0.16
0.14
0.12
0.1
0.08
0.06
0.04
0.02
0
200
400
600
800
1000
1200
1400
1600
1800
2000

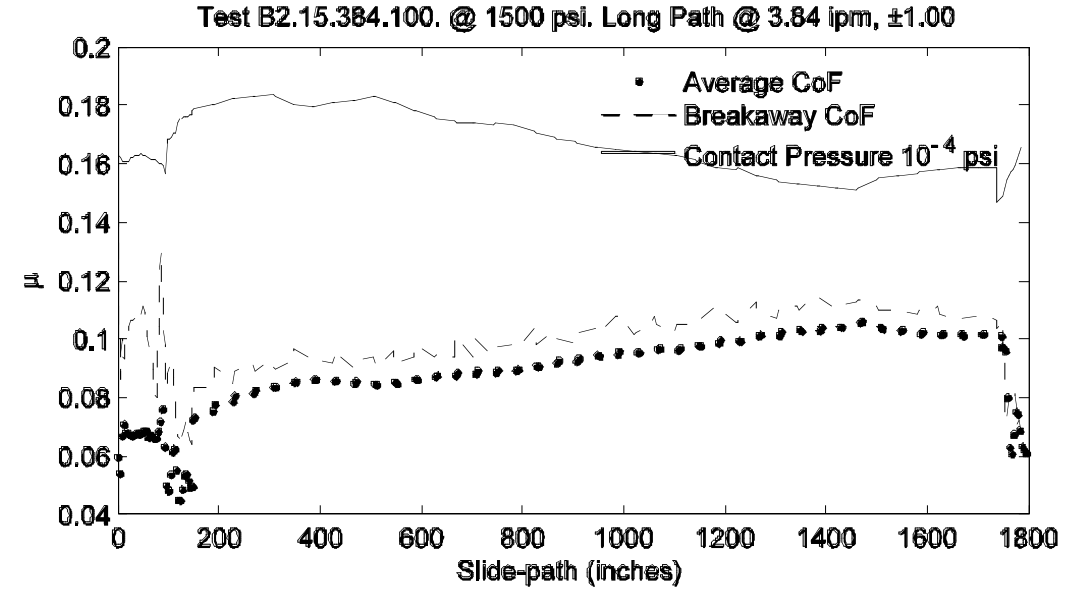
Test B2.15.384.100. @ 1500 psi. Long Path @ 3.84 ipm, ±1.00
Average CoF
Breakaway CoF
Contact Pressure 10^-4 psi
μ
Slide-path (inches)
0.2
0.18
0.16
0.14
0.12
0.1
0.08
0.06
0.04
0
200
400
600
800
1000
1200
1400
1600
1800

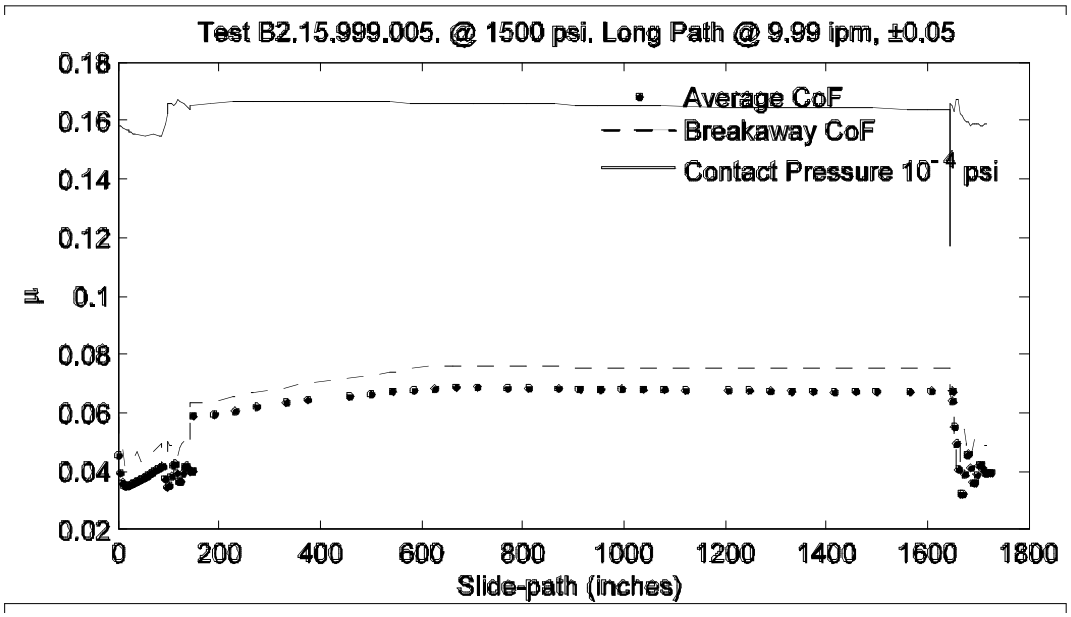
Test B2.15.999.005. @ 1500 psi. Long Path @ 9.99 ipm, ±0.05
Average CoF
Breakaway CoF
Contact Pressure 10^-4 psi
μ
0.18
0.16
0.14
0.12
0.1
0.08
0.06
0.04
0.02
0
200
400
600
800
1000
1200
1400
1600
1800
Slide-path (inches)

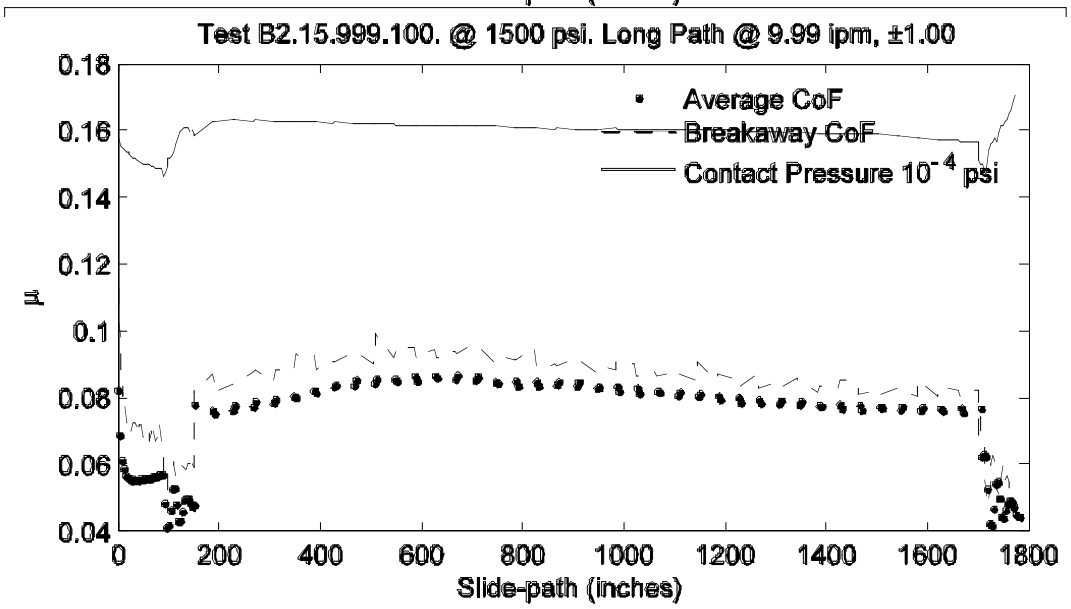
Test B2.15.999.100. @ 1500 psi. Long Path @ 9.99 ipm, ±1.00
Average CoF
Breakaway CoF
Contact Pressure 10^-4 psi
μ
0.18
0.16
0.14
0.12
0.1
0.08
0.06
0.04
0
200
400
600
800
1000
1200
1400
1600
1800
Slide-path (inches)

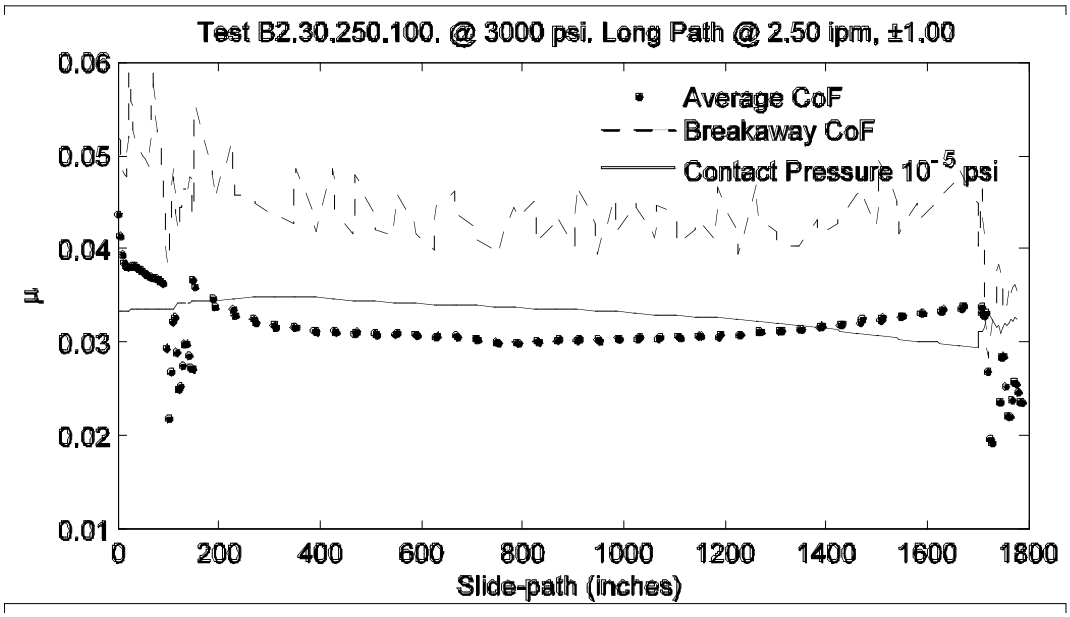
Test B2.30.250.100. @ 3000 psi. Long Path @ 2.50 ipm, ±1.00
Average CoF
Breakaway CoF
Contact Pressure 10^-5 psi
μ
0.06
0.05
0.04
0.03
0.02
0.01
0
200
400
600
800
1000
1200
1400
1600
1800
Slide-path (inches)

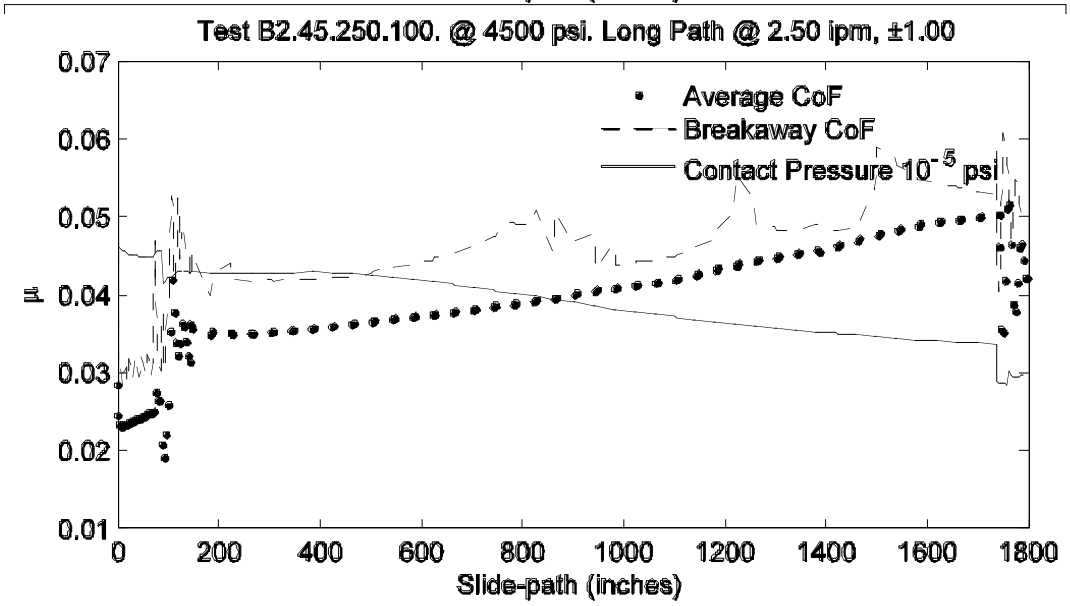
Test B2.45.250.100. @ 4500 psi. Long Path @ 2.50 ipm, ±1.00
Average CoF
Breakaway CoF
Contact Pressure 10^-5 psi
μ
0.07
0.06
0.05
0.04
0.03
0.02
0.01
0
200
400
600
800
1000
1200
1400
1600
1800
Slide-path (inches)

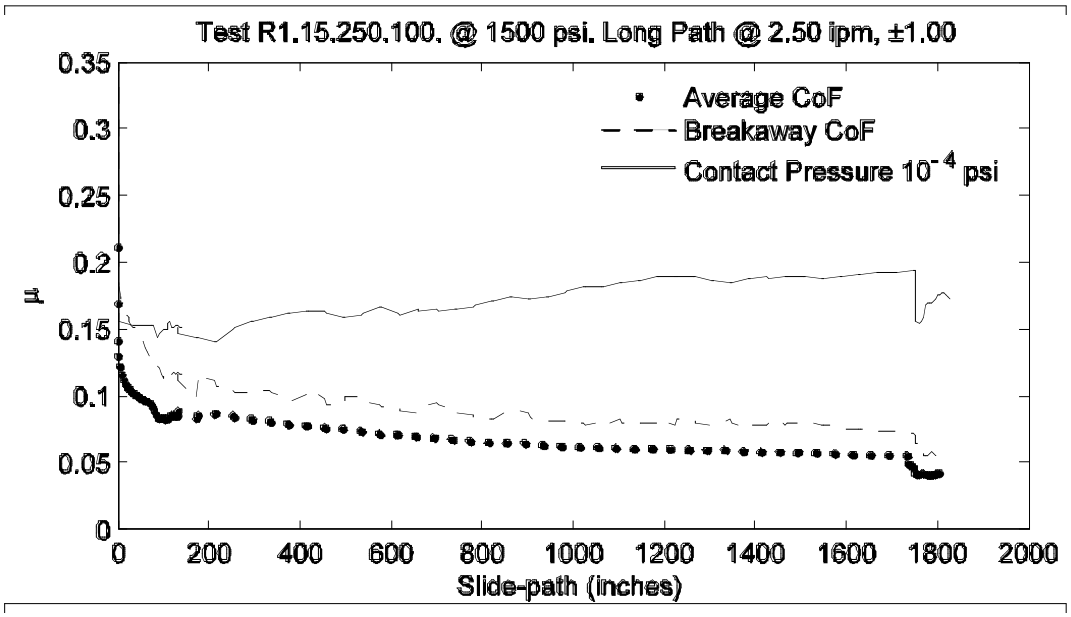
Test R1.15.250.100. @ 1500 psi. Long Path @ 2.50 ipm, ±1.00
Average CoF
Breakaway CoF
Contact Pressure 10^-4 psi
μ
0.35
0.3
0.25
0.2
0.15
0.1
0.05
0
0
200
400
600
800
1000
1200
1400
1600
1800
2000
Slide-path (inches)

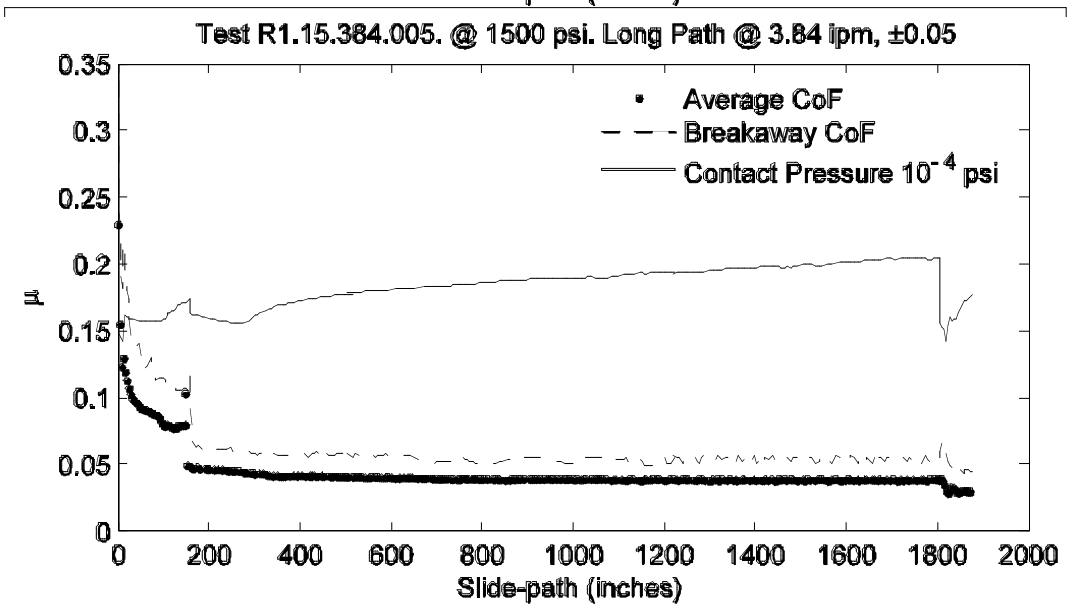
Test R1.15.384.005. @ 1500 psi. Long Path @ 3.84 ipm, ±0.05
Average CoF
Breakaway CoF
Contact Pressure 10^-4 psi
μ
0.35
0.3
0.25
0.2
0.15
0.1
0.05
0
0
200
400
600
800
1000
1200
1400
1600
1800
2000
Slide-path (inches)

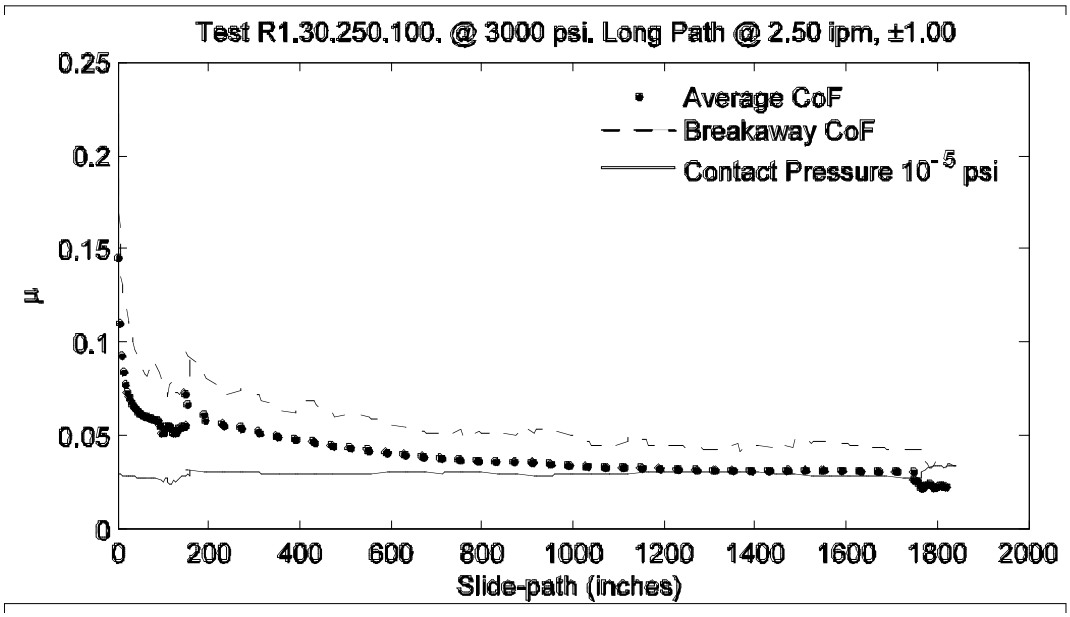
Test R1.30.250.100. @ 3000 psi. Long Path @ 2.50 ipm, ±1.00
Average CoF
Breakaway CoF
Contact Pressure 10^-5 psi
μ
0.25
0.2
0.15
0.1
0.05
0
0
200
400
600
800
1000
1200
1400
1600
1800
2000
Slide-path (inches)

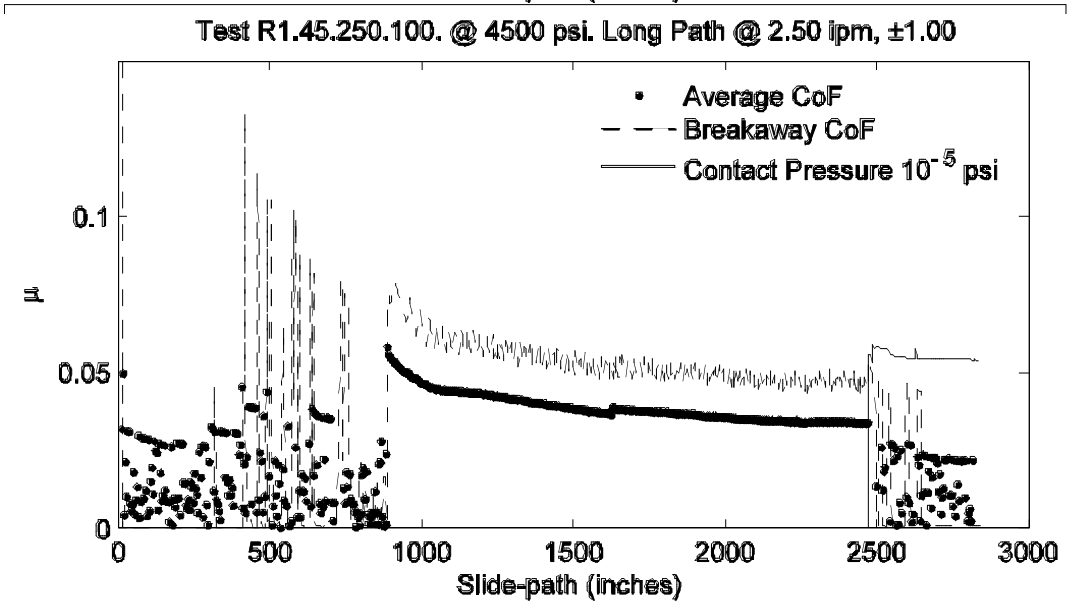
Test R1.45.250.100. @ 4500 psi. Long Path @ 2.50 ipm, ±1.00
Average CoF
Breakaway CoF
Contact Pressure 10^-5 psi
μ
0.1
0.05
0
0
500
1000
1500
2000
2500
3000
Slide-path (inches)